UNIVERSITY OF STELLENBOSCH

Diode-End-Pumped Solid-State Lasers

M.J. Daniel Esser

Thesis presented in partial fulfilment of the requirements for the degree of
Master of Science
at the University of Stellenbosch.

Dr. Christoph Bollig
Prof. Hubertus M. von Bergmann

Laser Research Institute
Physics Department

April 2005

Declaration

I, the undersigned, herby declare that the work contained in this thesis is my own original work and that I have not previously in its entirety or in part submitted it at any university for a degree.

Signature: …….

Date: …….

Abstract

This thesis consists of two parts: a discussion on diode-pumped solid-state lasers and a detailed description of the development of a diode-end-pumped Nd:YLF laser. A background motivation, which places this research area in perspective, is also given.

Part One introduces solid-state lasers and their physics. The focus is on the Nd^{3+} active ion and describes its energy level structure as a typical four-level solid-state laser. An overview of optical pump sources for solid-state lasers is given, focussing on the construction, operation and advantages of diode lasers.

It is motivated that diode-end-pumping solid-state lasers produce laser systems with the highest efficiency and diffraction limited beam quality. It is, however, emphasised that power scaling of diode-end-pumped solid-state lasers is problematic due to localised heat generation in the solid-state laser medium. The adverse effect of heat generation on the laser performance is also described. In the design of diode-end-pumped solid-state lasers, the management of thermal effects is suggested as the approach to scale the output power of these lasers.

Part Two of the thesis describes the design and the results of a novel high-power diode-end-pumped solid-state laser developed at the Laser Research Institute. The description of the design is split into three components: the laser material, the pump source and the laser resonator.

The choice of laser material is motivated in detail, focussing on Nd:YLF's advantage of having a very weak thermal lens when operated on the σ-polarization at 1053 nm. Its disadvantage of having a low fracture limit is also highlighted, but the approach to power scale it to the multi-10-watt level, with the use of low doping concentration, a low absorption pump wavelength, and a large pump beam, is described. It is further shown that this approach led to the development of a novel laser resonator, which allows a large fundamental mode in the laser material to match the large pump beam, and it can compensate for the astigmatic thermal lens in Nd:YLF.

The experimental results of the high-power diode-end-pumped Nd:YLF laser are presented, showing the influence of doping concentration, output coupling efficiency and resonator adjustments on the continuous wave and *Q*-switched laser performance.

It is shown that the optimum laser parameters were determined, resulting in the Nd:YLF laser producing more than 26 W of continuous wave output power with a close to diffraction limited beam quality ($M^2 < 1.4$), and more than 3 mJ of energy per pulse at a repetition rate of 6 kHz when *Q*-switched. It is concluded that the power-scaling concept proved to be efficient and that further power scaling would be possible with this scheme.

Opsomming

Hierdie tesis bestaan uit twee dele, naamlik ’n bespreking van diode-gepompde vaste-toestand lasers en ’n verslagdoening van die ontwikkeling van ’n longitudinale gepompde Nd:YLF-laser. Daar word vooraf ’n motivering gegee om hierdie navorsing in perspektief te plaas in vergelyking met wêreldwye laser ontwikkeling.

Deel een is ’n inleiding tot vaste-toestand lasers asook die fisika wat die lasers beskryf. Die Nd^{3+}-ioon word uitgesonder en sy kwantumenergiestruktuur word voorgestel as dié van ’n tipiese viervlak vaste-toestand laser. Bronne wat as optiese pomp kan dien vir vaste-toestand lasers word bespreek, met besondere verwysing na die werking en voordele van diode lasers as pompbron.

Daar word verder gemotiveer dat diode-gepompde vaste-toestand laser sisteme met hoë straal kwaliteit die hoogste doeltreffendheid het indien hulle longitudinaal gepomp word. Daar word egter aangetoon dat dit problematies is om hierdie lasers tot hoë drywing op te skaal as gevolg van die gelokaliseerde hittelading in die vaste-toestand laser materiaal. Die newe-effekte van hittelading op die gedrag van vaste-toestand lasers word uitgewys. Daar word aangetoon dat die bestuur van hittelading in die medium van uiterste belang is tydens die ontwerp van hoë drywing longitudinale gepompde vaste-toestand lasers

In deel twee van die tesis word ’n unieke hoë drywing longitudinale gepompde Nd:YLF-laser, wat by die Laser Navorsings Instituut ontwerp en gedemonstreer is, in diepte beskryf. Die ontwerp van die Nd:YLF-laser kan onderverdeel word in ’n bespreking van die laser materiaal, die pompbron en die laser resonator.

Die keuse van Nd:YLF as lasermateriaal word breedvoerig gemotiveer, met die klem op hierdie materiaal se geringe termiese lens indien laseraksie in die σ-polarisasie by 1053 nm plaasvind. Die lae termiese breekpunt word uitgewys as die beperkende effek van die materiaal. Die metode om hierdie materiaal egter na die multi-10-watt drywings vlak op te skaal word beskryf: dit is deur ’n lae konsentrasie van Nd^{3+} te gebruik, tesame met ’n pomp golflengte met ’n lae absorpsie koëffisiënt, en ’n groot

diameter pomp straal. Daar word aangetoon dat hierdie keuses gelei het tot die ontwerp van ’n unieke laser resonator wat ’n groot fundamentele resonatormodus het in die lasermedium (om te pas by die groot diameter pomp straal). Hierdie resonator ontwerp het ook die nie-uniforme termiese lens van Nd:YLF in ag geneem.

Die resultate soos verkry in die eksperimentele opstelling van die Nd:YLF-laser word daarna beskryf. Die invloed van verskeie parameters word weergegee, soos die uitkoppelingspersentasie, die resonatorlengte en die konsentrasie van Nd^{3+}-ione. Die effek van laasgenoemde faktore op die gedrag van die laser tydens kontinue- en *Q*-geskakelde werking word bespreek.

Die optimale werking van die laser soos verkry deur die regte keuse van parameters word aangetoon, met ’n hoogste uitset drywing van die Nd:YLF-laser van meer as 26 W met ’n bykans diffraksie-beperkte bundel kwaliteit wat tydens kontinue werking behaal is. In die *Q*-geskakelde modus is meer as 3 mJ energie per puls verkry teen ’n pulseringfrekwensie van 6 kHz. Opsommend kan gesê word dat ’n suksesvolle metode gevolg is om die drywing op te skaal, en dat die konsep verder ontwikkel kan word om selfs hoër drywing uitset te behaal.

To my Parents

Acknowledgements

The work presented here was supported by many people, all of whom cannot be mentioned. Nevertheless, I want to express my appreciation to:

my study leader, Dr. Christoph Bollig, for his technical leadership, his depth of knowledge, which he is always willing to share, and his friendship;

my supervisor, Professor Hubertus von Bergmann, for his ongoing support of the researchers and students in the solid-state laser laboratory at the Laser Research Institute, including the work presented here;

the students and personnel of the Laser Research Institute and Physics department, who gave me the opportunity to enjoy my studies in a diverse and intellectual environment;

the National Laser Centre for their financial support of my MSc studies, their support of this laser development project at the Laser Research Institute, and their support for the presentation of this work at two international conferences;

Dr. Andrew Forbes for his valuable comments and motivation;

my parents, for their financial and emotional support during my studies, as well as their unfailing trust in me;

and Irene-marié, who lovingly supported me throughout, being my girlfriend, fiancé and wife.

Contents

List of figures

List of tables

Background

Technological research is generally influenced by world economics and market trends. The market potential usually determines the research direction, since the research should provide solutions that are needed in the industry. In return, the industry provides further funding for research. Research supporting the optoelectronics industry, particularly laser development, is no exception and is influenced by the laser market trends to a large extent.

The importance of economic criteria in choosing or developing a laser source for industrial, medical and research applications is increasing. These include investment costs, overall efficiency of the laser source, reliability, maintenance costs and overall system capability. However, in many applications these economic criteria must be balanced with scientific criteria, for example beam quality, which could ensure increased efficiency, quality and flexibility of a particular process, which indirectly reduce the overall cost of such an application [1].

As stated in the latest laser market report in *Laser Focus World* [2], the overall market remains to be dominated by diode lasers (Figure 1-1). This is due to their wide range of applications and further improvement of the available output powers, increased beam quality and beam delivery techniques, reduced cost and wider range of wavelengths which are available [3].

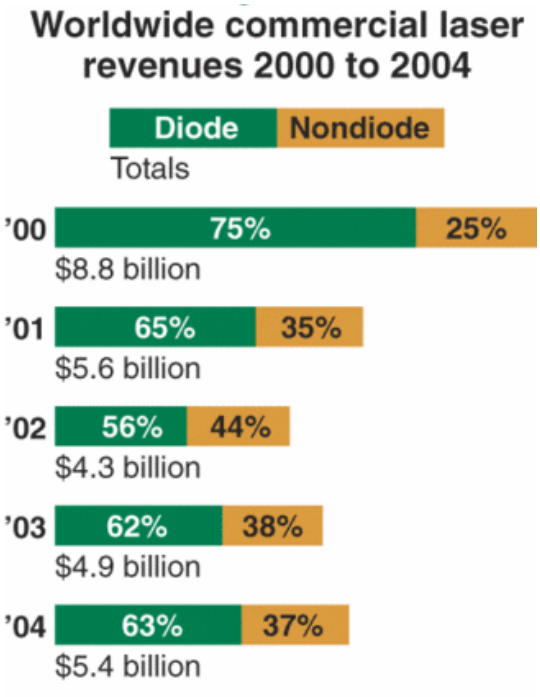

Figure 1-1: The trend in worldwide laser revenues from 2000 to 2003 and prediction for 2004 [2].

However, diode lasers do not dominate the market where high power lasers with fair or good beam quality are required. This market is still the domain of lamp-pumped solid-state lasers, as seen in Figure 1-2.

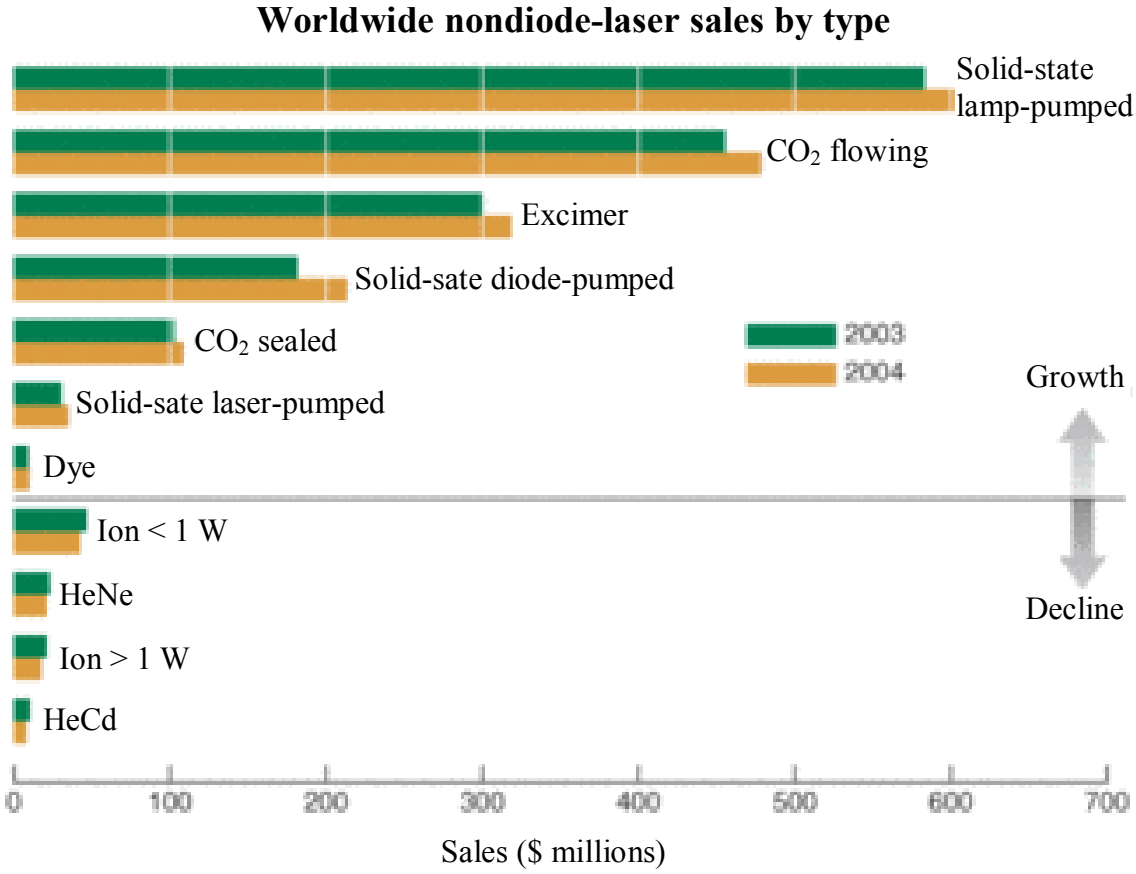

Figure 1-2: The worldwide laser (non-diode) sales for 2003 and prediction for 2004 [2].

Although the established technology of lamp-pumped solid-state lasers can provide high output power and fair beam quality, there is still improvement potential with regard to the efficiency and beam quality of these lasers [1]. However, diode-end-pumped solid-state lasers have proven to be highly efficient lasers with diffraction limited beam quality. These lasers could fill the need of the industry by providing laser systems of high efficiency and near diffraction limited beam quality. It is therefore of no surprise that the market for diode-pumped solid-state lasers has experienced robust growth over the past decade [4].

The main reason why diode-pumped solid-state lasers do not dominate the market is that their output powers are limited to a few watts [5]. With the motivation of many possible applications of such lasers, much research has gone into the understanding of the factors that limit the output power of these lasers, and into the further development of high power diode-end-pumped solid-state lasers.

With the above mentioned in mind, the research presented here on the development of a high-power diode-end-pumped solid-state laser is justified by the scientific impact and the economic value of lasers with high power, high efficiency and near diffraction limited beam quality.

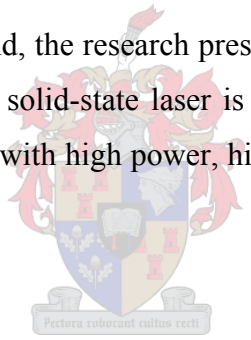

Part 1 – Diode-pumped solid-state lasers

1 Introduction to solid-state lasers

LASER action, or Light Amplification through Stimulated Emission of Radiation, is inherently linked to the principles governing the interaction of radiation with matter. When a laser material is excited in such a way that there are more atoms in a higher energy level than in some lower level, the material will be able to amplify incident radiation at the frequency corresponding to the energy level difference, as determined by Bohr's frequency relation $E = h\nu$ [6 Ch. 1].

The amplified (stimulated) emission is indistinguishable from the stimulating radiation field, which gives rise to the high coherence of the light emitted from a laser. The principles governing spontaneous emission, stimulated emission and absorption of radiation in matter, as described by Einstein and Plank, will not be discussed here but can be found in well known laser text books e.g. [6, 7, 8].

In its most basic form, a laser consists of a laser medium, a pump source to excite the medium, and an optical resonator [8 Ch. 1]. A solid-state laser medium is a crystal, glass or ceramic which contains a small amount of an active element in which optical transitions can occur. For the case where the active element is one of the rare-earth ions, these optical transitions occur between the energy states of inner, incomplete electron shells of the ion. To be a suitable laser source, the laser medium must possess sharp florescent lines, strong absorption bands for optical pumping and reasonably high quantum efficiency [6 Ch. 2].

The first laser, which was demonstrated in 1960, was a solid-state laser. It was a ruby laser which used the transition metal Cr^{3+} as active element and sapphire (Al_2O_3) as host material [9]. Since then, many solid-state laser systems have been demonstrated using trivalent rare earths, divalent rare earths and transition metals as active elements in various host materials [10]. However, the most widely used active element is the trivalent neodymium ion (Nd^{3+}).

Already in the early stages of solid-state laser development, it was recognised that continuous wave operation at room temperature could be achieved with lasers using Nd^{3+}. This is due to the ion's sufficiently long fluorescence lifetime, narrow fluorescence linewidth and its four-level laser structure, with the lower laser energy level high above the ground level [6 Ch. 2].

The Nd^{3+} ion has been used as active element in a large number of different host materials, including glasses, oxides, phosphates, silicates, tungstates, molybdates, vanadates, beryllates, fluorides and ceramics. Each of these host materials has its distinct properties, limitations and advantages [10 Sect. 1]. Probably the best known laser material is Nd doped yttrium aluminium garnet ($Nd^{3+}:Y_3Al_5O_{12}$) commonly known as Nd:YAG. It has been used extensively, especially in high power lamp-pumped lasers, due to its low threshold and high gain laser operation. Additionally, the crystal is very hard, is isotropic, and it can be grown in relatively large crystals with high optical quality [6 Ch. 2].

Since the advent of diode-pumped solid-state lasers, laser materials such as $Nd:YVO_4$, have increased in importance. Due to the narrow band output of diode lasers, materials that were not widely utilised in lamp-pumped systems, have been shown to be highly efficient diode-pumped lasers. This is because the laser diode spectral output can be chosen to overlap with the absorption band of a laser material [11].

The operation of solid-state lasers, including possible pumping schemes and limitations of output power and efficiency, will be discussed with Nd lasers as example. Nd lasers have been demonstrated with a wide range of pumping schemes and resonators, and the underlying principles of heat generation and thermal lensing in solid-state lasers can be explained well with Nd lasers.

An in-depth study of solid-state lasers, covering the increasing number of combinations of active elements and host materials, does not fall within the scope of this work. A comprehensive introduction to solid-state lasers can be found in [6].

2 The Nd^{3+} laser

2.1 Energy levels

The crystal in which the laser ion is hosted must have lattice sites that can accept dopant ions. For example, in the Nd:YAG material about 1% of Y^{3+} is substituted by Nd^{3+}, which has a similar atomic size. In addition, the local crystal fields in the crystal must have the correct symmetry and strength, which is needed to induce the desired spectroscopic properties of the laser material [6 Ch. 2].

The Nd^{3+} ion has three electrons in the unfilled *4f* subshell. The outer, complete 5*s* and 5*p* subshells shield the inner shell from the crystal field, such that optical transitions in the inner shell almost act as free electronic transitions. In the ground state of the ion, the orbital angular momentum of the three electrons in the 4*f* shell add up to six atomic units, i.e. L = 6, expressed by the letter *I*. The spin angular momentum of the electrons adds up to $^3/_2$ units, defining the ground state of the Nd^{3+} ion as $^4I_{9/2}$. The $^4I_{11/2}$, $^4I_{13/2}$ and $^4I_{15/2}$ states form the first few excited levels of Nd^{3+} [6 Ch. 2]. Other combinations between the orbital and spin angular momentum give rise to higher excited energy levels [12].

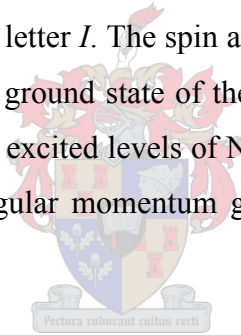

The energy level diagram of Nd^{3+} in the YAG crystal is shown in Figure 2-1. The crystal field splits the energy levels into Stark sublevels. The magnitude of the Stark effect and the degree to which the crystal field influences the energy levels of the ion depends on the host crystal in which the ion is doped [6 Ch. 2].

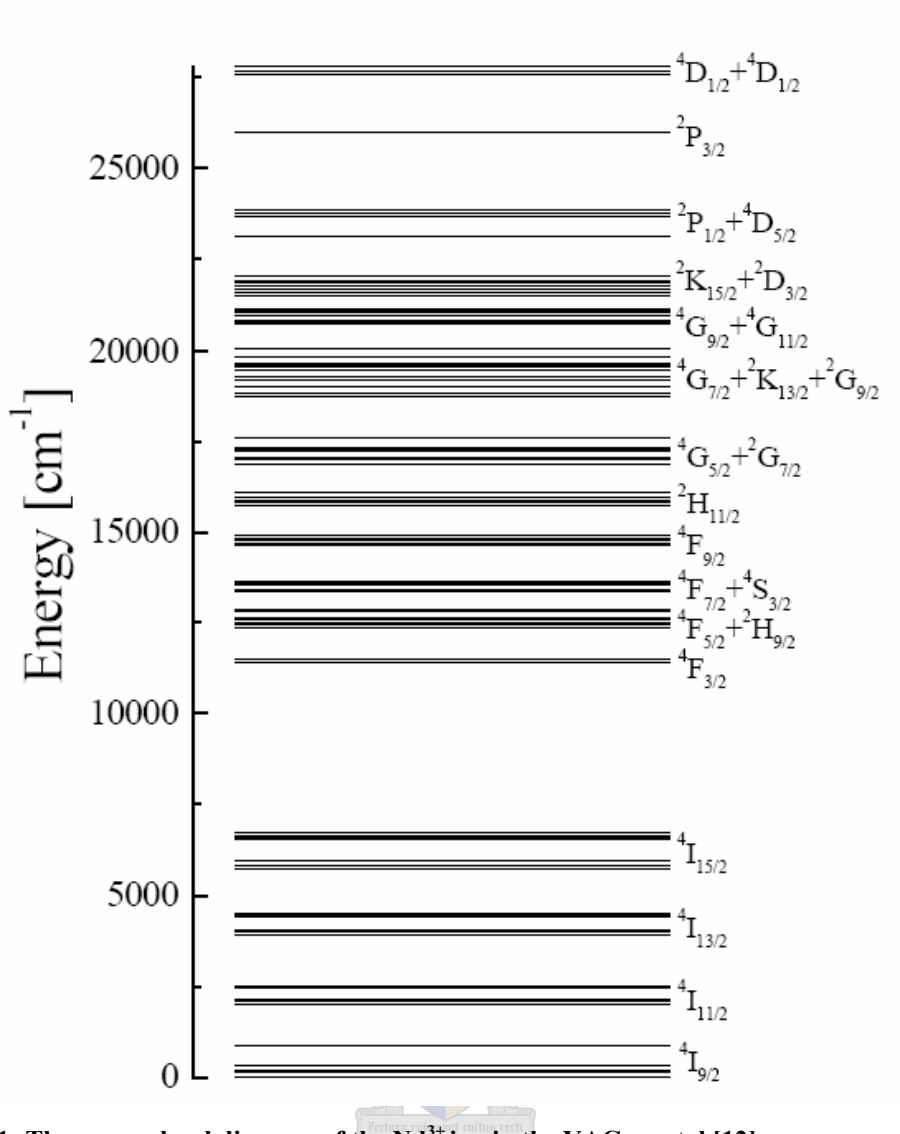

Figure 2-1: The energy level diagram of the Nd^{3+} ion in the YAG crystal [12].

The absorption spectrum of Nd:YAG, as determined by its energy level structure, is shown in Figure 2-2. The highest absorption cross section in the wavelength region shown is at 808 nm. This wavelength relates to the energy transition from the ground state $^4I_{9/2}$ to the excited state $^4F_{5/2}$ [13]. Other absorption bands exist below the wavelength range which is shown in Figure 2-2, which relate to transitions from the ground state to higher lying energy levels. These are of more interest for lamp-pumped systems [7 Ch. 6].

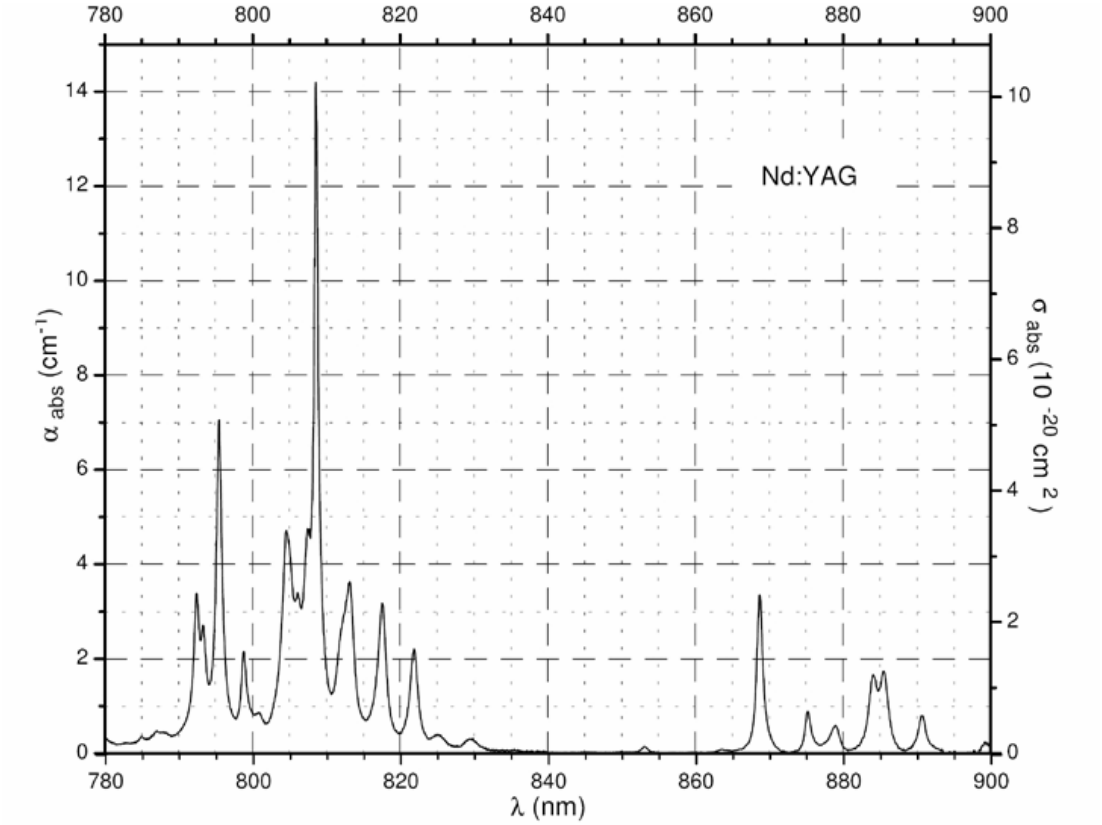

Figure 2-2: The absorption spectrum of Nd:YAG from 780 to 900 nm [13].

An excited ion will produce a fluorescence spectrum also according to its energy level structure. The strongest emission cross section of Nd:YAG is at 1064 nm, as seen in Figure 2-3. This wavelength relates to the energy transition from the $^4F_{3/2}$ excited level to the $^4I_{11/2}$ level [13]. The $^4F_{3/2}$ level of the Nd^{3+} ion has a long fluorescence lifetime, ranging from 100 μs in YVO_4, 230 μs in YAG to 500 μs in YLF, another well known laser material [6 Ch. 2].

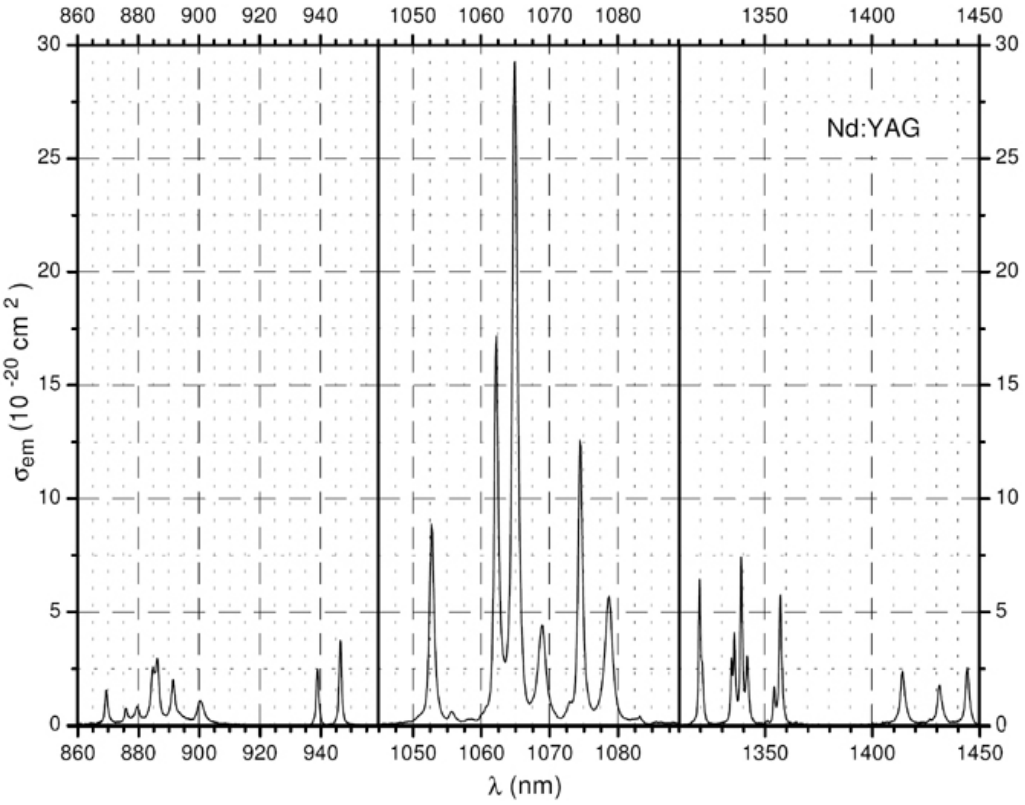

Figure 2-3: Fluorescence spectrum of Nd:YAG in the 900 nm, 1064 nm and 1.3 μm regions [13].

2.2 Four level laser

Because of its spectroscopic properties, the Nd^{3+} ion can form an almost ideal four-level laser. This well known scheme is illustrated in Figure 2-4 for the Nd^{3+} energy levels in YAG. The ions in the host material are excited from the ground level ($^4I_{9/2}$) to the pump level ($^4F_{5/2}$) by absorbing radiation (at 808 nm) which corresponds to the energy difference between these levels. The ions that are excited to the pump level relax very fast to the next lower lying level, the so-called upper laser level ($^4F_{3/2}$).

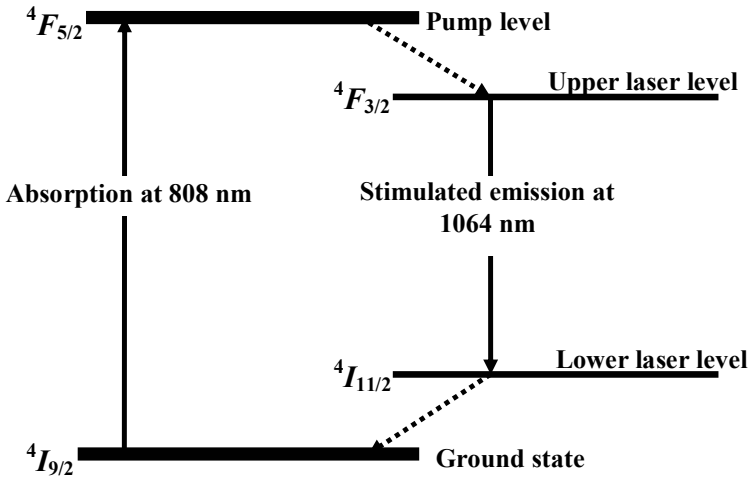

Figure 2-4: Schematic of the Nd:YAG four level laser.

The upper laser level is a meta-stable level and has a long lifetime. This allows a population inversion to exist between the upper laser level and the lower laser level. Through stimulated emission (at 1064 nm), the ions can relax down to the lower laser level ($^4I_{11/2}$). The lower laser level again relaxes very fast to the ground state [7 Ch. 1].

The energy gaps between the pump level and the upper laser level, and the lower laser level and ground state, have the same order of magnitude as the phonon energy in the crystal lattice. The transitions between these energy states therefore relate to a phonon being emitted by the ion and transferred to the crystal lattice, which is a fast non-radiative process, producing heat in the host material. The lifetime of the pump level, and the lower laser level, is therefore much shorter than the lifetime of the upper laser level, ranging from 10^{-8} to 10^{-11} s for different materials [6 Ch. 2].

The population dynamics of a laser greatly depend on the lifetimes of the excited energy levels, as well as the cross sections and linewidths of the absorption and emission spectra. The real life situation can be more complicated than the simple four level laser in Figure 2-4 and may involve more energy levels [6 Ch. 2]. It is also possible to force laser action on lines other than the one with the strongest emission cross section, for example into the $^4I_{13/2}$ level producing ~1.3 μm laser radiation [14], or into some high lying stark sublevel of the $^4I_{9/2}$ ground state resulting in laser action between 900 and 950 nm, depending on the host material [13, 15]. Laser rate equations and population dynamics of solid-state lasers can be found in [7 Ch. 5].

Another important factor that influences the feasibility and efficiency of a laser, other than the laser material, is the pumping scheme that is employed. The energy source that is used, and the technique how the energy is coupled into the laser material, is greatly influenced by the choice of laser material, and vice versa. This important subject will be discussed in detail in the next chapters.

3 Pump sources for solid-state lasers

As stated, solid-state lasers need to be optically pumped to excite the active medium inside the laser crystal or glass. Various light sources have been used to optically pump solid-state, and in particular Nd lasers. Nonelectric sources such as the sun, chemical flashbulbs and radiation from detonations have been used for special and rare applications [6 Ch. 6]. Commonly used electric sources vary from flashlamps and arc lamps, which have been used extensively, to modern diode lasers that are still under development [4].

The choice of pump source greatly influences the overall efficiency from electrical input power to optical output power and the beam quality of the laser. It furthermore influences the flexibility of the laser design and it can determine the overall operating environment.

3.1 Flashlamps and arc lamps

Flashlamps and arc lamps usually consist of a quartz tube sealed at the ends by two electrodes. The tube is filled with a gas, for example xenon or krypton, such that when a high voltage is applied to the electrodes, an arc discharge can take place in the gas. The spectral distribution of the emitted light from the gas discharge consist both of line and continuum components, and depends in complex ways on electron and ion densities and temperatures of the discharge [6 Ch. 6].

The light emission from the gas discharge can be coupled into a laser medium to excite it to the pump energy level, as discussed in the previous section. However, the coupling efficiency into the medium is usually low, due to the spatial and spectral characteristics of gas discharges. The broad spectral output of flashlamps and arc lamps poorly overlaps with the absorption spectrum of solid-state laser materials. In addition, only a small portion of the omni-directional radiation from a lamp source can be coupled with high optical density into the laser medium [6 Ch. 6].

Nevertheless, the electrical-to-optical efficiency of arc discharges is high (~70 %), and tens of mega joules of pulsed energy and hundreds of kilowatts of power can be delivered by lamp sources. Therefore, the amount of power that is coupled into the

laser medium, although a small portion of the total pump power, can be significant. The highest power solid-state lasers remain to be krypton-filled arc lamp-pumped systems [6 Ch. 6].

The overall electrical-to-optical efficiency of high power lamp-pumped solid-state lasers is in the order of a few percent. Additional disadvantages of lamp-pumped systems include the limited lifetime of flashlamps and arc lamps, the elaborate power supplies necessary to drive high voltage discharges, and instabilities in the laser output due to the statistical nature of gas discharges [16].

3.2 Diode lasers

Already in 1963 a solid-state laser was pumped using a semiconductor source, i.e. a Nd:$CaWO_4$ laser pumped with a 880nm GaAs light emitting diode (LED) [17]. Since then the development of diode-pumped solid-state lasers has grown alongside the development of diode lasers [18].

Light is emitted from a semiconductor material when a pn junction is forward biased so that holes and electrons can recombine. The photon energy of the emitted light is determined by the energy gap between the conduction and valance bands of the pn junction. It therefore follows from the relation $E = h\nu$ that the wavelength of the photons emitted is $\lambda = \frac{hc}{E}$, and if λ is expressed in μm and the energy gap (E_g) is in electron volt [6 Ch. 6], then the wavelength of the light emitted by the semiconductor material is

$$\lambda = \frac{1.24}{E_g}.$$

Such a device can emit laser radiation with a narrow spectral bandwidth when operated with sufficient injection current to establish a population inversion, and when the cleaved facets of the material produce optical feedback [19]. The very basic schematic of a laser diode is shown in Figure 3-1 [20].

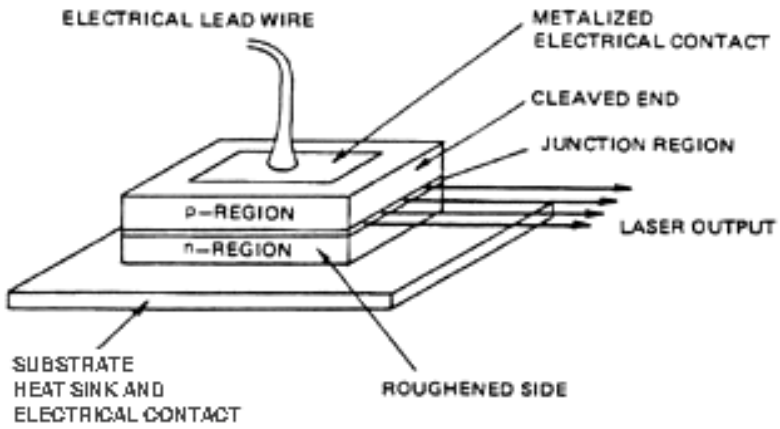

Figure 3-1: Basic construction of a laser diode [20].

There are ranges of wavelengths available from diode lasers, based on a large number of semiconductor materials. However, of main interest are the GaAs- and InP-based systems, which produce wavelengths in the 680 to 980 nm, and 1100 to 1650 nm regions, respectively [21].

InP-based laser diodes at 1300 nm and 1550 nm have been developed to deliver a few milliwatts of output power, which is sufficient for the optical fibre and telecommunications industries. In this wavelength region, only a few applications require more than 100 mW of output power, such as pump lasers for erbium-doped fibre amplifiers at 1480 nm [21].

Higher power laser diodes that are commercially available are based on GaAs-substrates, in the wavelength range from 780 to 980 nm. The biggest drive for higher power diode lasers is for direct industrial applications of diode lasers, and for pumping high power solid-state lasers, for example the Nd:YAG system at 808 nm.

These high power devices range from single stripe emitters, linear diode arrays containing tens of stripe emitters, linear bars that contain a few diode arrays, up to two-dimensional arrays, or stacks of diode bars. Output powers can be from a few milliwatts up to kilowatts in continuous wave operation. Even higher peak powers are available from these devices when they are operated in quasi-continuous wave mode [6 Ch. 6].

Various techniques have been developed to couple the radiation of diode lasers into solid-state laser media. The technique of coupling the radiation directly into the

medium without any intervening optics, which can make a laser system very compact, is especially suitable for microchip solid-state lasers. This technique has recently been implemented in a miniature green diode-pumped solid-state laser at the Laser Research Institute (LRI), University of Stellenbosch [22].

Other techniques to couple diode radiation into solid-state lasers include the use of standard optics [23], GRIN lenses [24], micro-optics [25], lens ducts [26] and optical fibres [27]. The technique of coupling a 1 W diode laser into an optical fibre by using a cylindrical micro lens is shown in Figure 3-2 [28] and Figure 3-3 [29].

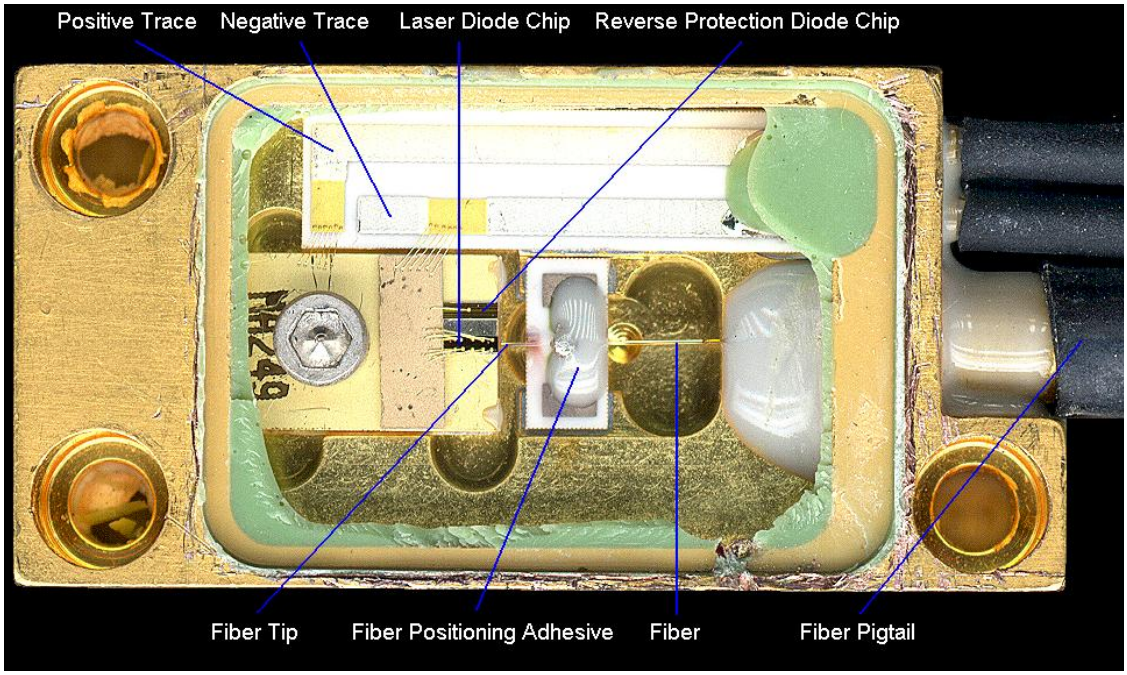

Figure 3-2: The interior construction of a typical 1 W fibre coupled diode laser, showing the method of coupling the diode radiation into an optical fibre [28].

The main advantage of using diode lasers to pump solid-state lasers, as compared to lamp-pumped systems, is the high coupling efficiency into the laser medium. Essentially all the optical power delivered by the laser diode can fall within the absorption band of the solid-state material. This improves the overall efficiency of the laser system, even if the electrical to optical efficiency of diode lasers is less than that of lamp sources, in the order of 25 to 50 %.

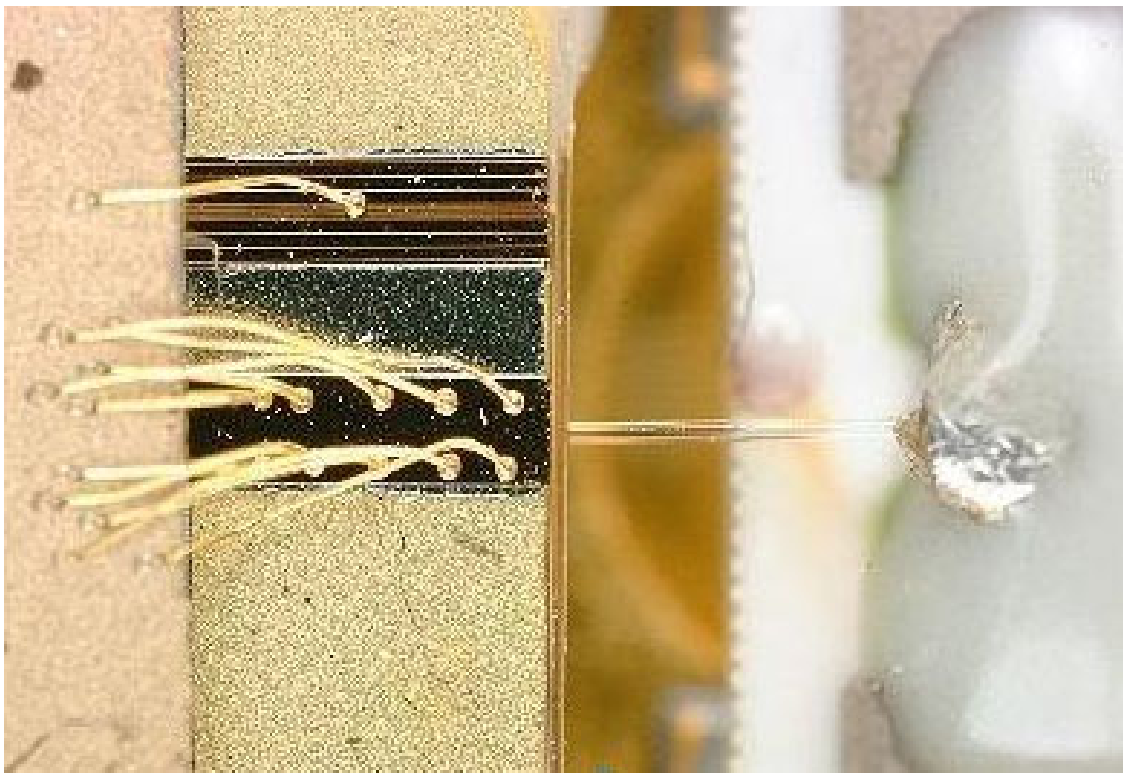

Figure 3-3: A close-up view of a 1 W laser diode focused into a fibre tip by a cylindrical micro lens [29].

Additional fundamental advantages of using diode lasers to pump solid-state lasers include the following [6 Ch. 6, 16, 18, 21]:

- the high brightness output of a diode laser allows the pump light to be focussed with high optical density, leading to high gain in the laser medium;
- the good spectral overlap between diode radiation and the absorption spectrum of a laser medium leads to a reduction in thermal load in the medium which can lead to better beam quality;
- the high coupling efficiency can lead to the development of lasers which are not feasible as lamp-pumped systems, such as three-level lasers and lasers operating on low gain transitions;
- laser diodes are quiet pump sources with good amplitude and spectral stability, leading to stable operation of solid-state lasers.

Favourable operating conditions of diode lasers, which have led to the wide-range implementation of diode-pumped solid-state lasers, are notably [6 Ch. 6, 16, 18, 21]:

- the separation of the pump source from the laser cavity due to delivery optics such as optical fibres, which allows compact and robust laser designs;

- the low voltage operation, which allows power supplies to be stable, compact and safe;
- the long lifetime of the laser diodes that enables “maintenance free” operation of laser systems.

The optical-to-optical efficiency of diode-pumped solid-state lasers is in the order of 30 to 50%, and even higher efficiencies have been demonstrated [30]. This efficiency is considered high since energy is converted from diode lasers, which has “poor” beam quality with a wide spectral output, into highly coherent laser beams with diffraction limited beam quality. The energy from continuous or quasi-continuous diode radiation can also be stored with high efficiency in a solid-state laser material, and can be released in high-energy laser pulses with high peak power [18].

The main disadvantage of diode-pumped solid-state lasers is the high cost of diode lasers. This, together with the unavailability of high power diode lasers with fair beam quality has hampered the development of diode-pumped solid-state lasers up to the middle 1990’s [18]. However, the cost of diode laser power has decreased from $ 600/W for a 10 W diode laser in 1987, to $ 100/W for a 40 W diode laser in 1996 [31]. Modern estimates of the future price for high power diode lasers are in the order of $ 15/W [32]. In addition to the lowering price, beam-shaping techniques have increased the brightness of diode lasers [33]. These beam-shaping techniques are increasingly used in commercial high power diodes, leading to the feasible development of high power diode-pumped solid-state lasers.

3.3 Summary

The advantages of diode lasers over flashlamps as pump sources for solid-state lasers are summarised in Table 3-1. A discussion on the well-established technology of lamp-pumped solid-state lasers can be found in [7].

	Flash lamp	**Laser diodes**
Lifetime	500 to 1 000 h	10 000 to 50 000 h
Supply voltage	2 to 5 kV	2 to 4 V
Power supply	Big	Compact
Modulation and control	Difficult	Easy
Spatial emission	Nearly isotropic	Focusable
Spectral emission	Broad	Narrow, tuneable
Efficiency P_{light}/P_{elec}	60 to 80 %	30 to 50 %
Transfer efficiency	4 to 8 %	~ 100 %
Laser efficiency P_{laser}/P_{elec}	0.5 to 2 %	5 to 15 %
Cooling	Easy	Sometimes complex

Table 3-1: Comparison between lamp-pumped and laser diode-pumped solid-state lasers [21].

Laser diodes are still under development and therefore diode-pumped solid-state lasers as well. The side-pumping and end-pumping configuration of diode-pumped solid-state lasers will be discussed in the next section.

4 Diode-pumped solid-state lasers

4.1 Diode side-pumping

Consider the cylindrical laser crystal rod shown in Figure 4-1, pumped from the side by diode laser radiation. The side-pump setup is usually such that the whole laser crystal is filled with diode radiation. The amount of active ions excited by the radiation (the excitation density), decays exponentially from the edge of the crystal. However, the diameter of the crystal is rarely longer than the absorption length of the pump light and therefore reflective pump cavities are necessary to reflect the pump light back into the laser crystal to improve the absorption efficiency of the system.

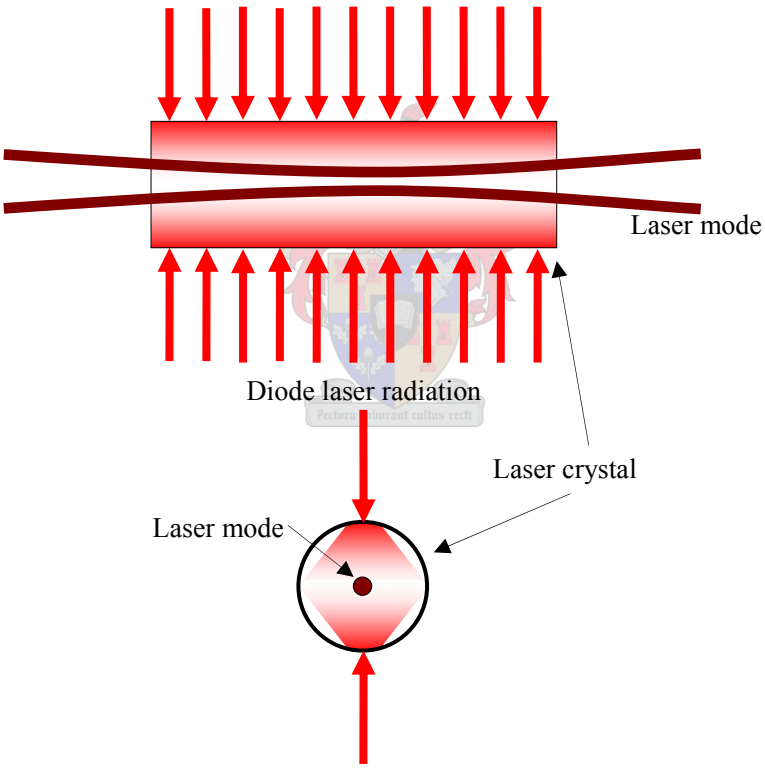

Figure 4-1: Diode-side-pumped solid-state laser rod with the resonator mode shown inside the crystal.

As stated, the whole crystal is excited and can act as gain medium for the laser. Nevertheless, the only energy that is extracted by the laser is the energy from the excited ions that spatially overlaps with the fundamental resonator mode. As seen in the figure, the laser mode does not fill the whole crystal and does not overlap with the region where the gain is the highest, i.e. at the edge of the crystal.

An additional concern of the side-pumping scheme is that higher order resonator modes have larger beam diameters than the fundamental TEM_{00} mode. These modes, overlapping better with the excited ions in the crystal, will have considerable gain and may oscillate in the laser. The additional higher order modes will impair the beam quality of the laser. Only with the addition of a hard aperture, which discriminates against the higher order modes but transmits the fundamental mode, will the laser be forced to oscillate on the fundamental laser mode alone and retain near diffraction limited beam quality. However, this technique will limit the energy that can be extracted from the gain medium and with this poor beam overlap efficiency, a large portion of the pump light is deposited as heat inside the crystal.

4.2 Diode end-pumping

Already in 1989, it was stated by T.Y. Fan [34]:

"The highest-efficiency diode-laser-pumped solid-state lasers with diffraction-limited output beams have been demonstrated in an end-pumped geometry."

If the laser rod is pumped longitudinally, collinear with the laser resonator mode, then it is referred to as end-pumping, as illustrated in Figure 4-2. This setup allows very good beam overlap efficiency because only the ions that spatially overlap with the resonator mode are excited by the pump radiation.

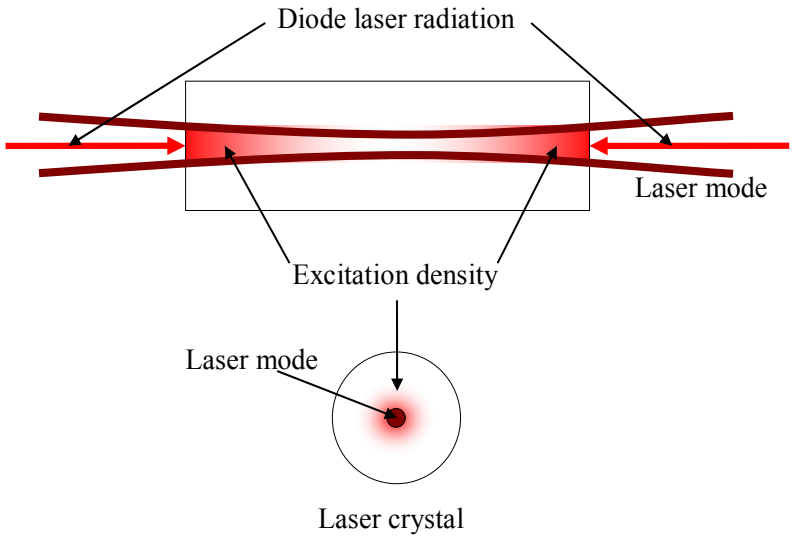

Figure 4-2: Diode-end-pumped solid-state laser rod with the excitation density shown inside the crystal.

High beam quality is ensured when only the fundamental laser mode has enough gain to oscillate. This is done by spatially overlapping the pump beam and the resonator mode. If this mode-matching is done successfully, the higher order modes are discriminated against by the soft aperture created by the limited gain in the outer parts of the crystal.

Good absorption efficiency is achieved since the laser crystal is usually chosen to be significantly longer than the absorption length of the pump radiation. The absorption length is the inverse of the absorption coefficient α, which is defined in Section 7.2. It is determined by the doping concentration of the active ions in the crystal, and the spectral overlap between the diode radiation and the crystal absorption spectra.

The practical advantage of end-pumping is that it usually enables flexible laser design since no additional pump cavities are necessary to reflect the pump light back into the laser crystal. This tends to lead to more compact designs since no provision needs to be made for coupling optics along the edge of the crystal. Rather, the design can be optimised for good heat extraction from the laser rod with either direct conductive or convective cooling. Discussions on diode-end-pumping can be found in [6, 18 and 35]

4.3 Summary

It can be concluded that the combination of the favourable properties of diode lasers and the advantages of the end-pump geometry result in the high efficiency and good beam quality of diode-end-pumped solid-state lasers. These advantages sparked the development of a large number of different designs for diode-end-pumped solid-state lasers [35].

However, these advantages are overshadowed by the onset of thermal distortions with the power scaling of these lasers above a few watts of output power. Although this geometry ensures overall less heat generation due to the good beam overlap efficiency, it does result in localised heating in the centre of the laser rod. With intense pumping, the localised heating causes highly distorted thermal lensing which impairs the beam quality [36, 37].

The problem of localised heating, and therefore considerable thermal lensing, is less in side-pumped systems. However, a balance between efficiency and thermal distortions

can be found if the thermal effects in solid-state lasers are understood and are incorporated in a laser design. The thermal effects in solid-state lasers will be discussed in the next section.

5 Thermal effects in solid-state lasers

One of the main design criteria for high power solid-state lasers is the management of thermal effects [38, 39]. Heat generation in the solid-state laser material has been the main obstacle in maintaining the good properties of low-power diode-end-pumped solid-state lasers while power scaling these lasers [35].

5.1 Heat generation in solid-state lasers

The energy that is pumped and absorbed in the laser medium which is not released as emission is deposited as heat in the medium. This heat is the consequence of [6 Ch. 7]

- the quantum defect between the pump wavelength and the emission wavelength;
- absorption of pump light to energy levels other than the pump level;
- non-radiative decay and fluorescence;
- upconversion processes such as excited state absorption (ESA) and energy transfer upconversion (ETU);

5.1.1 Quantum defect

The energy difference between the pump photon energy and the laser photon energy of an optically pumped laser is known as the quantum defect. This energy, which is absorbed in the laser medium through multi-phonon relaxations, is the minimum amount of heat generated in the laser [40]. For a three- or four-level laser the quantum defect, which can be expressed as the quantum efficiency, poses the fundamental upper limit for the efficiency of a laser. The quantum efficiency of such a laser can be expressed as

$$\text{Quantum eff.} = \frac{E_{\text{laser}\,\lambda}}{E_{\text{pump}\,\lambda}} = \frac{h\nu_{\text{laser}}}{h\nu_{\text{pump}}} = \frac{\lambda_{\text{pump}}}{\lambda_{\text{laser}}}.$$

Further discussions are limited to Nd^{3+} doped solid-state lasers, although the principles apply to most solid-state lasers.

In an "ideal" Nd^{3+} solid-state laser

- which is in continuous wave operation;
- where only the lowest $^4F_{5/2}$ pump level is populated by the pump source;
- which extracts all the energy from the upper laser level through stimulated emission;
- which has no additional absorption due to impurities;

the heat caused by the quantum defect would constitute all the heat generated in the medium [6 Ch. 7, 40]. The heat generated due to the quantum defect in a Nd:YAG laser is shown in Figure 5-1.

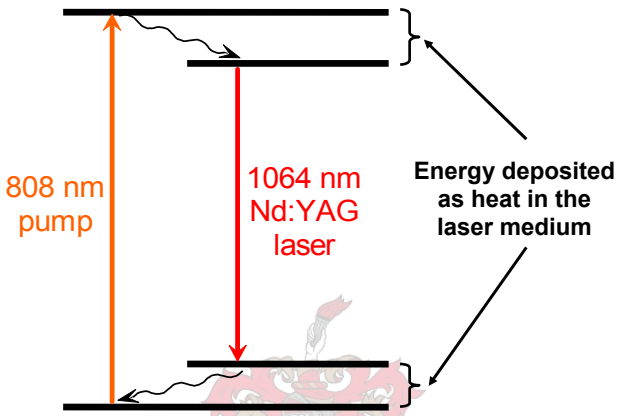

Figure 5-1: The energy level diagram of a Nd:YAG laser showing the heat deposited due to the quantum defect.

5.1.2 Absorption into other levels

Unfortunately, Nd^{3+} lasers have more effects contributing to the heat generated in the host material than just due to the quantum defect. This is especially true for lasers pumped by arc lamps or flashlamps which, in general, have a wide pump spectrum extending from the infrared into the ultraviolet [6 Ch. 6]. The Nd^{3+} ions absorb the pump radiation according to its absorption spectrum. Thus, a range of energy levels is populated, other than just the desired $^4F_{5/2}$ pump band. Even though the high lying populated energy levels relax very fast to the upper laser level $^4F_{3/2}$, the quantum defect is much higher than in the ideal case [6 Ch. 7]. Any populated energy level below the upper laser level decays to the ground state via multiphonon relaxation. This causes additional heat generation in the laser medium.

The spectral output of lamps can be filtered to match the ground state absorption to the $^4F_{5/2}$ level of the Nd^{3+} ion. This would reduce the quantum defect and additional heat generation inside the laser medium, although the system efficiency would remain low.

Diode-pumped Nd^{3+} lasers have an advantage over lamp-pumped lasers since the emission spectra of diode lasers are narrow and can range from sub-nanometre linewidths to a few nanometres. These narrow lines can be selected to have good spectral overlap with the $^4F_{5/2}$ pump level of the Nd^{3+} ions [6 Ch. 7]. If this is the case and if multi-photon absorption processes (i.e. ESA) [41] and energy-transfer upconversion [40] are not considered, only the $^4F_{5/2}$ level is populated, which decays to the upper laser level through multiphonon relaxation. Thus, the quantum defect can be minimized in a diode-pumped laser system due to the good spectral overlap.

5.1.3 Non-radiative decay and fluorescence

The other contribution to heat generated in the medium is the small amount from non-radiative decay and fluorescence from the ions that do not relax via stimulated emission. This contribution becomes very small if the laser has good beam overlap efficiency. A good spatial overlap between the excited ions and the laser beam would ensure that most of the energy is extracted via stimulated emission. If this is not the case, or if the laser medium is pumped but not lasing, the upper laser level decays spontaneously via fluorescence and multiphonon relaxation to the ground state. The amount of additional heat deposited in the medium depends on the branching ratio from the $^4F_{3/2}$ laser level, which determines the percentage of fluorescence and multiphonon relaxations [40].

Diode-end-pumped solid-state lasers have better spatial overlap of the pumped ions and the laser beam than side-pumped solid-state lasers. It is therefore not surprising that these lasers have the lowest amount of total heat deposited in the laser medium.

For example, a Nd:YLF laser end-pumped by a 797 nm diode laser, which lases on the 1047 nm line, has a quantum defect energy of ~3050 cm^{-1} which is deposited as heat in the crystal. With no other processes contributing significantly to heat generation, only ~24% of the absorbed pump power is converted to heat, independent of the pump power level [40].

5.1.4 Energy transfer upconversion

The phenomena of energy transfer upconversion and its effect on the performance of Nd:YAG [40], Nd:YLF [41], Nd:GLF [42], Nd:$KLiYF_5$ [43] and Nd:Glass [44] lasers has been investigated extensively [35, 45]. ETU in Nd:YLF is of particular interest and will be discussed further.

Energy transfer upconversion is a non-radiative process and can be described [41] as

"...a process in which two nearby excited ions interacts with each other, making one ion jump to a lower state and the other to be excited to a higher state using the energy released by the first ion."

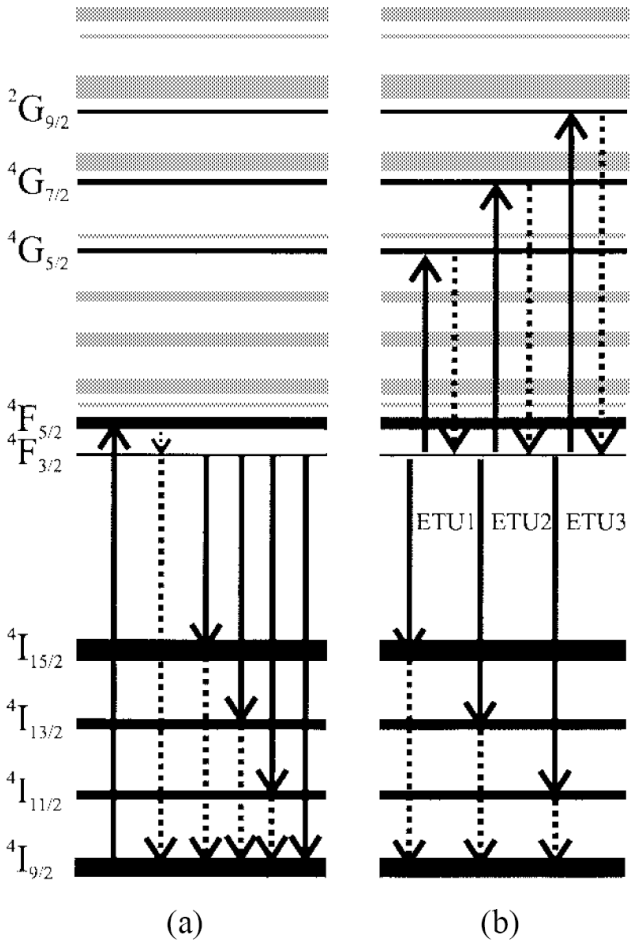

Figure 5-2: Energy level scheme of Nd:YLF without (a) and with (b) energy transfer upconversion. All transitions indicated by dashed lines contribute to heat generation in the crystal [47].

For this process to be significant there must be a direct or indirect (phonon-assisted) spectral overlap between emission and absorption from an energy level with a long

lifetime, i.e. the upper laser level. This is the case when the energy difference between the upper laser level and the lower laser levels is the same as (or close to) the energy difference between the upper laser level and higher lying levels [46]. The prominence of ETU therefore depends on the energy level structure of the specific laser crystal.

The three dominating upconversion transitions in Nd:YLF are shown in Figure 5-2(b), where one excited ion in the $^4F_{3/2}$ upper laser level relaxes down to a lower lying level, either $^4I_{15/2}$, $^4I_{13/2}$ or $^4I_{11/2}$. This ion transfers its energy to a neighbouring excited ion in the $^4F_{3/2}$ level which is upconverted to a higher level, either $^4G_{5/2}$, $^4G_{7/2}$ or $^4G_{9/2}$ respectively. The effect of the three processes on the population dynamics of the system is similar and can be summed in a single upconversion rate [47].

The upconversion rate has a quadratic dependence on the excitation density inside the crystal [46], which in turn depends on the pump intensity, absorption efficiency and the doping concentration of the crystal. In addition, the excitation density depends on the conditions under which energy is extracted from the crystal [40].

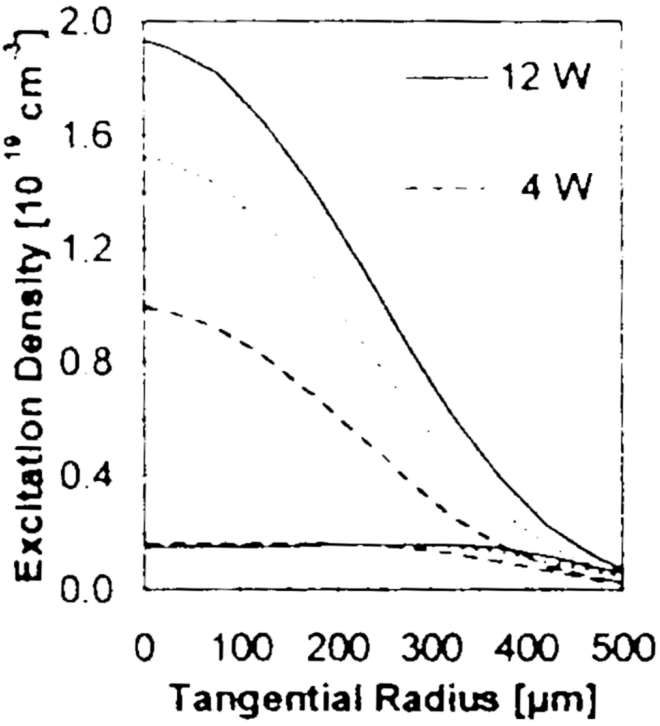

Figure 5-3: Calculated excitation density within the front 5% of a Nd:YLF crystal, versus the tangential radius (from the centre of the pumped region) for different pump powers under lasing (bottom curves) and nonlasing (top curves) conditions [40].

Figure 5-3 shows the calculated excitation density of a Nd:YLF crystal end-pumped with a Gaussian pump beam, for pump powers of 4 and 12 W. The strongest excitation

is found in the centre of the pump beam (tangential radius = 0). Under lasing conditions, the upper laser level is depleted by stimulated emission. In the region where the laser mode and the pump beam overlap, the excitation density is clamped to the laser threshold, as seen in the bottom curves of the figure.

Under nonlasing conditions such as in the "off time" of a *Q*-switched laser at low repetition rate or in an amplifier, the upper laser level is depleted by fluorescence, multiphonon relaxations and upconversion. The excitation density is an order of magnitude higher under nonlasing conditions than under lasing conditions, as seen in the top curves of Figure 5-3.

Since the upconversion rate has a quadratic dependence of the excitation density, the upconversion rate is two orders of magnitude larger under nonlasing conditions, compared to lasing conditions where inter-ionic upconversion has a marginal influence [40]. The relative upconversion rates for Nd:YLF under lasing and nonlasing conditions are shown in Figure 5-4. In this example the increase in upconversion rate under lasing conditions in the wings of the pumped region is due to lower beam overlap efficiency since the laser beam is smaller than the pump beam.

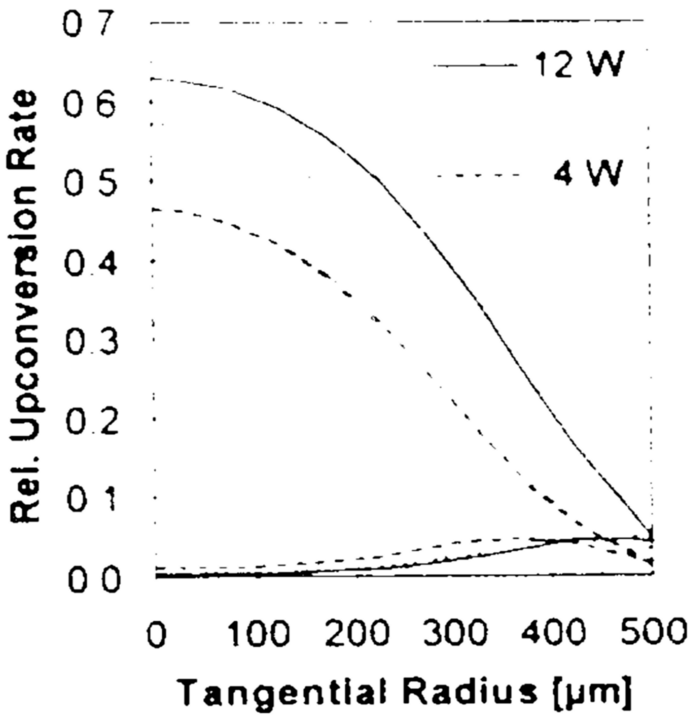

Figure 5-4: Calculated upconversion rates relative to the pump rate within the front 5% of a Nd:YLF crystal, versus the tangential radius for different pump powers under lasing (bottom curves) and nonlasing (top curves) conditions [40].

The effect of energy transfer upconversion, which is only significant under nonlasing conditions, is that it generates additional heat inside the crystal as indicated by the dashed lines in Figure 5-2. The heat generated in one such process in which two excited ions are involved, is equivalent to the energy difference between the upper laser level and the ground state of the ions. Since the upconversion rate has a nonlinear dependence on pump power, the heat generation increases nonlinearly with pump power under nonlasing conditions.

For example, 52% of the pump power is converted to heat in a Nd:YLF laser which absorbs 9.5 W pump power under nonlasing conditions. If upconversion is not considered, only 25% of this pump power is converted to heat through the processes of fluorescence and multiphonon decay [40].

An additional effect of upconversion is that it depopulates the upper laser level without contributing to the stimulated emission, and therefore reduces the efficiency of the laser and shortens the lifetime of the upper laser level. The full population dynamics of Nd:YLF under lasing and nonlasing conditions is modelled and discussed by Pollnau *et al* in [40] and should be considered when designing high energy *Q*-switched lasers or amplifiers.

5.2 Effects of heat generation in solid-state lasers

The principles of heat generation in Nd^{3+} solid-state lasers as discussed in the previous section are general. However, the effect thereof on the operation of the laser depends on the choice of laser parameters such as the laser medium, pumping configuration and cooling geometry. These parameters determine the temperature profile inside the medium, the thermal lens and the stress induced birefringence. The discussion of the thermal effects will be limited to edge-cooled, end-pumped Nd lasers. The catastrophic effect of thermal fracture will also be discussed.

5.2.1 Temperature profile of an end-pumped edge-cooled laser rod

The heat generated inside the laser medium due to the pumping process needs to be extracted by cooling the laser crystal. The simplicity and compactness of an end-pumped laser rod that is cooled along the edge of the rod is very attractive, and is used in many systems [35]. In this configuration, the laser rod is usually in good thermal contact with a water-cooled copper block.

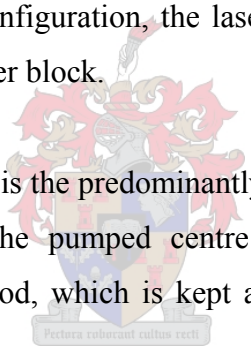

The effect of this setup however, is the predominantly radial heat flow due to the large temperature gradient between the pumped centre of the rod where the heat is generated, and the edge of the rod, which is kept at the temperature of the cooling block [35].

The exact temperature distribution inside the laser rod depends on the laser material; the pump absorption efficiency; the ratio between the pump beam size, laser mode size and the crystal size; the temperature of the cooling block; and the heat transfer coefficient between the laser rod and the cooling block.

Figure 5-5 shows the calculated temperature profile of an end-pumped Nd:YAG laser rod (r = 1.5 mm and l = 5 mm) which was mounted in a water cooled copper block at 290 K, pumped by a 3.3 W Gaussian beam with pump radius 125 μm. The authors assumed that 30 percent of the pump power was deposited as heat. The temperature increase (in K) from the edge of the laser rod is indicated by isobars, i.e. a solid line representing a constant temperature along the line [48].

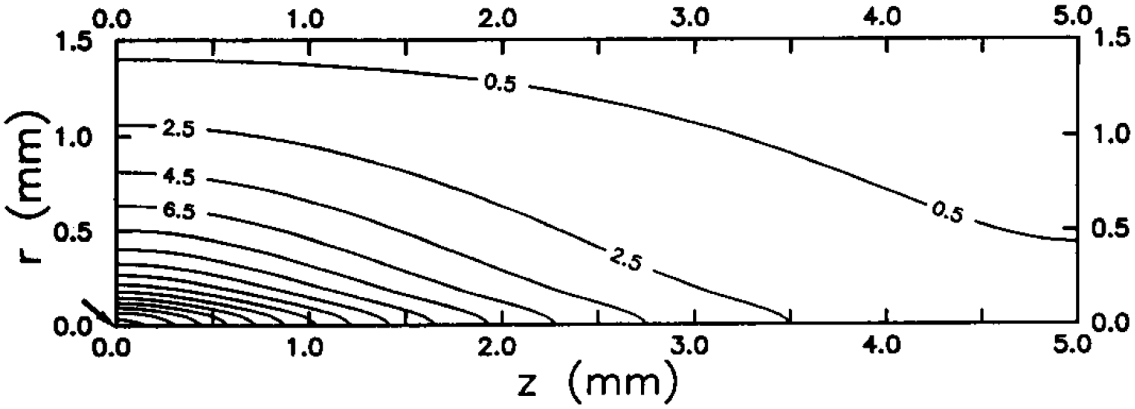

Figure 5-5: Radial and longitudinal temperature distribution in one half of an axial cross section of an end-pumped Nd:YAG rod [48].

It is evident from this example that the largest temperature increase is found at the crystal front surface in the centre of the pump beam where the strongest absorption occurs. Under nonlasing conditions, the temperature gradient is much more pronounced due to the additional heat generated in the medium [40], as discussed in the previous section.

The consequence of this temperature profile, is that

- there is a change of refractive index which follows the change in temperature;
- the crystal expands according to the temperature dependent expansion coefficient;
- the nonuniform expansion leads to stress in the crystal, which also cause a change in refractive index.

The change in the refractive index n_0 can therefore be expressed as

$$n(r,\phi,z) = n_0 + \Delta n_{temp}(r,\phi,z) + \Delta n_{stress}(r,\phi,z)\,,$$

with Δn_{temp} and Δn_{stress} the variation of the refraction index caused by temperature and stress respectively [38].

5.2.2 Thermal lens

The change in refractive index Δn_{temp} of the laser crystal causes a difference in longitudinal optical path length through the rod across the transverse temperature profile. This effectively forms a lens with the power of the same sign as the change in refractive index with temperature [40].

The thermal lens f_{th}, which is caused by the temperature dependence of the refractive index (dn/dT), can be approximated by

$$f_{th}(r) = \frac{2\pi K_c r^2}{P_p \gamma \eta_{abs} \left(\mathrm{d}n/\mathrm{d}T\right) s(r)}.$$

This approximation shows that the thermal lens depends on the thermal conductivity K_c of the crystal, the incident pump power P_p, and the fraction of pump power absorbed in the laser medium η_{abs}. γ is the fraction of absorbed pump power dissipated as heat, and $s(r)$ is the fraction of pump power contained in a disk of radius r. The derivation of this formula is shown in [35].

A more sophisticated model is developed by Pollnau *et al*. [40]. In this model the temperature dependence of (dn/dT) and the temperature dependence of the thermal conductivity are included. The change in dn/dT for a change in temperature is nearly linear for Nd:YAG around room temperature; and the thermal conductivity is inversely proportional to the temperature.

The expansion of the laser crystal (dL/dT), and the temperature dependence of this parameter is also considered in the above mentioned model. The expansion causes bulging of the end-faces of the laser rod, which causes an additional thermal lens with the same sign as the expansion of the crystal along the optical axis. End-face bulging can play an important role in the design of a high power end-pumped solid-state laser since it is influenced by the amount of heat generated close to the end-faces of the laser crystal. A uniform absorption of the pump power along the length of the crystal, and a large pump volume influence the magnitude of end-face bulging [49].

The model shows an almost linear increase in thermal lens power for increased pump power under lasing conditions. Under non-lasing conditions the thermal lens increases nonlinearly with increased pump power. This is attributed to the additional heat generated by energy transfer upconversion and the unfavourable temperature dependence of the thermal conductivity and other crystal parameters. The thermal lens of an end-pumped solid-state laser that is non-uniform will induce large aberrations, as shown in Figure 5-6(b).

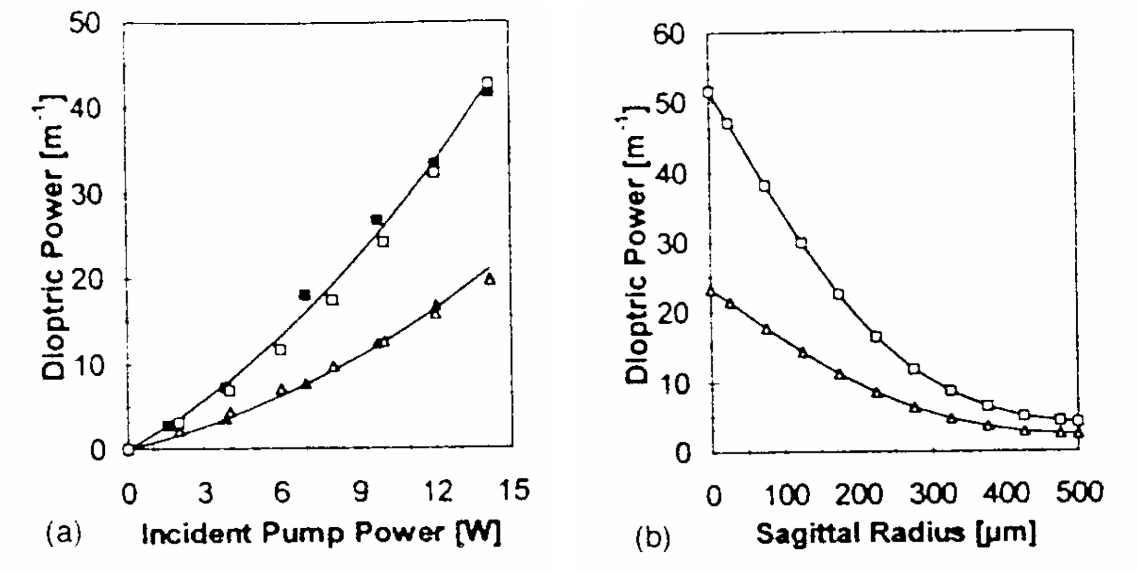

Figure 5-6: The calculated dioptric power (a) of the thermal lens of an end-pumped Nd:YAG laser versus the pump power; and the radial dependence (b) of the thermal lens at full pump power, under lasing (Δ) and nonlasing (□) conditions. The solid symbols indicate experimental data [40].

This aberrated lens has an adverse effect on the wavefront of the fundamental laser mode [50], and therefore it decreases the beam quality of a laser. In addition, degradation in beam quality usually causes an increase in resonator loss. Many schemes to compensate for a thermal lens have been developed, but it usually results in highly complicated resonator designs [51]. An alternative approach is to reduce the thermal lens in the crystal by careful choice of laser medium, pump scheme and resonator design [35, 40].

5.2.3 Stress-induced aberrations

As stated, the non-uniform temperature profile leads to non-uniform expansion, which causes stress in the laser crystal. The calculated stress in the Nd:YAG crystal of the previous example (Figure 5-5) is shown in the following figure.

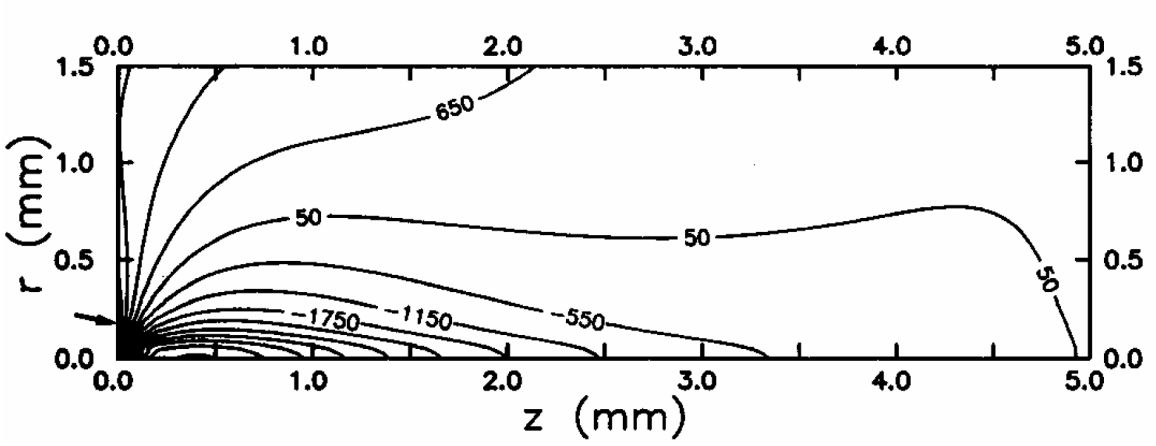

Figure 5-7: Radial and longitudinal hoop stress (in psi) in one half of an axial cross section of an end-pumped Nd:YAG rod [48].

Because the temperature in the centre of the rod is always larger than at the edge, the centre region of the rod is in compression (negative hoop stress values) while the outer regions and the rod edge are in tension (positive hoop stress values) [39].

The stress in the crystal leads to changes in the refractive index Δn_{stress} due to the photo-elastic effect and introduces an additional stress-induced thermal lens. The amount of refractive index change is determined by the elasto-optical properties of the specific laser medium, which can be different for the radial and tangential directions in the laser rod. This change in refractive index in the two directions is the cause of stress-induced birefringence [38].

The stress induced thermal lens power is small compared to the contribution from temperature, and is of minor importance for crystals which have a strong natural birefringence, such as Nd:YLF [40]. However, in non-birefringent laser materials such as Nd:YAG, stress-induced birefringence can cause degradation in laser beam quality due to bifocusing and depolarization loss [35].

Bifocusing occurs because the induced change in refractive index for radiation polarized parallel to a local strain component will be different from the change in refractive index for radiation polarized perpendicular to that local strain component in

the crystal. Therefore, the stress induced thermal lens shows different focal lengths for tangential and radial polarization [54]. This effect, if not compensated for, causes astigmatism. It gives rise to elliptically distorted beam profiles both inside and outside the resonator, thereby reducing the maximum extractable TEM_{00} power from the rod [52].

The other effect of stress-induced birefringence, depolarization, can cause a significant loss when attempting to select a linearly polarized output beam in a thermally stress-induced birefringent laser rod. A polarized laser beam travelling through such a rod will undergo a partial change in polarization due to the birefringence, and will therefore experience a loss at the polarizer [38].

There are a number of well-established techniques to reduce the effects of stress induced birefringence, but they add a significant extra complexity to the laser cavity design and can lead to reduced overall efficiency. [35]

5.2.4 Thermal fracture

Considerable effort should be made to reduce the losses in a laser resonator. Additional losses introduced by the effects of thermal lenses and stress induced birefringence can lead to undesirable results. In solid-state lasers where the pump light is focussed to high power densities or if the laser crystal is poorly cooled, the heat load can exceed the material strength and thermal fracture can occur.

There could also be a critical point in a laser configuration where an increase in resonator loss can cause a runaway temperature increase in the system. The higher loss increases the energy upconversion rate, which increases the heat load in the crystal. This in turn causes the temperature to increase, leading to a decrease in the thermal conductivity. The temperature therefore increases even further, causing a stronger thermal lens that would introduce more losses in the system. Ultimately, this would lead to thermal fracture of the laser rod.

Typically, the rod barrels that are under tension, as seen in Figure 5-7, are the weakest in terms of material strength due to the presence of scratches, pits or voids. In addition, crystalline and glassy optical materials are usually weaker in tension than in compression.

Even though the compression stresses in the centre of the rod are much larger, the maximum tensile stress component (in tension) lies on the rod surface, and is typically where catastrophic thermally induced failure of the rod occurs if the tensile stress exceeds the fracture strength. The fracture strength of a crystal depends on the condition of the crystal and on the medium's thermal shock resistance parameter [53]. The fracture strength ultimately determines the amount of heat and inversion power that can be tolerated before rapture [39].

Catastrophic damage can also occur if the melting point of the material is reached by the heat generated in the medium. Nd:Glass, with a low melting point and thermal conductivity is particularly susceptible for this effect.

5.2.5 Management of thermal effects

In summary, it can be stated that uncompensated steady-state or transient thermal lensing degrades beam quality. In addition, stress induced birefringence can cause depolarization loss with a reduction in laser efficiency. If the cooling of the laser crystal is non-uniform, it can lead to the formation of hotspots and beam wander. Without proper thermal management, the laser system will therefore be unreliable [54].

Part 2 - Design and development of a high power diode-pumped Nd:YLF laser

6 Design criteria

The aim was to develop a diode-end-pumped solid-state laser with output power in the tens of watt range. This was to be done while maintaining the desirable properties which are associated with low-power diode-end-pumped solid-state lasers, such as high efficiency and near diffraction limited beam quality [34].

The goal therefore was to demonstrate an end-pumped solid-state laser with the following properties:

- high average output power;
- diffraction limited beam quality;
- continuous wave and pulsed output;
- large dynamic range;
- high efficiency;
- compact and robust;

The power scaling of diode-end-pumped solid-state lasers is hindered by two problems, the first of which is the lack of high power diode lasers with beam parameters that are good enough for end-pumping [5]. High power diode lasers which are suitable as pump sources for high power end-pumped solid-state laser development have only recently become commercially available and are still being developed [55].

The second and main problem in power scaling high beam quality end-pumped solid-state lasers is the onset of thermal effects under intense pumping. These include thermal lensing and thermal stress-induced birefringence, which impairs the beam quality of the solid-state laser.

To be able to meet the gaols set out, the laser was designed to minimize the detrimental effects of thermal lensing and stress-induced birefringence, thereby maintaining near diffraction limited beam quality and overall high laser efficiency.

The laser design was split up into three parts: the choice of laser medium; the pump source and its setup; and the design of the laser resonator. It is important to note that although these parts are presented separately, the design of each influences the other greatly.

7 The laser medium

To minimize the effects of thermal lensing and stress-induced birefringence, Nd:YLF was used as laser material because of its good thermo-optical properties [5].

Nd:YLF is a uniaxial, birefringent crystal with two main lasing lines in the 1 μm wavelength region, namely 1047 nm and 1053 nm, on both the π- and σ-polarizations. The 1047 nm line on the π-polarization (E||c-axis) has 1.5 times higher gain than the 1053 nm line on the σ-polarization (E⊥c-axis).

An a-cut Nd:YLF crystal allows the polarization (E-field) of linearly polarized light to be either perpendicular or parallel to the c-axis. Therefore, such a crystal needs a resonator with some polarizing components or mechanisms to force the laser to operate on the weaker 1053 nm σ-polarized line [24].

The advantage of a Nd:YLF laser operating on the 1053 nm line is the overall weak thermal lens which is associated with the σ-polarization under lasing conditions. This is due to the combined effect of a negative change in refractive index with temperature (dn/dT) and a positive contribution to the thermal lens from the bulging of the end-faces of the laser rod. The balance between these two contributions lead to a very small thermal lens, either slightly positive or slightly negative.

The dn/dT on the π-polarization is stronger negative and dominates the thermal lens behaviour, resulting in a large negative thermal lens under intense pump power [47]. The thermal lens behaviour of an end-pumped, 1 % doped Nd:YLF crystal is shown in Figure 7-1 under lasing and non-lasing conditions.

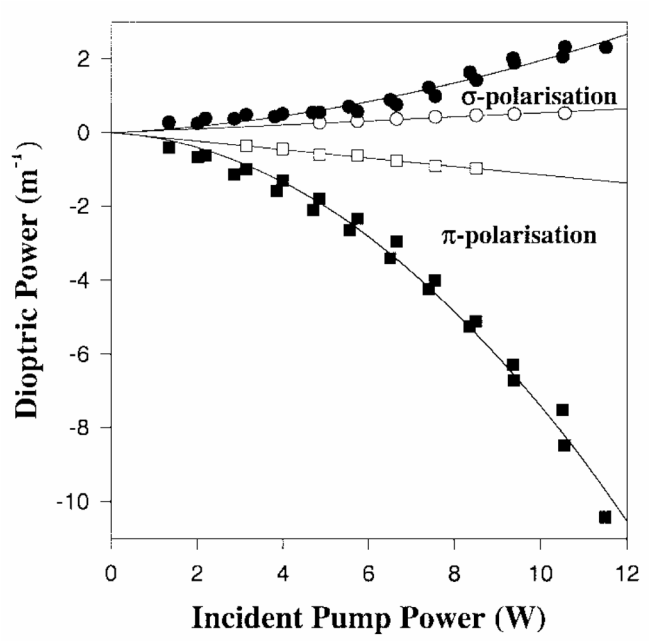

Figure 7-1: Measurements from [47] of the thermal lens power in the plane parallel with the c-axis, under lasing (open symbols) and nonlasing (closed symbols) conditions for both polarizations of a Nd:YLF laser.

The thermal stress-induced birefringence which is a significant problem for non-birefringent crystals, is negligible as compared to the natural birefringence of Nd:YLF [48]. Therefore, no additional components are needed in the resonator to compensate for this effect.

The disadvantage of Nd:YLF is that it has a very low thermal shock resistance parameter. The fracture limit of Nd:YLF is ~5 times smaller than Nd:YAG [5]. Since the laser should operate in pulsed mode (*Q*-switched), additional heat generation will be present due to energy transfer upconversion. Therefore precaution should be taken in the laser design to avoid thermal fracture of the Nd:YLF crystal [39].

7.1 Long crystals with low Nd doping concentration

The risk of thermally induced fracture was significantly reduced by using Nd:YLF crystals with low Nd^{3+} doping concentration. Crystals with 0.5% and 0.7% (at.) Nd^{3+} was used instead of the typical ~1% concentration [56] in the design of the high-power diode-end-pumped Nd:YLF laser.

It has been shown by Hardman *et al* [47] that a low doping concentration would minimize the overall heat generated in the crystal without compromising the laser

efficiency. It was stated that with a lower doping concentration, the excitation density is lower and the energy upconversion factor decreases. This would lead to a smaller influence of energy upconversion and the associated heat generation [40]. Crystals with Nd^{3+} doping concentration of 0.5% (at.) have successfully been used in a high power single frequency ring laser pumped with 25 W [57]; and in the amplifier stage of a high power Nd:YLF master oscillator power amplifier (MOPA) system [58].

A Nd:YLF crystal with low doping concentration needs to be long to have significant absorption of the pump radiation. This is a further advantage since the heat generated in the crystal is spread along the length of the crystal, which is fairly easy to cool if the crystal geometry is a cylindrical rod.

An additional measure to decrease the excitation density in the crystal was implemented by using a large pump beam diameter in the crystal [40]. This required a crystal with radius much larger (~3 times) than the pump beam radius to limit diffraction losses due to the hard aperture of the crystal edges [6 Ch. 5].

7.2 Absorption wavelength

A further measure to reduce the excitation density, and therefore the heat generated by energy upconversion, is by using a pump wavelength for which the laser medium has a low absorption coefficient [47]. The absorption coefficient α [cm^{-1}], which is wavelength dependant, is defined in

$$I(z) = I_0 e^{-z\alpha},$$

where *I(z)* is the intensity of pump light inside the medium (along *z*), and I_0 is the initial pump light intensity. The absorption spectrum of Nd:YLF as published by NASA is shown in Figure 7-2 [59].

It was shown in the literature that by detuning the pump wavelength from the absorption peak of Nd:YLF at 797nm, the heat generated due to energy upconversion was reduced and thermal fracture of the crystal was avoided, even with intense diode pumping under non-lasing conditions [40].

The risk for thermal fracture of the Nd:YLF crystal was reduced by using a pump wavelength of 805 nm, which has a low absorption cross section as compared to the

absorption peak of Nd:YLF at 793 nm or 797 nm. At this wavelength the absorption coefficient on the π-polarization for 1% (at.) doped Nd:YLF is only ~27 % of that at 797 nm.

Furthermore, the absorption coefficient has similar values for both the π-polarization and σ-polarization at 805 nm. This implies that the crystal can be uniformly pumped at this wavelength with an un-polarized pump source such as a fibre coupled laser diode. At any other absorption peak, the absorption from an un-polarized pump would be non-uniform for the two polarizations, which would lead to non-uniform heat generation and increased thermal distortions [60].

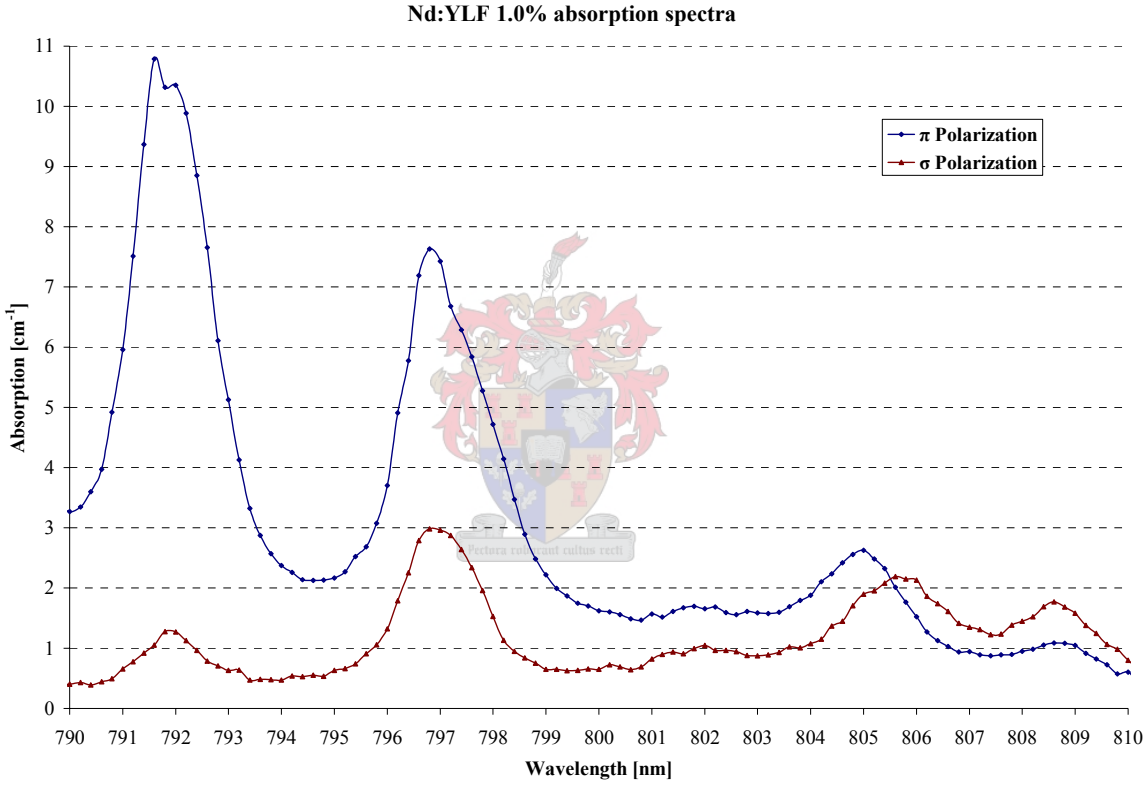

Figure 7-2: Absorption spectra of 1% (at.) doped Nd:YLF between 790 and 810 nm published by NASA [59].

An additional advantage of tuning the pump wavelength to the wide 805 nm absorption peak, instead of detuning from the steep 793 nm or 797 nm peak as in [47], is that the absorption in the wings of the pump radiation is low. It was shown that even by detuning the centre of the pump wavelength from the high absorption peak to get an overall low absorption coefficient, that a portion of the power in the wing of the pump radiation can still be absorbed at the absorption peak [60]. This method was sensitive to small changes in diode temperature (pump wavelength) which lead to non-uniform

absorption along the length of the crystal. In addition, it lead to a significant increase in excitation densities at the front surface of the laser crystal. This could lead to a significant increase in heat generation due to energy transfer upconversion and as a result, an increase in risk of thermal fracture of the laser crystal [40].

It has been shown that high efficiencies are possible even when end-pumping at wavelengths at which the absorption coefficient of Nd:YLF is low [61, 62], but it increases the requirement of the crystal to be long in order to absorb all of the pump power.

7.3 Cooling of the laser medium

A cylindrical rod geometry was chosen for the Nd:YLF laser crystals because diode-end-pumping permits efficient conductive cooling of edge-cooled laser rods. A cylindrical geometry allows uniform cooling along the edge of the rod, in contrast to a square rod clamped in a heat sink, which allows good thermal contact only on two crystal faces.

The design for the cooling of the high power Nd:YLF laser ensured uniform radial heat extraction from the pumped centre of the laser crystal. Each laser crystal was mounted in a cylindrical copper rod. The inner diameter of the copper cylinder was reamed to the diameter of the crystal to allow a smooth fit of the crystal inside the rod.

The copper cylinder with the mounted crystal, was placed in a water cooled copper heat sink inside the laser cavity, as shown in Figure 7-4. This cooling configuration was very compact and robust. The design also facilitated easy exchangeability of the mounted crystals, with little or no realignment necessary when the copper rods were exchanged or replaced after cleaning of the crystal faces. Furthermore, it allowed easy rotation of the crystal, as it was necessary to align the crystal c-axis parallel to the resonator plane while it was lasing.

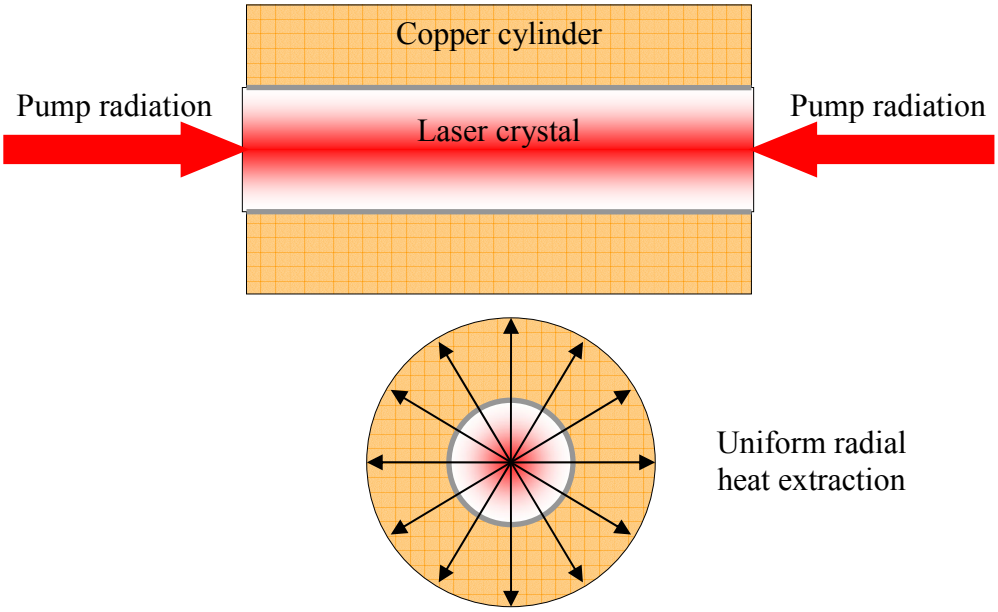

Figure 7-3: Side and axial view of the uniform radial heat extraction from an end-pumped Nd:YLF laser rod mounted in a cylindrical copper rod.

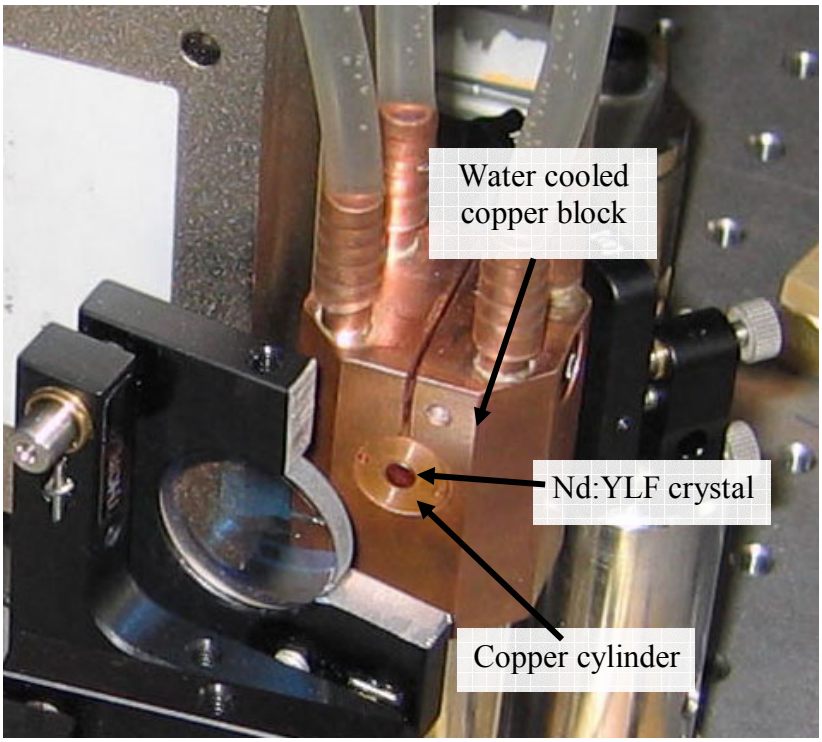

Figure 7-4: The laser rod was mounted in a water cooled copper block to ensure uniform cooling.

7.4 Choice of crystals

The choice of crystals was determined by the above mentioned design parameters. The need was for long crystals with low doping concentration and with cylindrical rod geometry with a diameter significantly larger than the pump beam diameter.

The range of available crystals was supplied by VLOC [63] and was anti-reflection (AR) coated for the pump wavelength at 805 nm and the laser wavelength around 1.05 μm. The results obtained in Section 11 was for Nd:YLF crystals with 4.0 mm ∅ and 30 mm long with Nd concentration of 0.5% and 0.7% (at.).

7.5 Requirements placed on the rest of the laser design

The choice of laser material, concentration and geometry placed a few requirements on the rest of the laser design.

The requirement of pumping at 805 nm was easily met since high power diode lasers at this wavelength are more readily available than at lower wavelengths, due to the commercial development of diode-pumped Nd:YAG laser systems which are pumped close to this wavelength [1].

To fulfil the requirement of having a large pump beam to pump the laser crystal over a long absorption length, required a pump source with good beam quality and high power [35]. This implied the pump beam had to have a confocal length longer than the absorption length of the crystal. To allow proper mode-matching between the pump beam and the TEM_{00} laser mode, the beam profile of the pump needed to be circular. These requirements were met by using commercial fibre coupled diode lasers. These commercial devices can deliver high output power and have sufficient beam quality with un-polarized, circular beam profiles. The coupling of diode power into the optical fibre is commercially done and is similar to what is described in Ref. [27]. The choice of pump source is discussed in the next section.

The requirements placed on the resonator design are that it should enable end-pumping of the laser crystal; it should force the laser to operate on the weaker 1053 nm laser transition; it should ensure good mode-matching of the pump beam and the resonator mode; and it should also be possible to compensate for the thermal lens to some degree. The laser resonator design is discussed in Section 9.

8 The pump source

Two Jenoptik 30 watt fibre coupled laser diode modules (JOLD-30-CPFX-1L) [64] were used as continuous wave pump sources for the high power solid-state laser. The optical output power was delivered with 0.4 mm diameter, 0.22 numerical aperture (NA) fibres. This related to a M^2 value of ~175 with the far-field approximation [65].

The fibres were connected to fibre collimators, manufactured by OZ Optics [66]. For reference, the diodes were named LD1 (serial number: 20414) and LD2 (serial number: 20418).

The manufacturer of the laser diodes specified the operating wavelength at 25 ˚C as 806.2 nm and 806.3 nm for LD1 and LD2 respectively, with 2.7 nm and 2.0 nm FWHM (Full Width Half Maximum) spectral width and with 3.1 nm and 2.9 nm 90%-width.

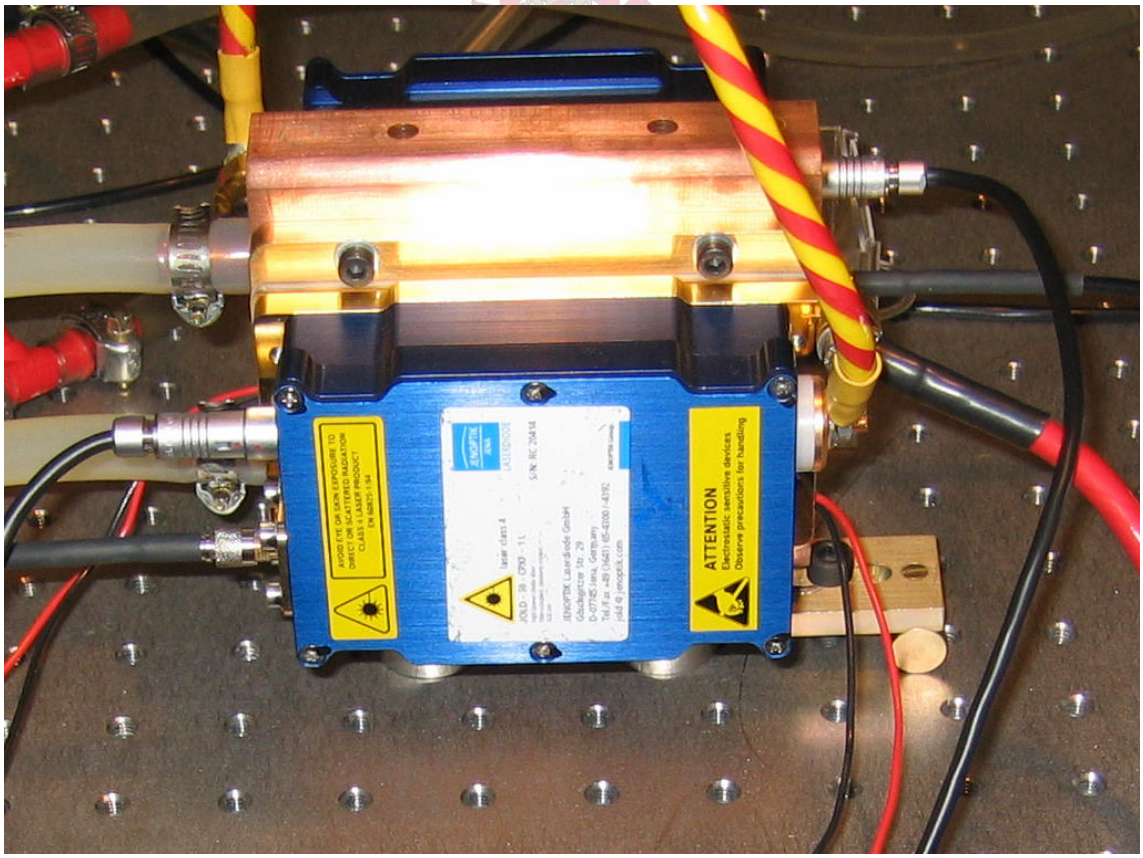

Figure 8-1: Two Jenoptik 30W laser diode modules mounted on a water cooled heat sink.

Both laser diodes were mounted on a single water-cooled copper heat sink. The cooling water for the diode lasers and the laser crystal was circulated by a Neslab "RTE 110 Basic" water controller with adjustable water temperature.

In addition to the water-cooling, the temperature of the diodes was actively controlled with a temperature controller to maintain the diode temperature within 0.01 °C of the set point. The temperature controller consisted of a PC with a data acquisition card to measure the temperature, custom control software and a GPIB interface to two HP 66332A power supplies, which controlled the cooling power of the integrated thermo-electric coolers (TEC's) of the laser diodes. A schematic of the control system is shown in Figure 8-2.

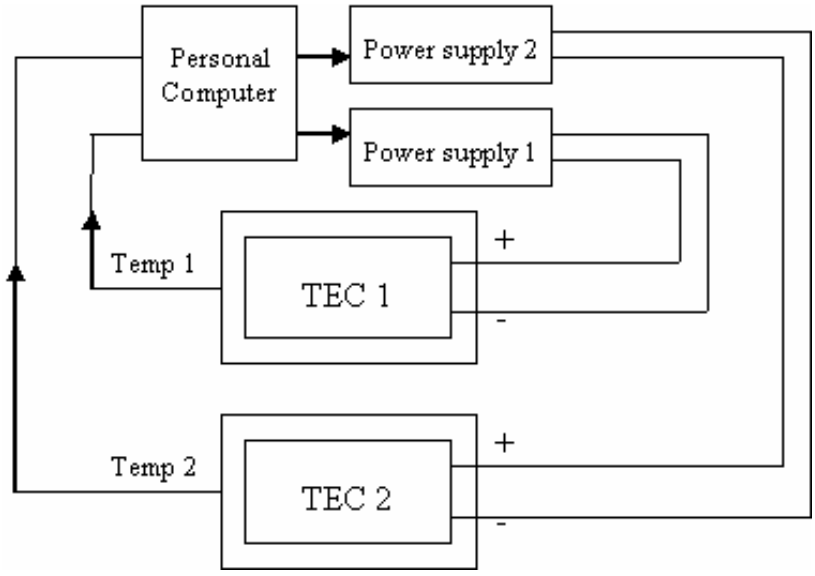

Figure 8-2: Schematic of the temperature controller that was used to actively cool the laser diodes.

The electrical input power of up to ~167 watts for the laser diodes was supplied by two HP 6652A power supplies (0-20V / 0-25A) connected in parallel. The specified operating currents for 30 W optical output from the diode lasers were rated as 41.7 A for LD1 and 42.7 A for LD2, though they were always operated in parallel and up to 42 A.

8.1 Efficiency and calibration of the laser diodes

The efficiency of the laser diodes was determined by measuring the combined optical output power and noting the electrical input power, at a controlled diode temperature. The output power was measured with a Coherent LM-200 power head and Coherent

Fieldmaster power meter. The result shown in Figure 8-3 was achieved with the diode temperature at 24 ˚C [1].

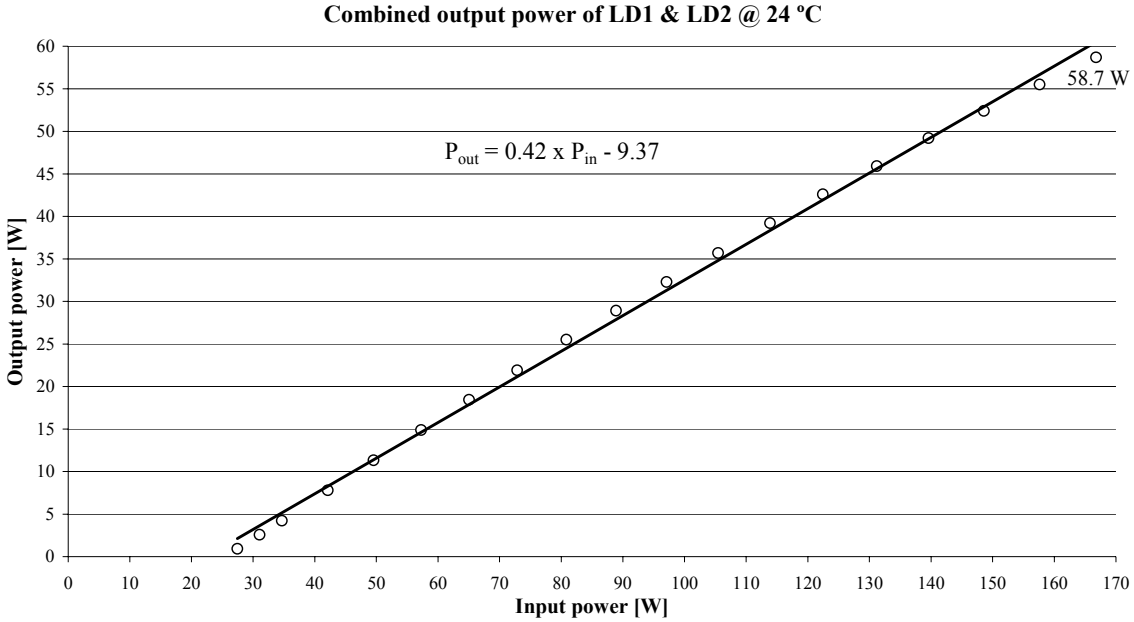

Figure 8-3: Slope efficiency of the diode lasers at 24 ºC. The combined output was 58.7 W at the maximum input current of 42 A.

As shown in Figure 8-3 the straight line $P_{out} = 0.42 \times P_{in} - 9.37$ closely approximates the output power of the laser diodes. From this result it was concluded that the laser diodes had a linear increase in output power with an increase in input power, with a slope efficiency of 42%. The overall electrical to optical efficiency of 35.2% was slightly lower than the value specified by the manufacturer. The small losses introduced by the optical fibres and collimators can attribute to this lower value [27].

The output power of each diode laser at full pump power (42 A) was measured for different diode temperatures. The measurements for LD2 are shown in Figure 8-4. The result of this experiment showed a slight variation (~2 W) in output power over the whole temperature range, which is inversely proportional to the diode temperature. Although this result indicated that a lower operating temperature yields higher output power, the operating temperature, which determines the pump wavelength, was determined by the absorption spectrum of the laser material.

[1] Note: The actual temperature of the diodes was ~4°C below the temperature as measured by the temperature controller. All diode temperatures are given as measured, unless otherwise specified.

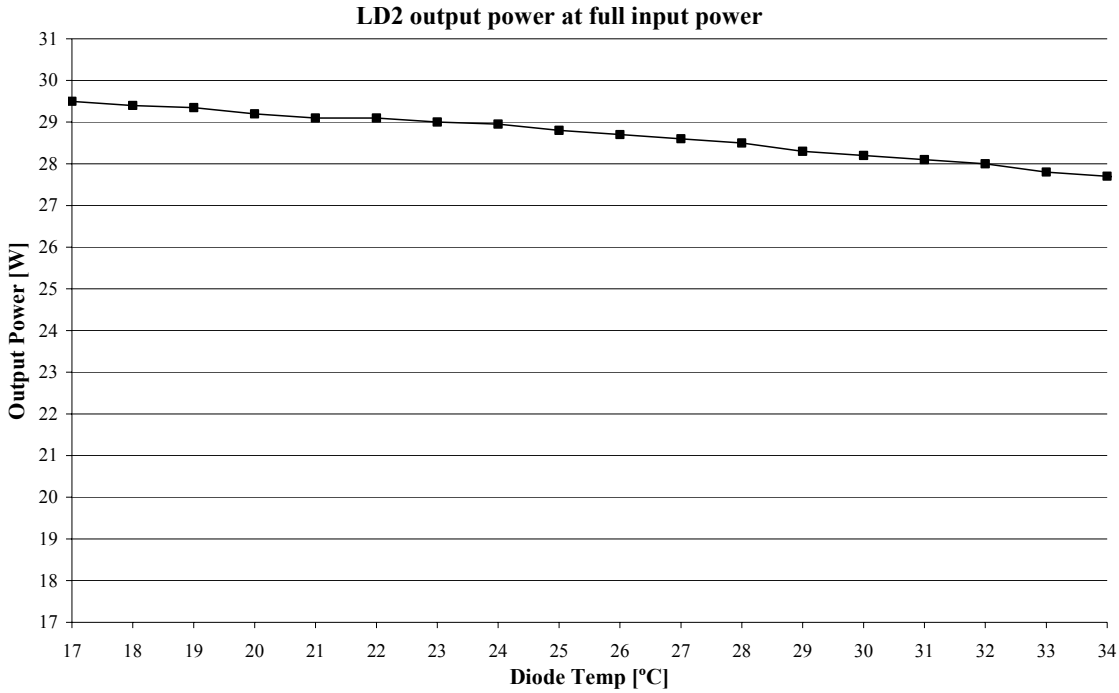

Figure 8-4: The measured change in optical output power of LD2 with a change in diode temperature.

8.2 Crystal absorption of diode power

The effective absorption spectrum of the 30 mm long Nd:YLF crystal with 0.7% doping concentration was calibrated against the diode laser temperature and is shown in Figure 8-5. A change of one degree Celsius in diode temperature relates to a change in wavelength of ~0.25 nm [18]. The resolution of the absorption curve was limited by the spectral bandwidth of the diode laser, which is 2.0 nm FWHM.

The data from this experiment was compared to the absorption spectrum of Nd:YLF in Figure 7-2. It was concluded that the measured peak in un-polarized absorption at the diode temperature of ~24 ºC corresponds to the 805 nm peak of the absorption spectrum.

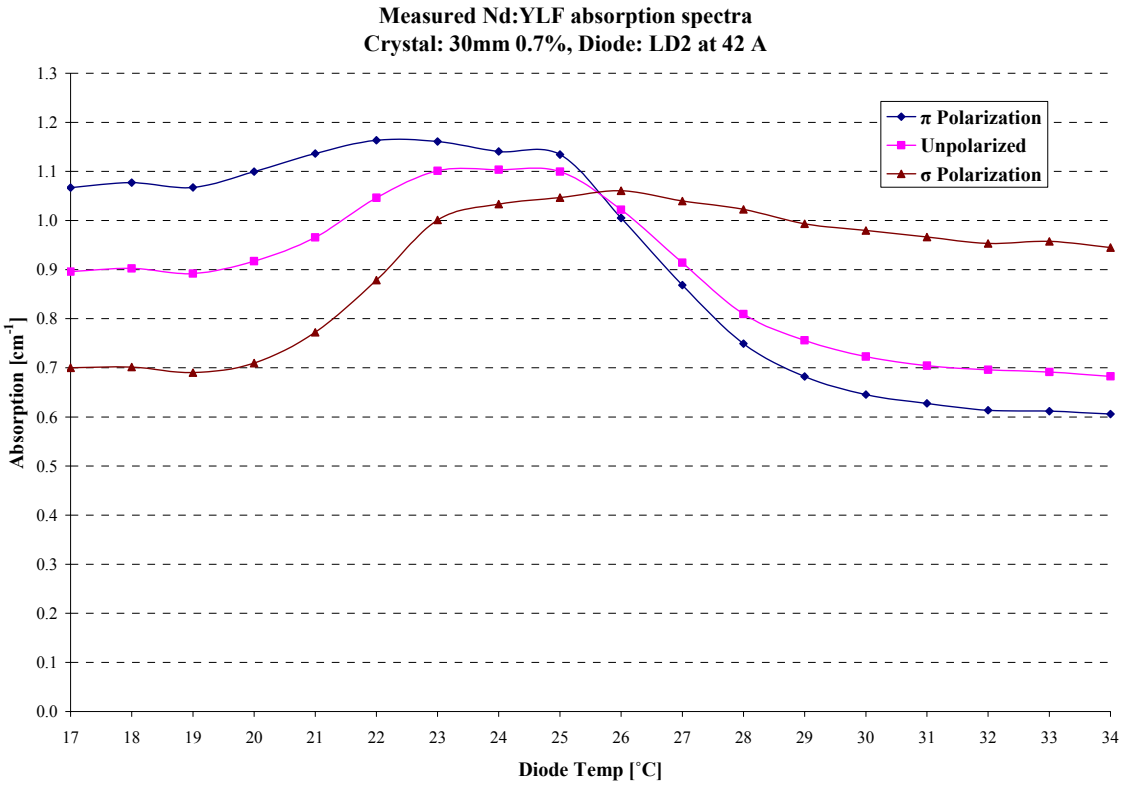

Figure 8-5: The measured effective absorption coefficient of the 30 mm long 0.7% Nd:YLF crystal at different laser diode temperatures, at 42 A operating current.

From this result it was concluded that the diode operating temperature should be in the region of 24 ºC when operating at maximum input current to fulfil the requirements as stated in Section 7.2. In this wavelength region, the un-polarized absorption is at a maximum, and is insensitive for a small change in diode temperature. Furthermore, the absorption coefficient is quite similar for both polarizations, which would lead to uniform absorption of the un-polarized pump radiation.

The measured effective absorption coefficient of ~1.1 cm^{-1} determined that the absorption length of the crystal was ~9 mm at this pump wavelength. Therefore a pump beam radius of 0.5 mm was used, which corresponded to a confocal length of ~16 mm inside the laser crystal, as calculated from Gaussian beam propagation theory [6 Ch. 5]. This was almost twice the absorption length of 0.7% doped Nd:YLF at the pump wavelength to ensure minimal diffraction spreading of the pump beam over the length of the crystal [5].

8.3 Summary

As discussed in Section 7, the large pump beam and long absorption length ensured reduced heat generation due to energy transfer upconversion. By implementing these measures the good thermo-optical properties of Nd:YLF were exploited, with a reduced risk of thermal fracture of the laser crystal under intense diode-end-pumping.

The large pump beam placed the restriction on the resonator design to have a large resonator mode in the crystal to ensure good spatial overlap with the pump beam. The resonator design will be discussed in the next section.

9 The laser resonator

From the choice of laser crystal and pumping setup, the resonator for the high power Nd:YLF laser should

- enable end-pumping of the laser crystal from both ends;
- force the laser to operate on the weaker 1053 nm laser transition which has the weak thermal lens;
- have a large resonator mode in the crystal to ensure good mode-matching with the large pump beam.

9.1 Traditional approach

The traditional approach to establish a large mode size in a resonator is to use the three-mirror cavity as shown in Figure 9-1. Such a cavity has a short arm with a small waist and a long arm with a large collimated mode.

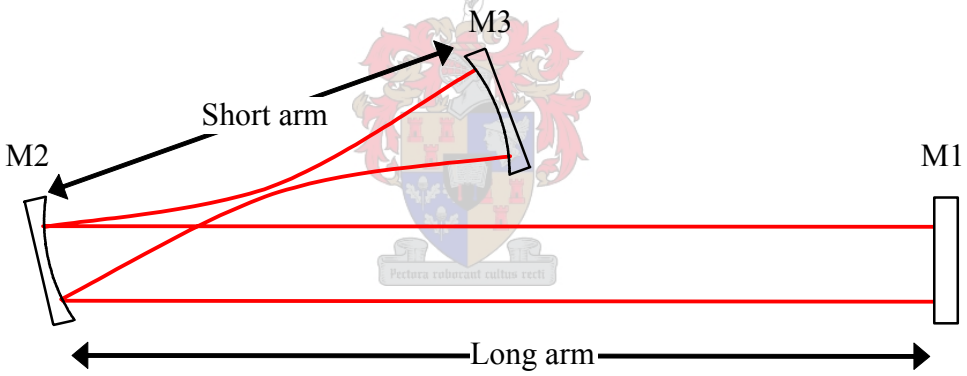

Figure 9-1: Simple three mirror resonator with a long arm between mirrors M1 and M2, and a short arm between mirrors M2 and M3.
Note: the resonator mode size and mirrors are not drawn to scale.

Resonators based on this principle have been used extensively in dye lasers, Kerr-lens mode locked lasers and intra-cavity frequency doubled lasers, where the small waist in the short arm was utilised [6 Ch. 5, 67]. However, it was shown by Clarkson *et al* that the large collimated mode in the long arm can be used to match a large pump beam in an end-pumped Nd:YLF laser [5]. They achieved an average output power of just above 10 W with good beam quality.

The same concept was used for the high power Nd:YLF laser. The features of this resonator and implementation thereof in the Nd:YLF laser will be discussed in more detail.

9.1.1 Large resonator mode for matching the pump beam

The main feature of the resonator that was utilised is the large resonator mode size in the long arm. The mode in the long arm is large and collimated when the long arm is significantly longer than the short arm, and when the short arm length is adjusted such that the resonator is close to the stability edge. Without taking the effects of a thermal lens or astigmatism into account, the stability edge is at the point where the short arm length L_0 is

$$L_0 = \frac{R_2}{2} + R_3,$$

with R_2 and R_3 the radii of curvature (positive for concave) of mirrors M2 and M3 respectively [68].

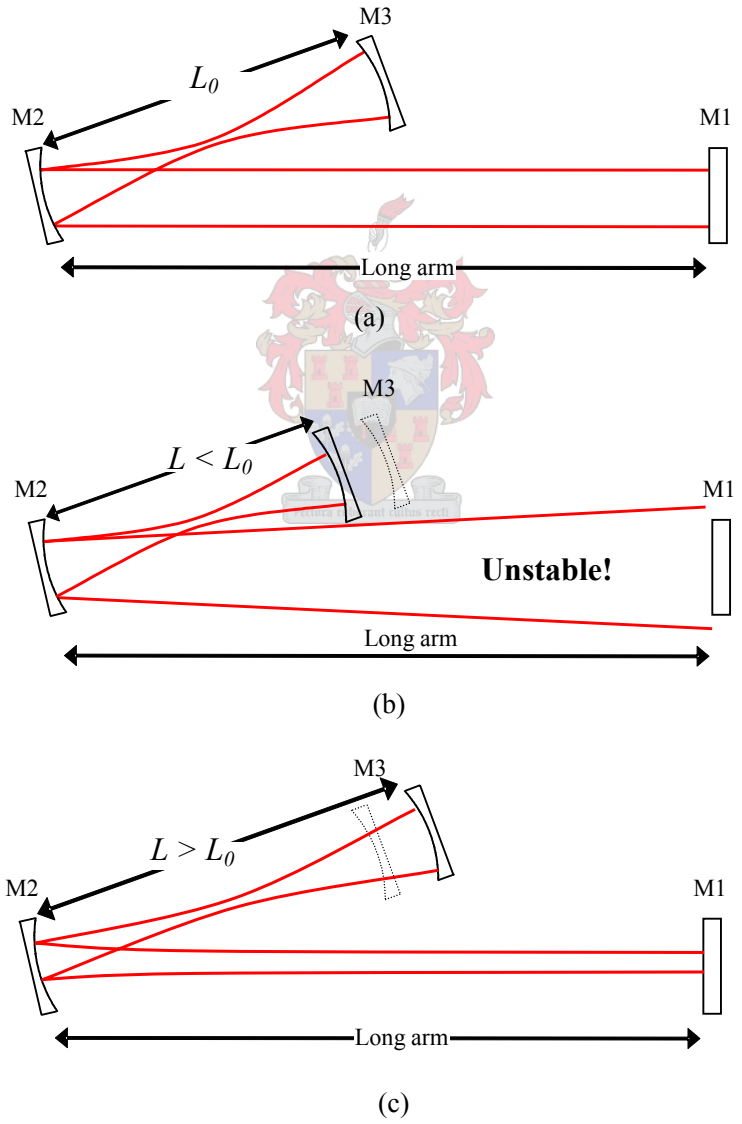

Figure 9-2: The effect of the short arm length on the resonator mode size in the long arm. At the stability point, the resonator mode is the largest (a). At shorter lengths, the resonator is unstable (b) and at longer lengths, the resonator mode size in the collimated long arm becomes smaller (c).

At the stability point, the resonator mode size in the long arm is at its largest and well collimated, as shown in Figure 9-2 (a). When the short arm length is made shorter than L_0, the resonator becomes unstable (Figure 9-2 b) and if the short arm length is longer than L_0, then the mode size in the collimated long arm becomes smaller (Figure 9-2 c).

For efficient mode-matching between the resonator mode and the large pump beam in the Nd:YLF crystal, the resonator can be set up with the laser crystal in the long arm. The radii of curvature of the mirrors and the short arm length can be chosen such that the mode size in the long arm has the same size as the pump beam. During laser operation, the short arm length can be adjusted to change the spatial overlap between the pump beam and the resonator mode to compensate for thermal lensing and therefore optimise the beam overlap efficiency and the beam quality of the laser.

9.1.2 Polarization selection through thermal lenses

With the property of an a-cut Nd:YLF crystal of having a strong negative thermal lens when operating on the π-polarization (1047 nm) and a weak positive thermal lens when operating on the σ-polarization (1053 nm), a resonator can be designed to force the laser to operate on the 1053nm line which has the weaker emission cross section. This can be done without any additional components in the resonator and has been demonstrated in a Nd:YLF laser with a diode-end-pumped geometry [40] and in a lamp-pumped system [69].

The resonator with the short arm and long arm described above can be set up to be stable either for a positive thermal lens or for a negative thermal lens. If the short arm length of the resonator is set up such that the resonator is at or close to the stability edge as in Figure 9-2 (a), and a negative thermal lens is introduced in the long arm, the mode size would increase and the resonator would become unstable. To compensate for this, the short arm length can be increased which would make the mode size smaller and the resonator stable, as shown in Figure 9-3.

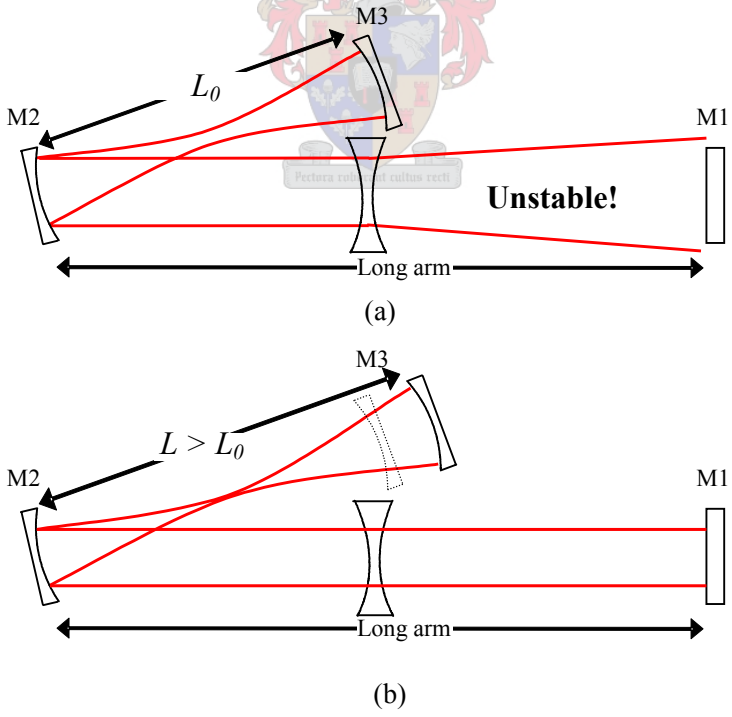

Figure 9-3: The effect of a negative thermal lens on the resonator mode size. The short arm can be adjusted to make the resonator stable (b).

If a positive thermal lens is introduced in the stable resonator of Figure 9-2 (a), it would decrease the mode size in the long arm. By shortening the short arm length, the mode size can be increased again up to the stability point, as shown in Figure 9-4.

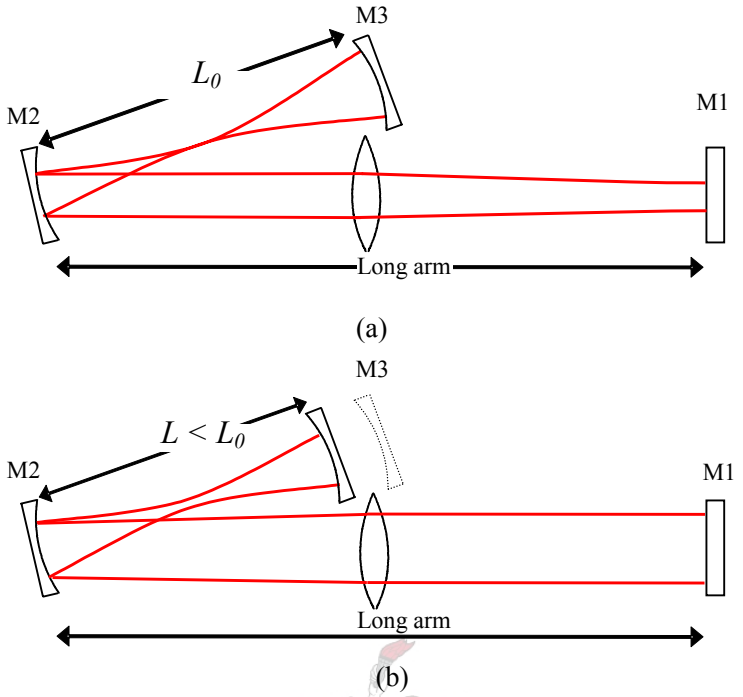

Figure 9-4: The effect of a positive thermal lens on the resonator mode size. The short arm can be adjusted to increase the mode size in the long arm (b).

Based on this principle, the short arm length was chosen such that the resonator forced the laser to operate on the weaker 1053 nm line. When the Nd:YLF crystal was operated at very low power, the thermal lens power was small and the laser operated on the strong 1047 nm line (π-polarization). With an increase in pump power, and an increase in thermal lens power, the resonator became unstable for the strong negative thermal lens of the π-polarization and switched to the σ-polarization with the weak positive thermal lens, for which the resonator was stable.

9.1.3 Compensation for an astigmatic thermal lens

Another feature of this resonator that was used for the high power Nd:YLF laser is its ability to compensate for an astigmatic element in the resonator. This is due to the adjustable incident angle on the curved folding mirror M2 in Figure 9-1. The effective radii of curvature in the horizontal and vertical resonator planes are

$$R_{\text{hor}} = R\cos\theta \text{ and } R_{\text{vert}} = \frac{R}{\cos\theta}$$

respectively, with θ the half angle between the long arm and the short arm [6 Ch. 5].

With the c-axis of the laser crystal aligned parallel to the horizontal axis of the resonator, the astigmatism due to the curved mirror can compensate for the astigmatic thermal lens of Nd:YLF operating on the σ polarization. This astigmatic thermal lens is due to the different crystal properties along the two different crystal axes [13], namely the refractive indices

$$n_o = 1.454 \text{ and } n_e = 1.477 ,$$

the temperature dependence of the refractive indices

$$\frac{dn_{\text{a-axis}}}{dT} = -0.9 \text{ and } \frac{dn_{\text{c-axis}}}{dT} = -2.9 \left[10^{-6}\,\text{K}^{-1}\right],$$

and the expansion of the laser crystal

$$\frac{dL_{\text{a-axis}}}{dT} = 13 \text{ and } \frac{dL_{\text{c-axis}}}{dT} = 8 \left[10^{-6}\,\text{K}^{-1}\right].$$

9.2 Resonator setup

The resonator design described above has the desired features of discriminating against the stronger emission at 1047 nm, it can compensate for changes in thermal lens powers due to the choice of incident pump power while it ensures a large mode size in the crystal to enable good spatial overlap with the large pump beam.

This resonator was modified to

- facilitate longitudinal pumping into both ends of the laser crystal;
- avoid optical damage on the resonator mirrors;
- and to minimize the resonator length for short-pulse operation

of the high power Nd:YLF laser.

The concave end-mirror of the basic resonator was replaced by a convex end-mirror. The result of this was a virtual focus outside the cavity, but otherwise the same operation of the resonator, in that by changing the short arm length between mirrors M2 and M3, the resonator mode size in the long arm was adjusted.

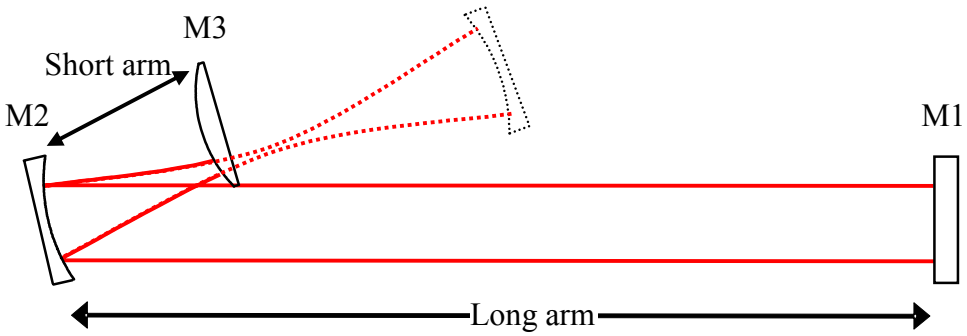

Figure 9-5: Concave end-mirror replaced by a convex end-mirror. The principle of the resonator is the same as the basic resonator.

Note: the resonator mode size and mirror sizes are not drawn to scale.

The criteria for the stability edge of the resonator changed to

$$L_0 = \frac{R_2}{2} - |R_3|.$$

The advantage of this setup was a shorter overall resonator length, which was necessary for the desired short pulse *Q*-switch operation. Previously demonstrated setups [5] used a plane mirror in the focus of the short arm in an attempt to shorten the resonator, and to use it as the output coupler of the resonator. The disadvantage of such a setup would be high optical densities on the mirror, which could lead to optical damage. In contrast, the setup of a convex end-mirror allowed an even shorter resonator and a large spot size on the mirror to avoid optical damage. (Note: the mode size and position of the resonator mirrors are not drawn to scale in Figure 9-5.)

The long arm of the resonator was folded at 45˚ (Figure 9-6) which had a threefold effect, without changing the working principle of the basic resonator. The laser crystal was placed between the concave folding mirror (M2) and the 45˚ mirror. This allowed the crystal to be longitudinally pumped from both ends, through M2 from one side, and through the 45˚ mirror from the other side. These mirrors were anti-reflection (AR) coated for transmission at the pump wavelength, and high-reflection (HR) coated for the laser wavelength.

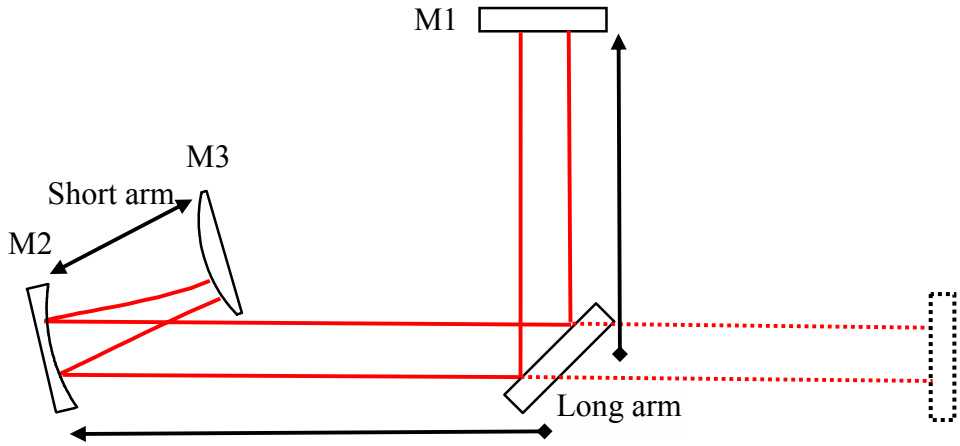

Figure 9-6: The resonator long arm was folded at 45° to facilitate longitudinal pumping into both ends of the laser rod.

This setup allowed mirror M1 to be replaced with an output coupler for the laser. The advantage of using a plane output coupler in the long arm was significant. Plane output couplers with different reflectivity were readily available and were exchanged with fair ease without major re-alignment of the laser. Furthermore, the output beam of the laser was well collimated.

The third effect of this setup was that when it was needed for *Q*-switch operation, an acousto-optic modulator (AOM) was placed in the long arm, between the 45° mirror and the output coupler. By placing the AOM in the collimated part of the resonator, it only changed the optical path length, and did not influence the alignment of the resonator significantly.

9.2.1 Initial setup

With the desired beam parameters determined (Section 8.2) and all the requirements taken into account (Section 9.2), the resonator was modelled to determine the resonator lengths and radii of curvature of mirrors M2 and M3. The following values for the resonator mirrors and arm lengths were calculated and used as a first setup (Figure 9-7): radius of curvature of M3 = -30 mm and radius of curvature of M2 = 150 mm. Adjustable short arm length ~48 mm, and total long arm length ~205 mm.

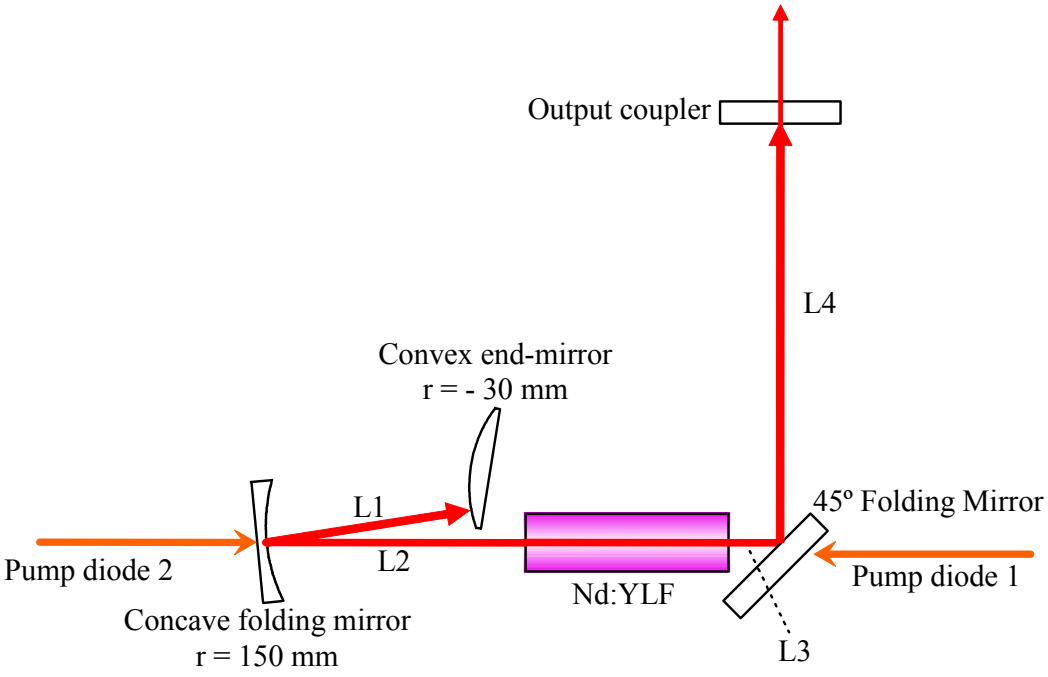

Figure 9-7: Laser resonator for the high power diode-end-pumped Nd:YLF laser.

The half angle between L2 and L1 was made as small as practically possible during the first setup to minimize the effect of astigmatism on the concave folding mirror. It was later measured to be ~6.8°.

As stated, mirror M2 and the 45° mirror were AR coated for the pump wavelength (805 nm), and HR coated for the laser wavelength (1053 nm). The end-faces of the laser crystal were AR coated for both the pump and the laser wavelengths. The 30 mm long Nd:YLF crystal with 0.5% (at.) doping concentration was initially used. The c-axis of the crystal was aligned to be within the resonator plane.

For pulsed operation, the laser was *Q*-switched with an acousto-optic modulator (AOM). The AOM that was available for the setup was produced by Gooch & Housgo and had an RF-driver integrated in the device. The RF-driver was water cooled by the same water controller as the laser diodes and laser crystal. The driving frequency was 27 MHz and the material was fused silica. The switching frequency was controlled by a block pulse generator, from 5 kHz to 100 kHz. The AOM was mounted in such a way that it was easy to insert and remove from the laser resonator as shown in Figure 9-8, without major realignment of the laser.

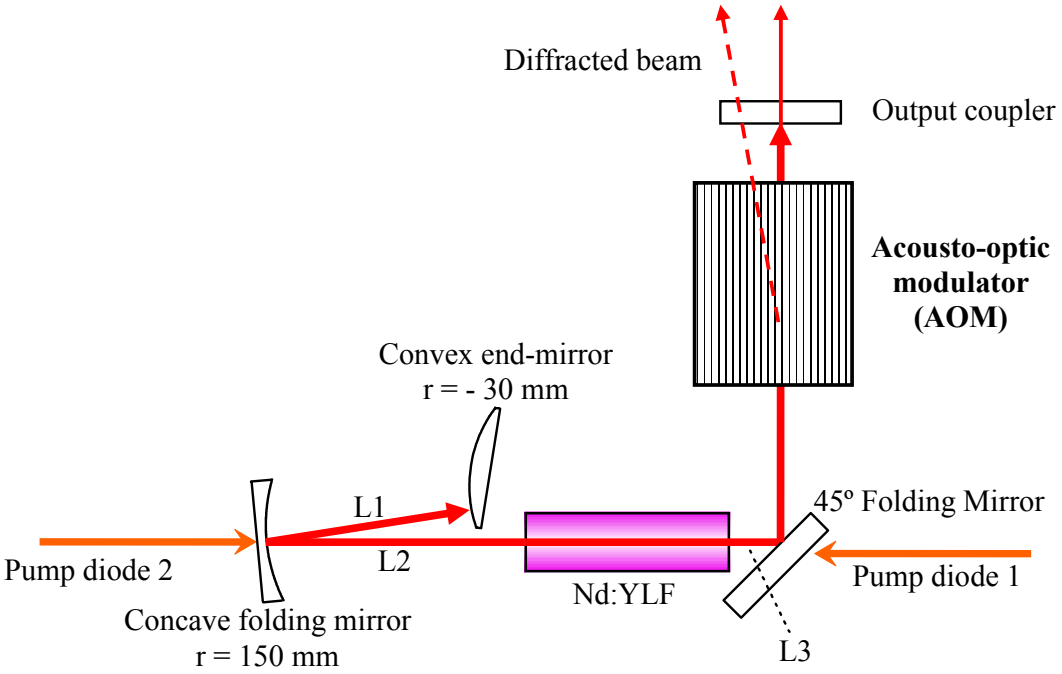

Figure 9-8: Laser resonator for the *Q*-switched Nd:YLF laser, showing the placement of the AOM.

The optics for delivery of the pump radiation was set up as shown in Figure 9-9. The lengths L5 to L8 and the choice of focusing lenses f_{LD1} and f_{LD2} were calculated to allow the desired pump radius of ~0.5 mm inside the Nd:YLF crystal, as discussed in Section 8.2. It was initially set up with L5 = 378 mm, L6 = 57 mm, L7 = 117 mm and L8 = 362 mm. The focal length of f_{LD1} was 100 mm and f_{LD2} was 80 mm. Only uncoated lenses were available during the initial setup.

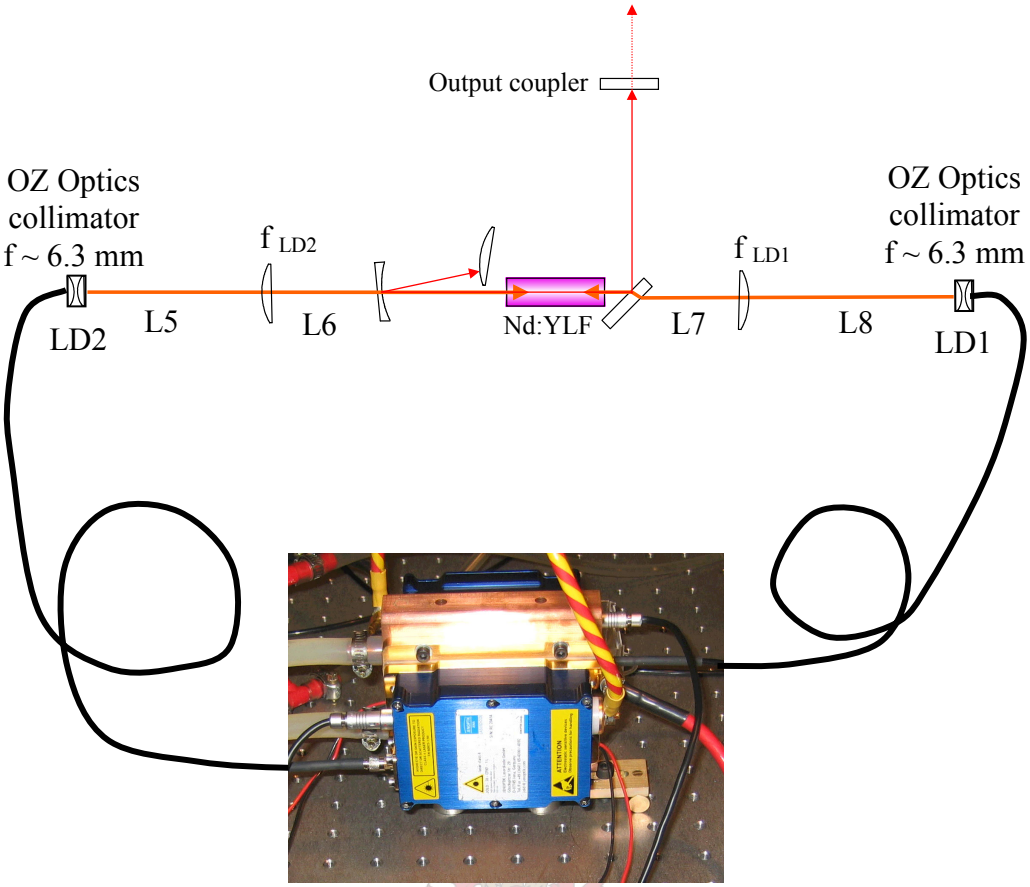

Figure 9-9: Laser setup including pump delivery optics.

The adjustable OZ Optics fibre collimator was used to image the fibre end onto the focusing lens, for both f_{LD1} and f_{LD2}. This allowed an approximate Gaussian pump beam profile at the foci inside the crystal.

The focus lenses were mounted on three-dimensional translation stages, to allow accurate positioning of the pump waists inside the crystal. By aligning both pump waists to overlap with the resonator mode, the maximum coupling efficiency was achieved. The optimum pump waist position along the optical axis were determined experimentally during laser operation.

A photo of the initial resonator setup with the AOM in the resonator is shown in Figure 9-10.

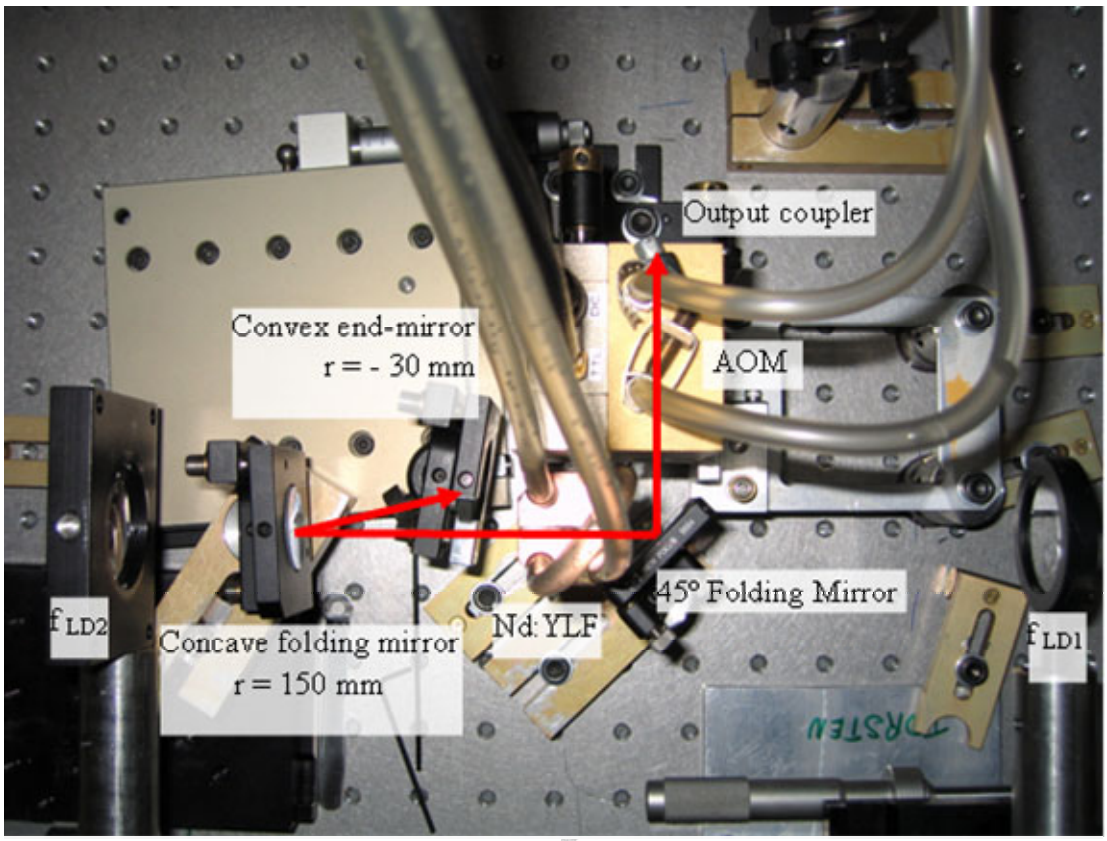

Figure 9-10: Photo of the resonator setup, showing the positions of the resonator mirrors and other components. The laser beam inside the resonator is also indicated.

9.2.2 Final setup

The 0.5% doped Nd:YLF crystal was replaced with a 0.7% crystal of the same dimensions. The final dimensions of the resonator after extensive optimization were L1 = 49 mm, L2 = 63.5 mm, L3 = 14 mm and L4 = 77.5 mm. The pump focus lenses were replaced by AR coated lenses, with f_{LD1} 100 mm and f_{LD2} 75 mm, and the lengths were changed accordingly to L5 = 367 mm, L6 = 48.5 mm, L7 = 105 mm and L8 = 413 mm. The half angle between the shot arm and the long arm was set to 8.0° to compensate for the astigmatic thermal lens of Nd:YLF. This setup related to the best results obtained as discussed in Section 11.5.

10 Diagnostic setup

The following equipment was used to determine the laser performance. The continuous wave power as well as the average power under pulsed operation was measured with a Coherent LM-200 power head and a Coherent Fieldmaster power meter. From this and the calibration of the diode lasers in Section 8.1, the overall efficiency of the laser was determined.

The external beam profile, which is an indication of the beam quality, was captured by a Coherent LaserCam IIID digital laser camera. The M^2 beam quality factor was measured with the slit-scan technique, using an automated device which was developed in-house at the LRI. The user interface allowed easy and quick determination of the M^2 value in both the horizontal (x-plane) and vertical (y-plane) resonator planes, as seen in Figure 10-1.

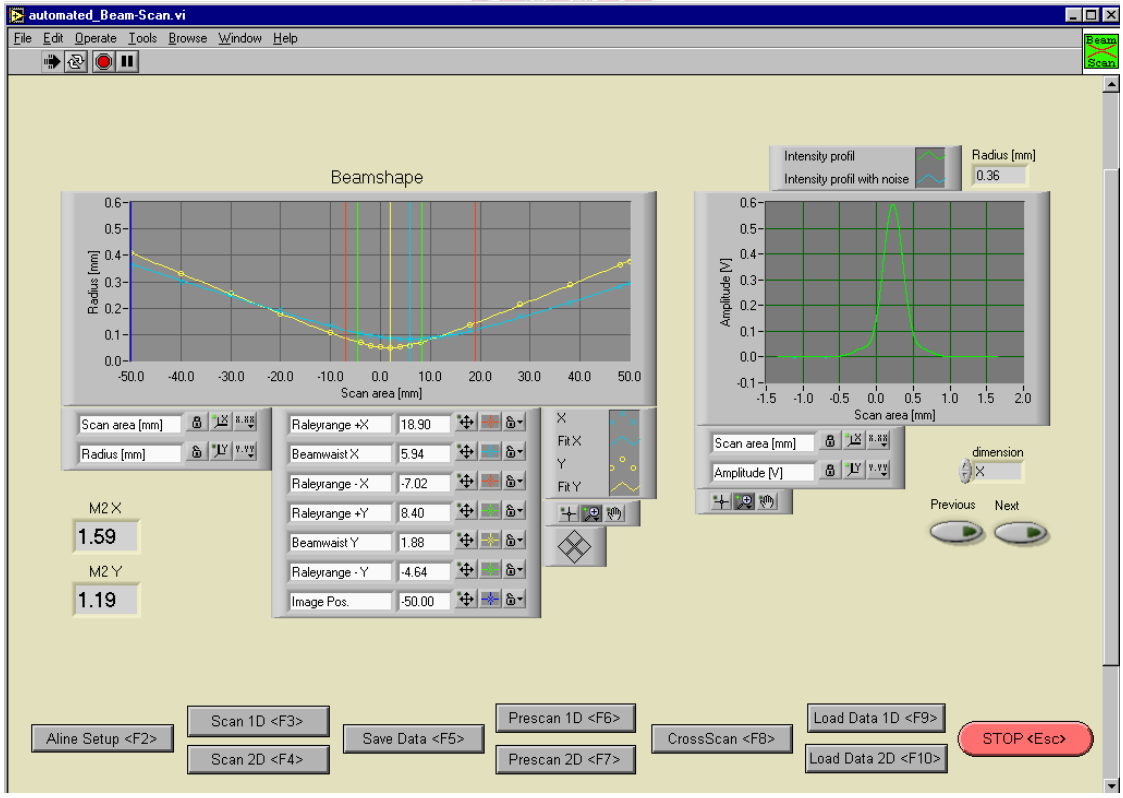

Figure 10-1: The user control interface of the automated M^2 measuring device.

Under pulsed operation, the time resolved pulse length was either measured with a BPX 65 photo diode (~5 ns rise time) or with a ThorLabs DET210 fast photo detector (~1 ns rise time), connected to a Tektronix (300 MHz, 2.5GS/s) fast oscilloscope. The

energy per pulse was determined by the pulse repetition rate and the average output power of the laser.

11 Results

The Nd:YLF laser was operated in a number of parameter configurations. Almost all parameters were varied under both continuous wave and pulsed operation in order to get an indication of the dependence of laser performance on a certain parameter. The laser performance, as measured by the output power, beam quality and pulse length, was influenced by the choice of doping concentration, output coupling efficiency, short arm length and diode wavelength.

11.1 Influence of doping concentration

The graph in Figure 11-1 shows the efficiency curves of the Nd:YLF laser operated without the AOM in the cavity, with both a 0.5% and 0.7% Nd doped crystal. The output coupler reflectivity was 90%. The diode temperature and short arm length were the same for the two cases.

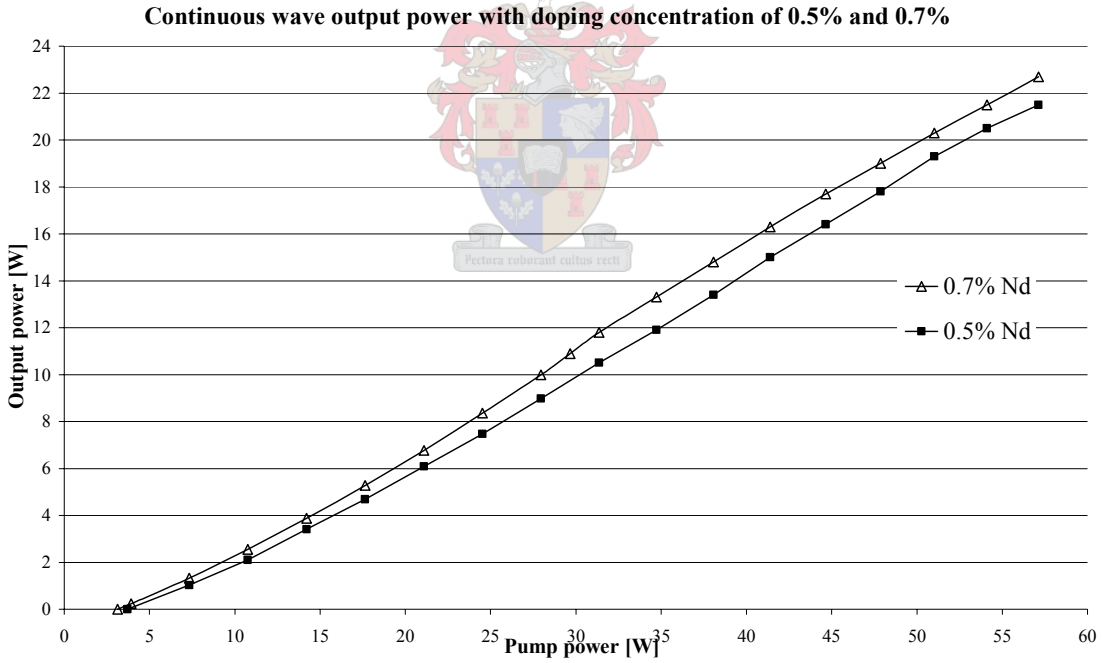

Figure 11-1: The continuous wave slope efficiency of the Nd:YLF laser with Nd concentration of 0.5% and 0.7%.

At the maximum pump power the laser with the 0.5% Nd:YLF crystal delivered 21.5W of output power and with the 0.7% Nd:YLF crystal it produced 22.7 W. This related to an optical-to-optical efficiency of 37.6% and 39.7% respectively.

The far field beam profile of the output laser beam at full pump power is shown in Figure 11-2. In both cases the beam profile was nearly circular which indicated that the laser operated in the TEM_{00} transverse laser mode. The experiment was also performed for output coupler reflectivity of 60% and 80%, which delivered similar results for the output powers and beam profiles.

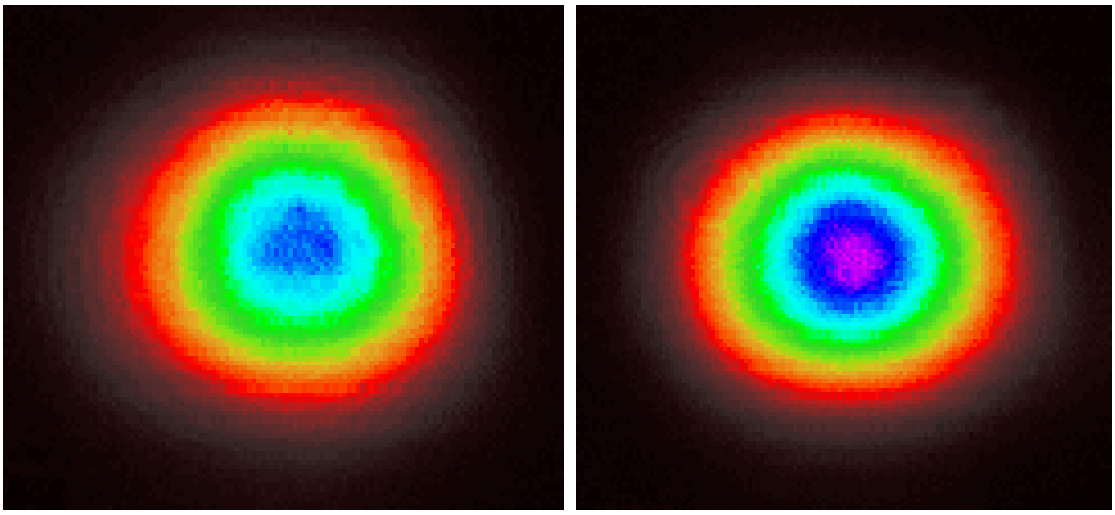

(a) **(b)**

Figure 11-2: The far field beam profiles at maximum output power of the Nd:YLF crystal of (a) 0.5% and (b) 0.7% doping concentration.

The influence of doping concentration on the performance of the *Q*-switched laser at 50 kHz was also investigated. The difference in average output power for the two different crystals was similar to that observed under continuous wave operation. The average pulse lengths at different pump powers for the two doping concentrations are shown in Figure 11-3. For both crystals, the pulse length decreased with increased pump power. At the maximum pump power the laser with the 0.5% Nd:YLF crystal produced pulses of 136 ns duration, and the laser with the 0.7% crystal had pulse lengths of 100 ns. A similar behaviour in pulse length was also observed for output coupler reflectivity of 60% and 90% for the two different doping concentrations.

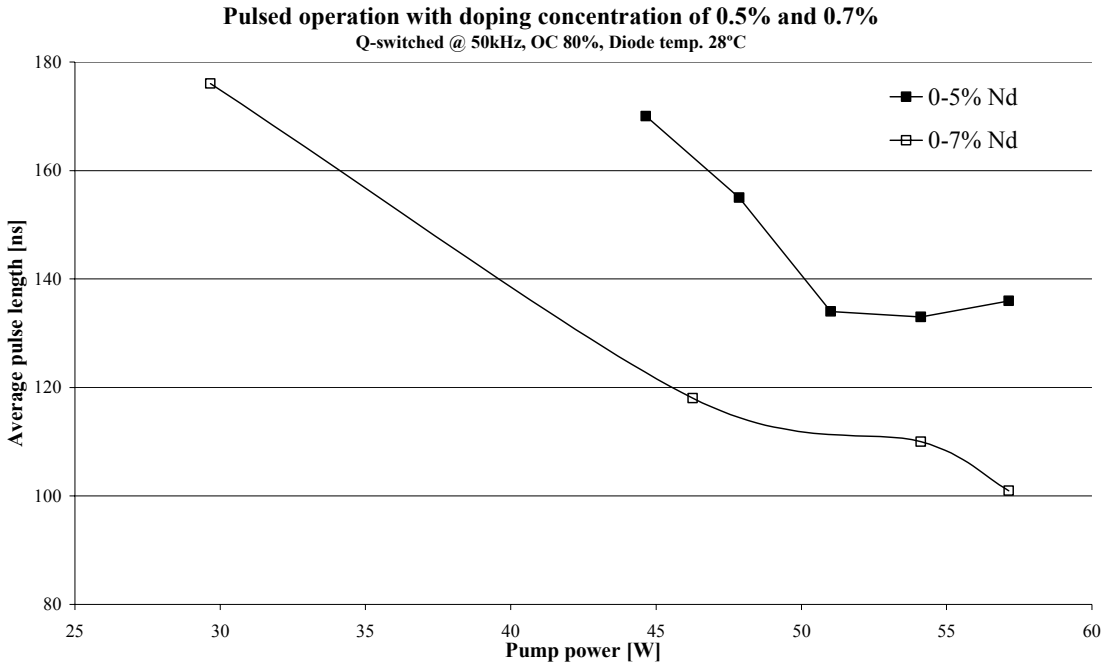

Figure 11-3: The pulse length of the *Q*-switched Nd:YLF laser at different pump powers with Nd doping concentration of 0.5% and 0.7%.

11.2 Influence of output coupling

The choice of output coupling efficiency influenced the average output power, pulse length and beam quality of the *Q*-switched laser. The slope efficiencies of the *Q*-switched laser under three output coupling values are presented in Figure 11-4.

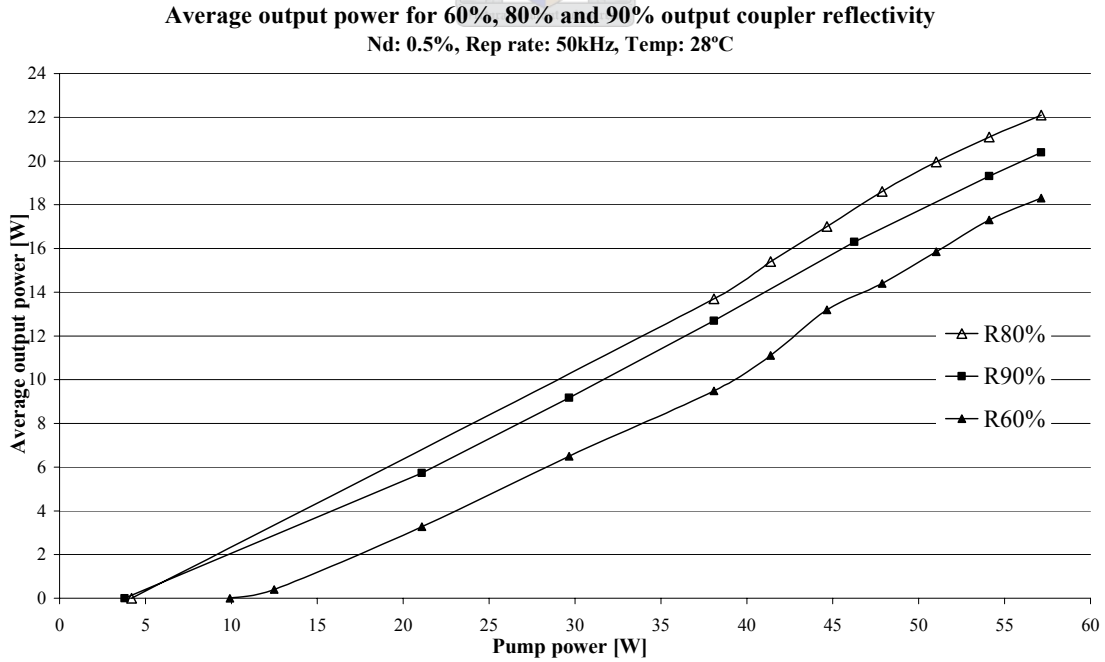

Figure 11-4: Performance of the *Q*-switched Nd:YLF laser with different output coupler reflectivity.

The laser was *Q*-switched at 50kHz, had a 0.5% Nd:YLF crystal and the diode temperature was at 28°C. The short arm length was the same for all three configurations. As seen in Figure 11-4, the laser with the 80% output coupler reflectivity had the highest efficiency over the whole pump power range. At full pump power, the laser with 80% output coupler reflectivity also delivered shorter pulse lengths than the laser with the 60% and 90% output couplers.

Similar results were observed for the laser with Nd concentration of 0.7%, for which the pulse length and pulse shape together with the beam profile for 90%, 60% and 80% reflectivity is shown in Figure 11-5 to Figure 11-7. Note: the beam profiles of the three cases were captured under different attenuation values.

The laser with 90% output coupler was only pumped up to 38 W since the beam quality deteriorated at this level. At this pump level it delivered 13.7 W and the pulse length was ~139 ns, as seen in Figure 11-5.

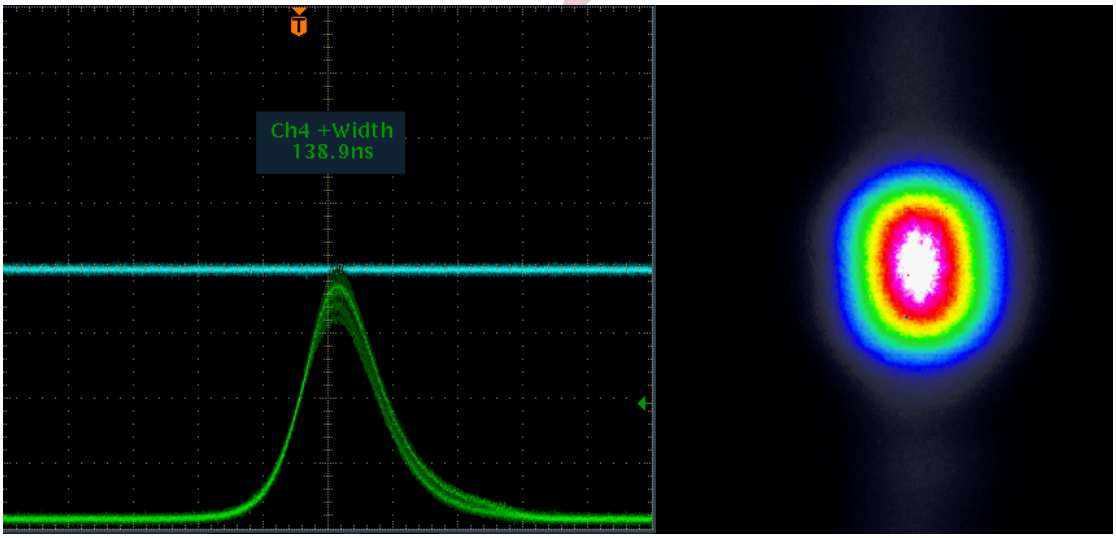

Figure 11-5: Pulse and beam profile of the Nd:YLF laser with 90% output coupler reflectivity at 38 W pump power and 13.7 W average output power.

The laser with the 60% output coupler reflectivity was pumped at full pump power. It delivered 18.0 W of average output power and pulse lengths of ~113 ns, which is shown in Figure 11-6.

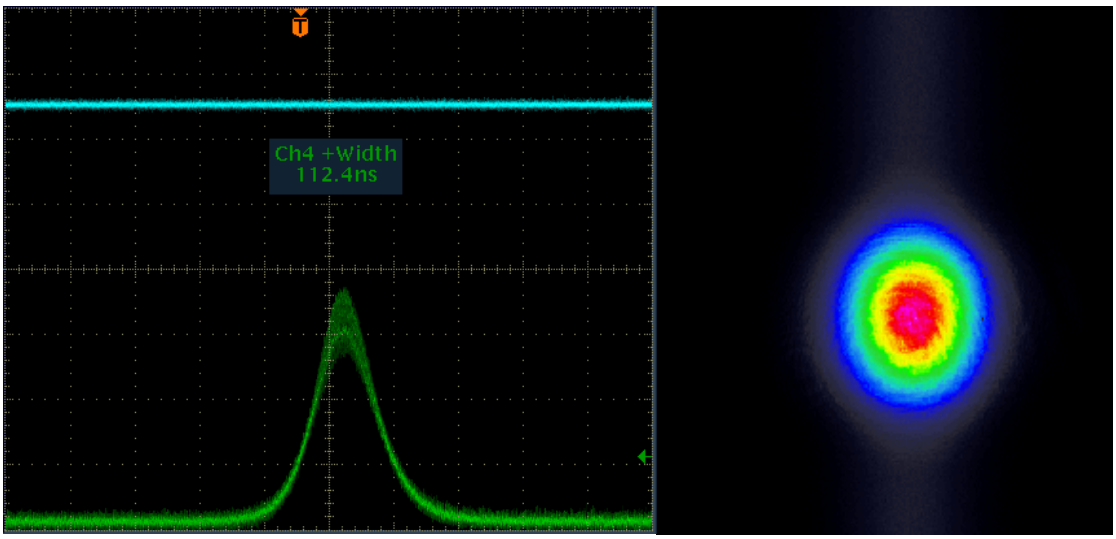

Figure 11-6: Pulse and beam profile of the Nd:YLF laser with 60% output coupler reflectivity at full pump power and 18.0 W average output power.

The laser with 0.7% Nd and 80% output coupler reflectivity showed an average output power of 21.2 W with a pulse length of ~101 ns, while maintaining good beam quality, as seen in Figure 11-7.

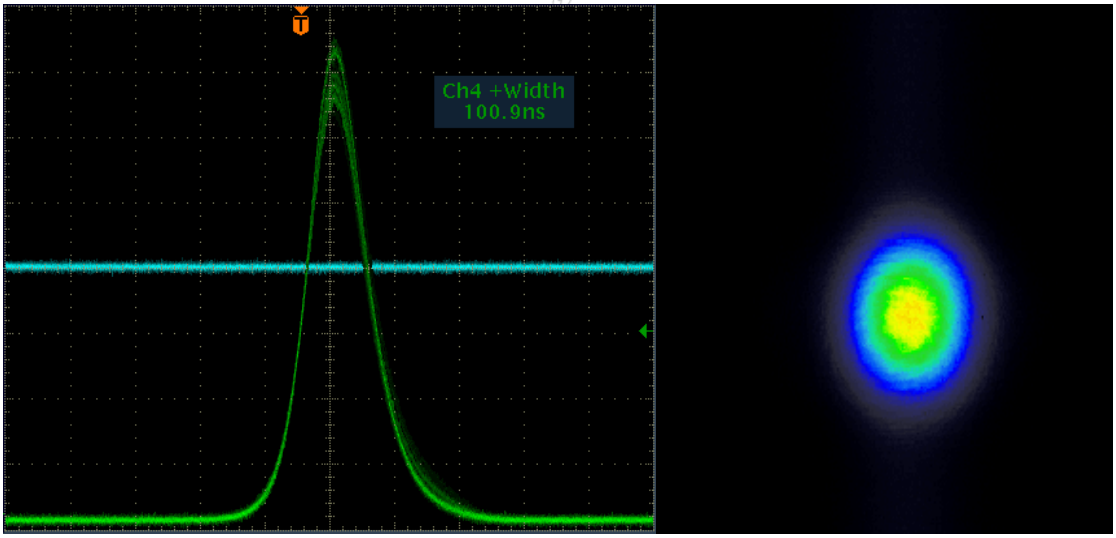

Figure 11-7: Pulse and beam profile of the Nd:YLF laser with 80% output coupler reflectivity at full pump power and 21.2 W average output power.

The above results are summarised in Table 11-1.

	R = 80%	R = 60%	R = 90%
0.5%			
Average power [W]	22.1	20.4	18.3
0.70%			
Average power [W]	21.2	18.0	13.7
Pulse length [ns]	101	113	139

Table 11-1: The influence of the output coupler reflectivity on the average power and pulse length of the Nd:YLF laser.

11.3 Influence of the short arm length

The influence of the short arm length of the resonator on the far field beam profile is shown in Figure 11-8. The laser was pumped at full power with an output coupler reflectivity of 80%. The Nd:YLF crystal had a doping concentration of 0.7% Nd and the diode temperature was kept at 28°C. The short arm length was decreased by moving mirror M2 in steps of 0.5 mm closer to M1.

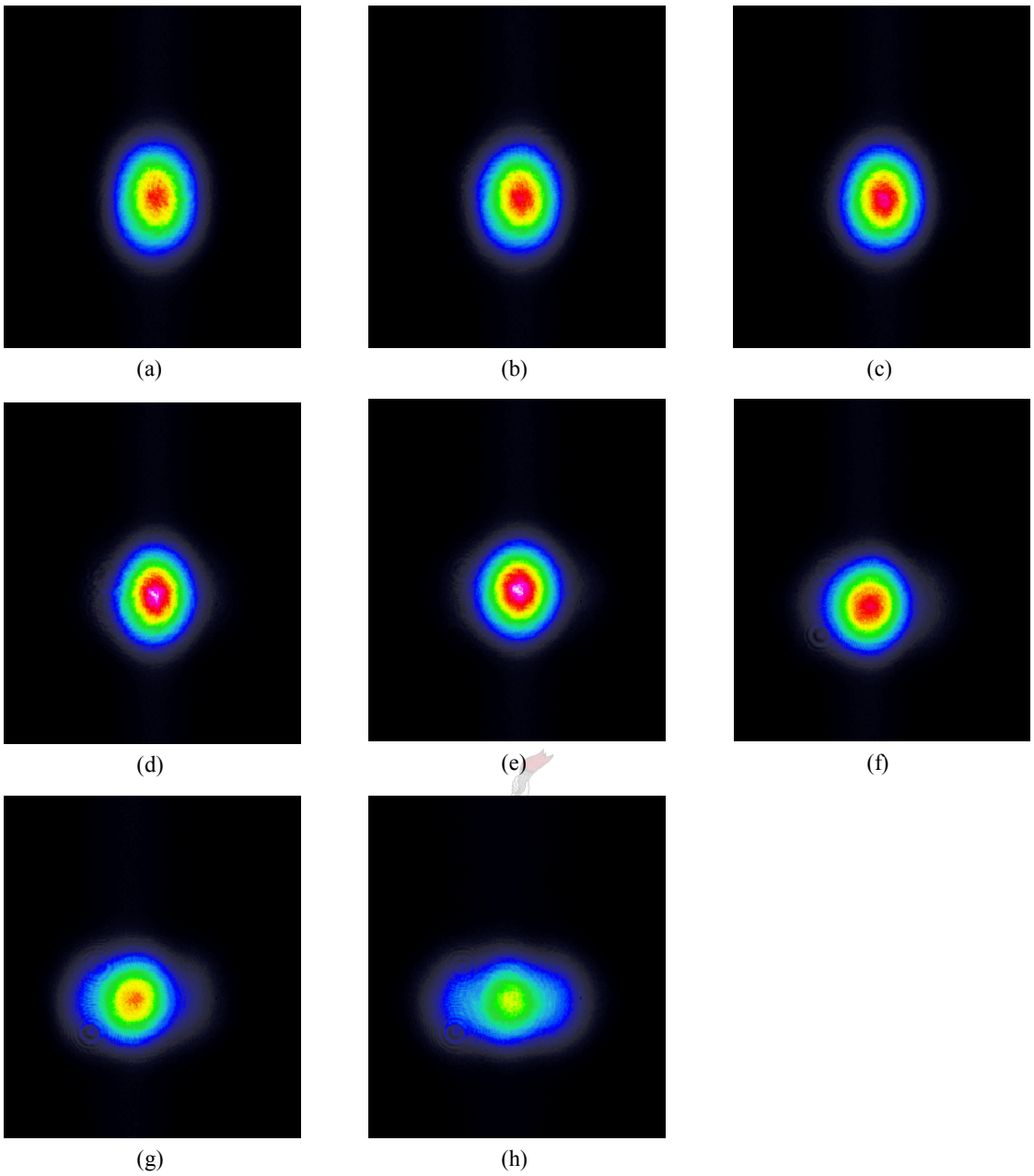

Figure 11-8: The influence of the short arm length on the beam profile of the laser at full pump power. All other parameters were kept constant while the short arm length was decreased in 0.5mm steps from a long distance (a) to a short distance (h).

As the short arm length was decreased, the output power increased slightly from 23.2 W in Figure 11-8(a) up to 23.5 W in Figure 11-8(e), and decreased again to 21.0 W in Figure 11-8(h). The decrease in short arm length also required an increase in input power to establish laser threshold. When the short arm length was decreased further than in Figure 11-8(h), the laser resonator came close to the stability edge.

In order to quantify the influence of the short arm length, the M^2 beam quality factor was measured for different short arm lengths under full pump power. The change in

M^2 for the change in short arm length from 47.25 mm to 52.25 mm, together with the output power, is shown in Figure 11-9. The laser was pumped with the diode temperature at 24 °C.

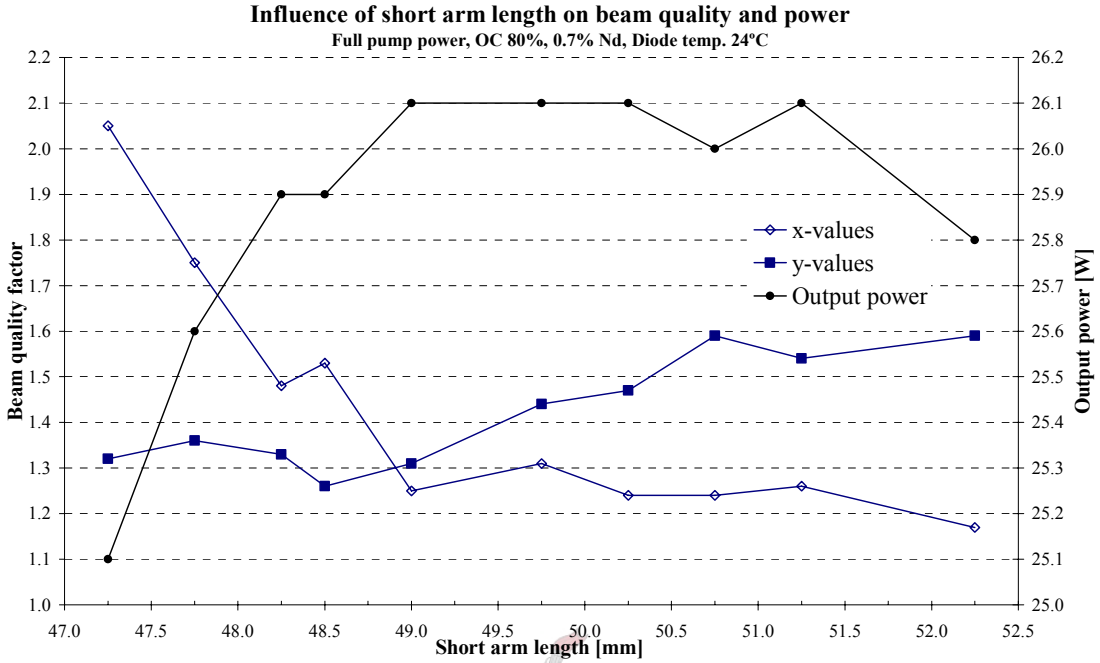

Figure 11-9: The influence of the short arm length on the beam quality factor as measured in the x- and y-planes, and on the output power of the Nd:YLF laser.

11.4 Output power dependence on pump wavelength

It was concluded from the pump absorption measurements in Section 8.2 that the optimum absorption of the un-polarized pump power was at the diode temperature in the region of 24 °C. This result was compared to the output power of the Nd:YLF laser at full pump power for different diode temperatures. The laser with output coupler reflectivity of 80%, short arm length of 48.5 mm and doping concentration of 0.7% Nd was operated in continuous wave mode while the diode temperature, and thus the pump wavelength, was varied. The result is shown in Figure 11-10.

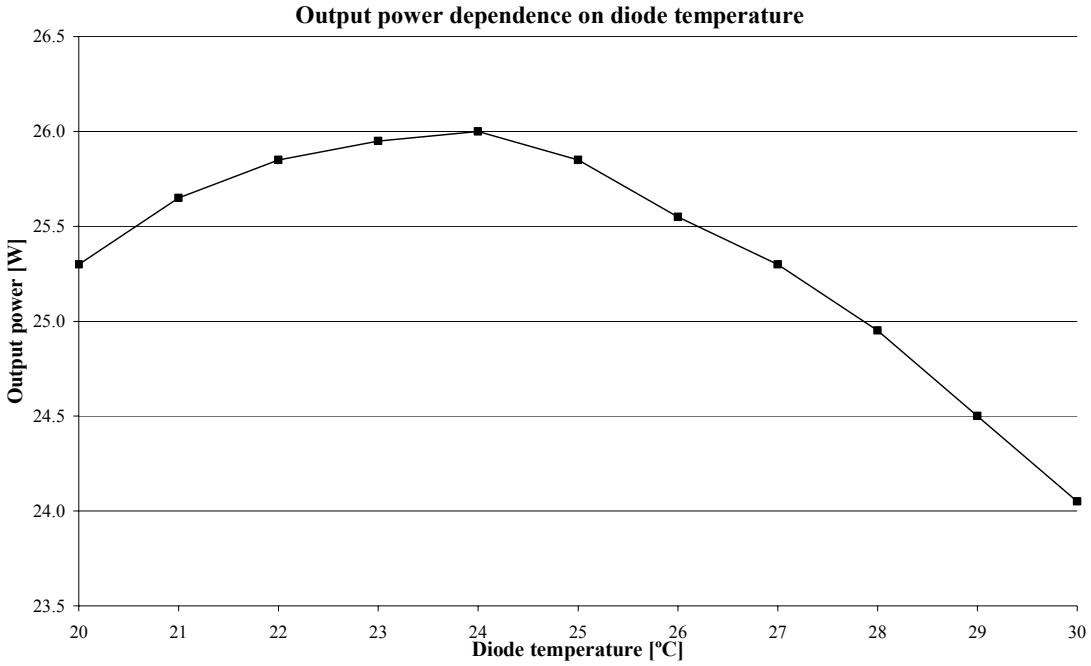

Figure 11-10: The change in continuous wave output power of Nd:YLF laser as the diode temperature was varied from 20°C to 30°C.

The diode temperature was increased from 20° C to 30º C. The maximum output power of 26.0 W was achieved at the diode temperature of 24º C. The far field beam profile of the laser was monitored during the experiment, which indicated no significant change in the beam quality over this temperature range.

11.5 Discussion of results

The foregoing results suggested an optimum combination of doping concentration, output coupling efficiency, short arm length and diode temperature.

11.5.1 Doping concentration

From the results presented in Section 11.1 it was concluded that the laser with the Nd:YLF crystal of 0.7% Nd atomic doping concentration delivered higher continuous wave output power than the laser with the 0.5% doped crystal. Under *Q*-switched operation, the higher doped crystal also delivered shorter pulses. Although the risk for thermal fracture was higher for the 0.7% doped crystal (as discussed in Part 1), the laser was operated safely at full pump power without thermal fracture or indication of detrimental thermal effects.

11.5.2 Output coupling efficiency

The optimum output coupler reflectivity for the *Q*-switched Nd:YLF laser was experimentally determined in Section 11.2. The laser with the 80% reflectivity output coupler delivered the highest average output power and shortest pulse lengths, as compared to the other two output coupling efficiencies. The beam quality, as estimated from the beam profiles of Figure 11-5 to Figure 11-7, also suggested that the output coupler of 80% reflectivity was the optimum for this laser.

11.5.3 Short arm length

As discussed in Section 9 the short arm length was be adjusted to optimise the overlap of the resonator mode, which is influenced by the thermal lens, with the pump beam of the laser. The change in the far field beam profile for a change in the short arm length, as shown in Figure 11-8, was an initial confirmation that through fine adjustment of the short arm length the optimum mode-matching between the resonator mode and the pump beam, and thus the beam overlap efficiency for the laser, can be found.

The result was quantified in Figure 11-9 where the relationship between beam quality and output power was directly observed. At a short arm length of 49.0 mm the beam quality was good for both directions and the laser produced 26.1 W of output power. This short arm length was the optimum length for simultaneously producing good beam quality in both planes and ensuring good beam overlap efficiency.

However, the investigation of the beam quality at different short arms lengths showed that there were two different optimum short arm lengths for the beam quality factor in the horizontal and vertical planes when considered independently. This was due to the astigmatic thermal lens of Nd:YLF that influenced the resonator mode. The astigmatic thermal lens caused a different optimum short arm length in the two planes. As discussed in 9.1.3 this effect could be compensated for by increasing the incident angle on the concave folding mirror M2.

11.5.4 Diode temperature

The graph shown in Figure 11-10 of the output power of the 0.7% doped Nd:YLF laser versus the pump diode temperature shows the overall laser efficiency at different diode temperatures. The maximum output power was at a diode temperature of 24 °C.

This was expected from the measured effective absorption data for the Nd:YLF crystal (Figure 8-5). However, the efficiency of the laser diodes at different diode temperatures, as shown in Figure 8-3, also influenced the overall efficiency of the laser even if only slightly. The effect contributing more to the overall efficiency was the beam overlap efficiency that changed due to the different thermal lens at different diode temperatures.

11.5.5 Efficiency of the optimised Nd:YLF laser

From the above discussion of the results it is clear that the optimum parameters for the high power Nd:YLF laser were

- Doping concentration: 0.7 % (at.) Nd
- Output coupler reflectivity: 80 %
- Short arm length: 49.0 mm
- Laser diode temperature: 24 °C.

Figure 11-11 and Figure 11-12 summarise the performance of this laser when operated in continuous wave mode.

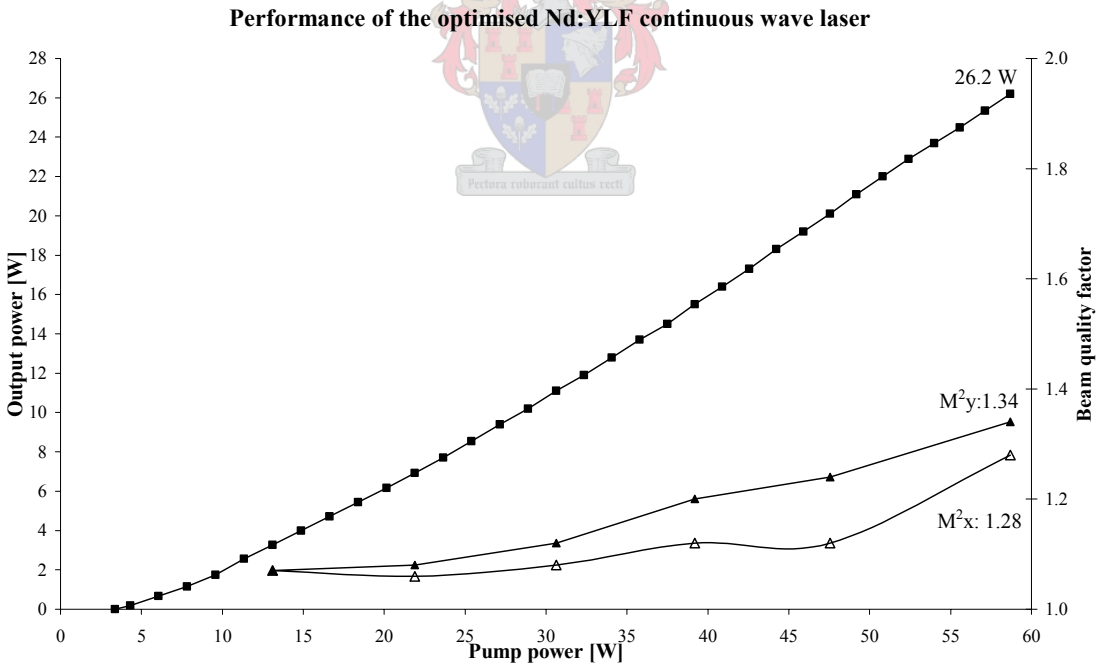

Figure 11-11: The slope efficiency and beam quality of the optimised continuous wave Nd:YLF laser.

At full pump power, the optimized Nd:YLF laser had a continuous wave output power of 26.2 W, more than twice the previously highest reported value in the literature [5].

The optical-to-optical efficiency was 44.6 % at full output power and the pump power for threshold of the Nd:YLF laser was 3.4 W.

The output power showed an almost linear increase for an increase in pump power, with a slope efficiency of 43 % at low pump power (below 30 W) and 55 % at higher pump power. This difference can be attributed to the increase in junction temperature of the laser diodes for an increase in drive currents, leading to a slightly different pump wavelength, which was optimised at full pump power. It would be possible to optimise the diode temperature at each current setting. For example, the optimum diode temperature at drive current of 25 A was 28 °C. This approach would lead to a more linear output graph. Nevertheless, the results show that the laser had a large dynamic range.

From the beam quality measurements in Figure 11-11 it can be seen that the beam quality changed from an almost diffraction limited beam at low power, to a beam with M^2 values of 1.28 and 1.34 in the horizontal and vertical planes respectively.

The corresponding beam profiles of the measured M^2 points are shown in Figure 11-12. It can be seen that the laser stays in the TEM_{00} transverse mode even if it becomes slightly oval at the maximum output power. The change in beam profile and beam quality factors at high output power is due to the increase in the thermal lens power. However, it must be noted that although the beam is oval at this point, the beam quality is still good in both planes with M^2 values below 1.4. This indicates that the oval beam can be corrected external to the laser resonator with standard cylindrical optics without any diffraction losses.

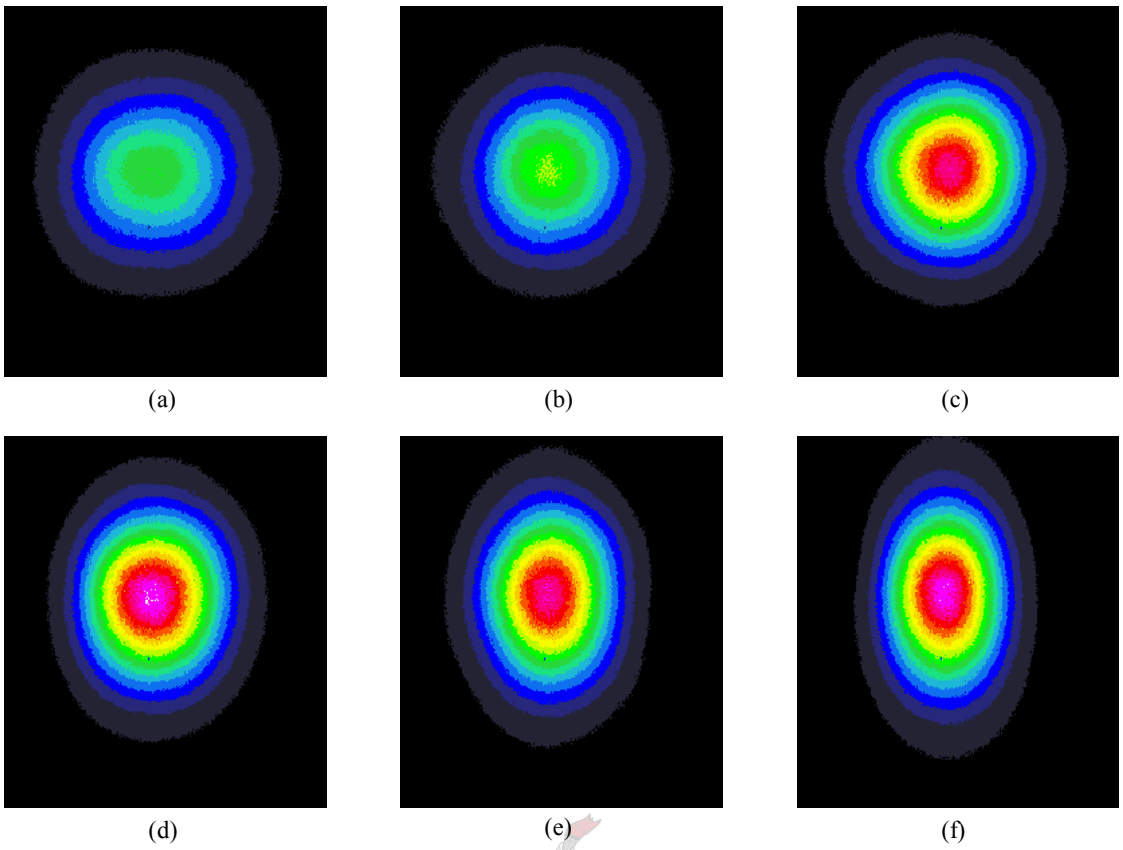

Figure 11-12: The far field beam profile of the optimised Nd:YLF laser at output power of (a) 3.3, (b) 6.9, (c) 11.1, (d) 15.5, (e) 20.1 and (f) 26.2 W.

Note: the shown beam profiles were measured under different attenuation levels.

11.5.6 Pulsed operation of the optimized laser

The AOM *Q*-switch was inserted in the optimised Nd:YLF laser to operate it in pulsed mode. The pulse repetition frequency was varied between 5 and 100 kHz while the laser was pumped at full power. The change in average output power and energy per pulse over the pulse repetition frequency range is shown in Figure 11-13 and the average pulse length is shown in Figure 11-14.

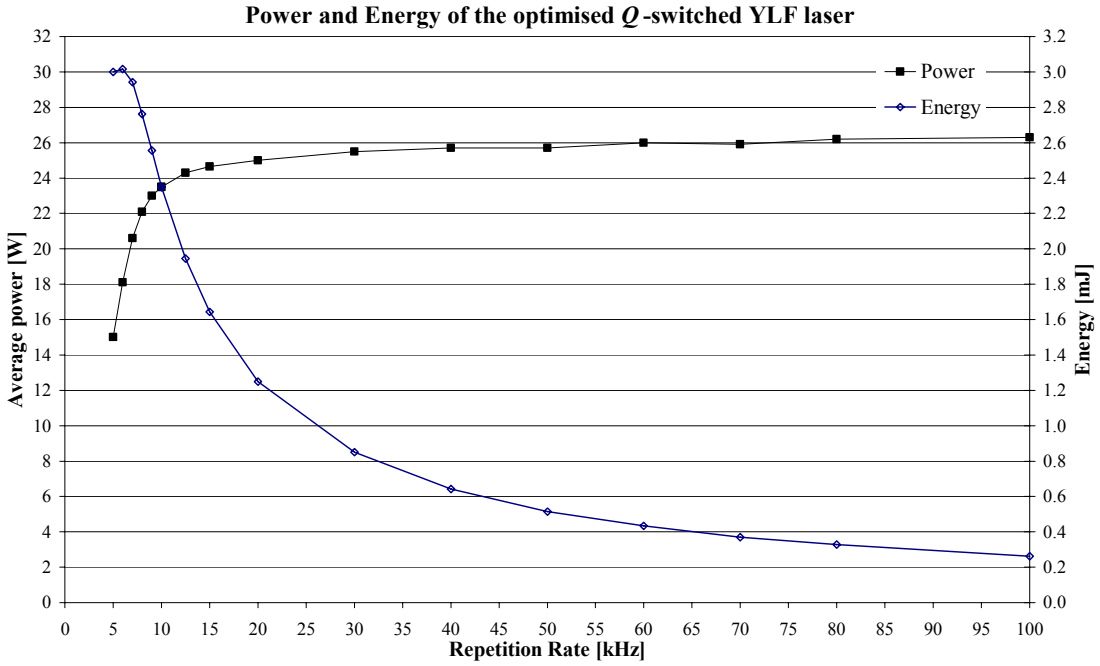

Figure 11-13: The average power and energy per pulse of the Nd:YLF laser at different repetition rates.

The average power approached the continuous wave power level at high repetition rate, reaching 26.2 W at 100 kHz. The pulse length was 195 ns at this rate, resulting in pulse energies below 0.3 mJ. With a decrease of pulse repetition rate, the pulse length of the laser decreased linearly, as seen in Figure 11-14.

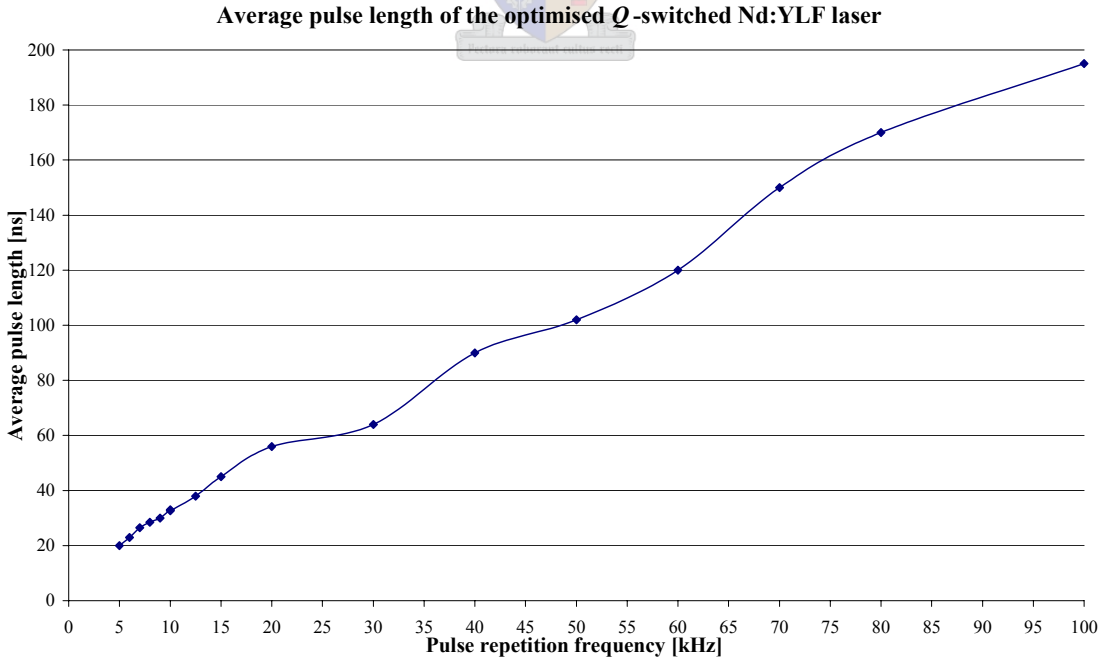

Figure 11-14: The average pulse length of the optimised Nd:YLF laser at different repetition rates.

The pulse energy reached a maximum of 3 mJ at a pulse repetition frequency of 6 kHz. Below this repetition rate, the average power dropped sharply, the energy per pulse decreased and the pulses became unstable. The instability can be attributed to an insufficient hold-off of the *Q*-switch due to the high gain in the laser medium and possibly, to a slow switching time of the *Q*-switch. The average pulse length of the laser at 5 kHz was 20 ns.

12 Summary & Conclusions

Part One formed a discussion of diode-pumped solid-state lasers. It consisted of an introduction to solid-state lasers in general, but focussed mainly on the well-known Nd^{3+} active ion, its energy levels and the four-level laser structure it can have.

The pump sources for solid-state lasers were discussed, comparing modern diode lasers against conventional lamp pump sources. The construction and operation of these devices were detailed, highlighting the advantages of diode lasers as pump sources for solid-state lasers.

It was motivated that diode-end-pumping of solid-state lasers ensured the desirable properties of high efficiency and diffraction limited beam quality, to a higher degree than side-pumping with diode lasers. However, it was noted that power scaling of diode-end-pumped solid-state lasers proves to be problematic, mainly due to localised heat generation in the laser medium.

The fundamental reasons for heat generation in solid-state lasers were discussed, including the phenomena of energy transfer upconversion (ETU), and its adverse effect on the performance of solid-state lasers. The generation of a highly aberrated thermal lens, which also depends on laser material properties, were discussed, and thermal fracture of the laser material were given as the ultimate limit for power scaling these lasers.

Part Two detailed the design and development of a high power diode-end-pumped solid-state laser. The approach was to use Nd:YLF, a laser material that has favourable thermo-optical properties. In particular, it has the advantage of a very weak thermal lens when operating on the σ-polarization. It has however, a major disadvantage of having a low fracture limit, which is worsened by its susceptibility to ETU.

The laser design incorporated these material properties to establish a high power Nd:YLF laser delivering more than 26 W output power in continuous wave and in pulsed operation with its output beam quality close to being diffraction limited. This power scaling concept was based on the unique combination of pumping a Nd:YLF

crystal with low doping concentration at 805 nm. This was to ensure a low excitation density in the pump volume to avoid the detrimental effect of ETU. At this wavelength, the absorption of the un-polarized emission from two commercial 30 W fibre-coupled diode lasers was uniform, reducing the aberrated thermal effects.

The development of the novel laser resonator design was discussed, in particular its main feature to allow good spatial overlap of a large fundamental resonator mode with a large pump beam in the laser medium, and its ability to discriminate against the Nd:YLF laser operating on the π-polarization.

The influence of doping concentration, output coupling efficiency, resonator setup and pump wavelength on the performance of the Nd:YLF laser were investigated experimentally, and the optimum combination of these parameters were determined. The results of the optimised high power diode-end-pumped Nd:YLF laser were presented and showed an efficient laser, with near diffraction limited beam quality over a large dynamic range. The optimised laser was also operated in *Q*-switched mode, which highlighted the energy storage capability of Nd:YLF at low pulse repetition rates.

With these results limited only by pump power, and not by thermal fracture of the laser material, it confirmed the power and energy scaling possibility of this approach for high power diode end-pumped solid-state lasers. Further work conducted at the Laser Research Institute that was based on this novel approach, saw the realisation of a Nd:YLF laser with more than 60 W of continuous wave output power in a diffraction limited beam, and more than 10 mJ pulse energy in *Q*-switched operation.

List of publications

International Conference Papers

1. **M. J. D. Esser**, C. Bollig and H. M. von Bergmann, "Efficient power scaling of an end-pumped Nd:YLF laser at 1053 nm," *EPS-QEOD Europhoton Conference, Lausanne* 2004.
2. C. Bollig, **M. J. D. Esser**, T. Stehmann and H.M. von Bergmann, "High-power end-pumped Nd:YLF laser," *Conference on Optics and Laser Applications,* Windhoek 2003.
3. **M. J. D. Esser**, C. Bollig and H. M. von Bergmann "Short pulse diode-pumped solid-state lasers," *Conference on Optics and Laser Applications,* Windhoek 2003.

National Conference Papers

1. **M. J. D. Esser**, C. Bollig and H. M. v. Bergmann, "Short pulse diode-pumped solid-state lasers," in *South African Institute of Physics 47th annual conference, Potchefstroom 2002*, talk E6, (2002).
2. **M. J. D. Esser**, C. Bollig, T. Stehmann and H. M. v. Bergmann, "Multi-Watt Diode-End-Pumped Solid-State (Nd:YLF) Laser," in *South African Institute of Physics 48th annual conference, Stellenbosch 2003*, talk D2, (2003).
3. T. Kapp, **M. J. D. Esser** and C. Bollig, "Compact Diode-Pumped Green Nd-vanadate Laser," in *South African Institute of Physics 48th annual conference, Stellenbosch 2003*, talk D3, (2003).
4. C. Bollig, **M. J. D. Esser** and T. Stehmann, "Visible Diode-Pumped High-Power Solid-State Lasers," in *South African Institute of Physics 48th annual conference, Stellenbosch 2003*, talk D17, (2003).
5. **M. J. D. Esser**, C. Bollig and H. M. v. Bergmann, "Electronic Feedback to Stabilize Pico-Second Diode-Pumped Solid-State Lasers," in *South African Institute of Physics 48th annual conference, Stellenbosch 2003*, poster D31, (2003).
6. N. Rumble, C. Bollig and **M. J. D. Esser**, "The Construction of a Miniature Solid-State Green Laser," in *South African Institute of Physics 48th annual conference, Stellenbosch 2003*, poster D 32, (2003).

References

[1] H. Hügel "New solid-state lasers and their application potentials" *Optics and Laser in Engineering* **34** 213-229 (2000).

[2] K. Kincade and S. Anderson "Review and forecast of the laser markets: Part I: Nondiode lasers" *Laser Focus World* (January 2004).

[3] D. Vivien "Recent advances in solid-state laser materials: An introduction" *Annales de Chimie Science des Matériaux* **28** (6) 1-3 (November-December 2003).

[4] R. Steele "Review and forecast of the laser markets: Part II: Diode lasers" *Laser Focus World* (February 2003).

[5] W. A. Clarkson, P. J. Hardman and D. C. Hanna "High-power diode-bar end-pumped Nd:YLF laser at 1.053 μm" *Optics Letters* **23** (17) 1363-1365 (1998).

[6] W. Koechner "Solid-state laser Engineering" 5th rev and updated ed. *Springer series in Optical Sciences Volume 1*, Springer-Verlag Berlin Heidelberg, Germany (1999).

[7] O. Svleto "Principles of lasers" second edition, translated and edited by D. C. Hanna, *Library of Congress Cataloging in Publication Data*, Plenum Press, New York (1982).

[8] A. E. Siegman "Lasers" *University Science Books* Sausalito, California (1986).

[9] T. H. Maiman *Nature* **187** 493 (1960).

[10] M. J. Weber "Handbook of Laser Science and Technology, Supplement 1: Lasers" *Library of Congress Cataloging-in-Publication Data*, CRC Press Inc. (1991).

[11] H. Zhanga, M. Chaoa, M. Gaoa, L. Zhanga and J. Yaob "High power diode single-end-pumped Nd:YVO4 laser" *Optics & Laser Technology* **35** 445 – 449 (2003).

[12] S. Kück, L. Fornasiero, E. Mix and G. Huber "Exited state absorption and stimulated emission of Nd^{3+} in crystals. Part I: $Y_3Al_5O_3$, $YAlO_3$, and Y_2O_3" *Applied Physics B* **67** 151-156 (May 1998).

[13] C. Czeranowsky "Resonatorinterne Frequenzverdopplung von diodengepumpten Neodym-Lasern mit hohen Ausgangsleistungen im blauen Spektralbereich" *PhD Dissertation*, University of Hamburg (2002).

[14] Y. Louyera, F. Balemboisb, M. D. Plimmera, T. Badra, P. Georgesb, P. Juncara and M. E. Himbert "Efficient cw operation of diode-pumped Nd:YLF lasers at 1312.0 and 1322.6 nm for a silver atom optical clock" *Optics Communications* **217** 357–362 (2003).

[15] L. Gao and H. Tan "Compact 600mW blue laser with a composite Nd:YAG" *Optics & Laser Technology* **35** 575 – 578 (2003).

[16] T. S. O. Fan and R. L. Byer "Diode Laser-Pumped Solid-State Lasers" *IEEE Journal of Quantum Electronics* **24** (6) 895-912 (June 1988).

[17] R. Newman "Excitation of the Nd^{3+} fluorescence in $CaWO_4$ by recombination radiation in GaAs" *Journal of Applied Physics* **34** 437 (1963).

[18] D. W. Hughes and J. R. M. Barr "Laser diode pumped solid state lasers" *Journal of Physics D: Applied Physics* **25** 563-586 (1992).

[19] B. D. Sinclair and M. H. Dunn "All-solid-state lasers" *Physics Education* **29** (1994).

[20] V. Gavryushin and A. Žukauskas "Semiconductor Lasers"
http://www.mtmi.vu.lt/pfk/funkc_dariniai/diod/led.htm (2002).

[21] C. Hanke "High power diode lasers" *Solid-state lasers: New Developments and Applications* Edited by M. Inguscio and R. Wallenstein, Plenum Press, New York (1993).

[22] N. Rumble, C. Bollig and M. J. D. Esser, "The Construction of a Miniature Solid-State Green Laser" *South African Institute of Physics 48th annual conference Stellenbosch 2003* poster D 32 (2003).

[23] J. R. Leger and W. C. Goltsos "Geometrical Transformation of linear Diode-Laser Arrays for Longitudinal Pumping of Solid-State Lasers" *IEEE Journal of Quantum Electronics* **28** (4) (April 1992).

[24] J. M. Auerbach and R.L. Schmitt, "Diode-laser-pumped monolithic Nd:YLF laser operating at 1.053 μm" *Optics Letters* **16** (15) 1171-1173 (1991).

[25] Th. Graf and J. E. Balmer "High-power Nd:YLF laser end pumped by a diode-laser bar" *Optics Letters* **18** (16) 1317-1319 (1991).

[26] R. Beach, P. Reichert, W. Benett, B. Freitas, S. Mitchell, A. Velsko, J. Davin and R. Solarz "Scalable diode-end-pumping technology applied to a 100-mJ Q-switched Nd^{3+}:YLF laser oscillator" *Optics Letters* **18** (16) 1326-1328 (August 1993).

[27] B. Ehlers, K. Du, M. Baumann, H. Treusch, P. Loosen and R. Poprawe, "Beam shaping and fiber coupling of high-power diode laser arrays" *Lasers in Material Processing* Proc. SPIE **3097** 639-644 (1997).

[28] S. M. Goldwasser "Sam's Laser FAQ" http://www.repairfaq.org/sam/fcld1.jpg (2004).

[29] S. M. Goldwasser "Sam's Laser FAQ" http://www.repairfaq.org/sam/fcldc1.jpg (2004).

[30] V. Lupei, N. Pavel, Y. Sato and T. Taira "Highly efficient 1063-nm continuous-wave laser emission in Nd:$GdVO_4$" *Optics Letters* **28** (23) 2366-2368 (December 2003).

[31] M. A. Apter (Coherent semiconductor division) "High Power Diode Lasers – Present Status and New Developments" *International Laser Marketplace 2001, München* (June 2001).

[32] Peter Loosen, *Summer School Lecturer*, *EPS-QEOD Europhoton Conference, Lausanne* 2004.

[33] W. A. Clarkson and D. C. Hanna *Optics Letters* **21** 375-377 (1996).

[34] T. Y. Fan, A. Sanchez and W. E. DeFeo "Scalable, end-pumped, diode-laser-pumped laser" *Optics Letters* **14** (19) 1057-1059 (October 1989).

[35] W. A. Clarkson "Thermal effects and their mitigation in end-pumped solid-state lasers" *Journal of Physics D: Applied Physics* **34** 2381-2395 (2001).

[36] Y. F. Chen, C. F. Kao, T. M. Huang, C. L. Wang and S. C. Wang "Influence of Thermal Effect on Output Power Optimization in Fiber-Coupled Laser-Diode End-Pumped Lasers" *IEEE Journal of Selected Topics in Quantum Electronics* **3** (1) (February 1997).

[37] S. B. Sutton and G. F. Albrecht "Optical distortion in end-pumped solid-state rod lasers" *Applied Optics* **32** (27) 5256-5269 (September 1993).

[38] R. Weber, B. Neuenschwander and H. P. Weber "Thermal effects in solid-state laser materials" *Optical Materials* **11** 245-254 (January 1999).

[39] D. C. Brown "Ultrahigh-Average-Power Diode-Pumped Nd:YAG and Yb:YAG Lasers" *IEEE Journal of Quantum Electronics* **33** (5) (May 1997).

[40] M. Pollnau, P. J. Hardman, M. A. Kern, W. A. Clarkson and D. C. Hanna "Upconversion-induced heat generation and thermal lensing in Nd:YLF and Nd:YAG" *Physical Review B* **58** (24) 16076-16092 (1998).

[41] T. Chuang and R. V. Verdún "Energy Transfer Up-Conversion and Exited State Absorption of Laser Radiation in Nd:YLF Laser Crystals" *IEEE Journal of Quantum Electronics* **32** (1) 79-91 (1996).

[42] L. C. Courrol, E. P. Maldonado, L. Gomes, N. D. Vieira Jr., I. M. Ranieri and S. P. Morato "Diode pumping Nd-laser efficiency limitations due to up-conversion processes in Nd:YLF and Nd:GLF" *Optical Materials* **14** 81-90 (2000).

[43] D. L. Russell and K. Holliday "Upconversion and energy transfer dynamics in Nd^{3+}:$KLiYF_5$" *Optics Communications* **191** 277-294 (May 2001).

[44] S. A. Payne, G. D. Wilke, L. K. Smith and W. F. Krupke "Auger upconversion losses in Nd-doped laser glasses" *Optics Communications* **111** 263-268 (October 1994).

[45] Y. Chen, Y. Lan and S. Wang "Modelling of diode-end-pumped Q-switched solid-state lasers: influence of energy-transfer upconversion" *Journal of the Optical society of America B* **19** (7) 1558-1563 (July 2002).

[46] M. Pollnau, P. J. Hardman, W. A. Clarkson and D. C. Hanna "Upconversion, lifetime quenching, and ground-state bleaching in Nd^{3+}:$LiYF_4$" *Optics Communications* **147** 203-211 (February 1998).

[47] P. J. Hardman, W. A. Clarkson, G. J. Friel, M. Pollnau and D. C. Hanna "Energy-Transfer Upconversion and Thermal Lensing in High-Power End-Pumped Nd:YLF Laser Crystals" *IEEE Journal of Quantum Electronics* **35** (4) 647-655 (April 1999).

[48] C. Pfistner, R. Weber, H. P. Weber, S. Merazzi and R. Gruber "Thermal Beam Distortions in End-Pumped Nd:YAG, Nd:GSGG, and Nd:YLF Rods" *IEEE Journal of Quantum Electronics* **30** (7) 1605-1615 (July 1994).

[49] *Private discussion,* Christoph Bollig.

[50] A. E. Siegman "Analysis of laser beam quality degradation caused by quartic-phase aberrations" *Applied Optics* **32** (30) 5893-5901 (October 1993).

[51] R. Weber, T. Graf and H. P. Weber "Self-adjusting Compensating Thermal Lens to Balance the Thermally Induced Lens in Solid-state Lasers" *IEEE Journal of Quantum Electronics* **36** (6) 757 (June 2000).

[52] H. Vanherzeele "Thermal lensing measurement and compensation in a continuous-wave mode-locked Nd:YLF laser" *Optics Letters* **13** (5) 369-371 (May 1988).

[53] R. Gaume and B. Viana "Optical and Thermo-mechanical Properties of Solid-State Laser Materials" *Annales de Chimie Science des Matériaux* **28** (6) 1-3 (November-December 2003).

[54] D. A. Rockwell "A Review of Phase-Conjugate Solid-State Lasers" *IEEE Journal of Quantum Electronics* **24** (6) 1124 (June 1988).

[55] Coherent Scientific "40 W Fibre Array Packaged (FAP) Diode Laser Bar for Pumping Applications" *Coherent News*, (October/November 2003). http://www.coherent.com.au/physical/cohnews/2003/5303_psdnews.pdf

[56] B. Frei and J. E. Balmer, "1053-nm-wavelength selection in a diode-laser-pumped Nd:YLF laser" *Applied Optics*, **33** (30) 9642-9646 (1994).

[57] P. J. Hardman, W. A. Clarkson and D. C. Hanna, "Efficient operation of an acousto-optically-induced unidirectional and single-frequency Q-switched Nd:YLF ring laser" *TOPS - ASSL '99* Washington 1999 26 pp.236-239 http://www.orc.soton.ac.uk/publications/19xx/1975.pdf

[58] T. M. J. Kendall, W. A. Clarkson, P. J. Hardman and D. C. Hanna, "High-power Nd:YLF master oscillator power amplifier with 15W single-frequency output at 1053b nm" *Lasers and Electro-Optics, 2001. CLEO '01 Technical Digest* 417-418 (6-11 May 2001). http://ieeexplore.ieee.org/iel5/7534/20509/00947991.pdf

[59] NASA database of lasers, http://aesd.larc.nasa.gov/gl/laser/spectra/ndspec.htm.

[60] P. J. Hardman, W. A. Clarkson and D. C. Hanna, "High Power Diode-Bar-Pumped Intracavity-Frequency-Doubled Nd:YLF Ring Laser" *Optics Communications* **156** 49-52 (1998).

[61] K. Babushkin and W. Seka, "Efficient 1053-nm Nd:YLF laser end pumped by a 100-W quasi-cw diode array" *Lasers and Electro-Optics, 1998. CLEO '98 Technical Digest* 180-181 (3-8 May 1998).

[62] E. P. Maldonado, I. M. Ranieri, N. D. Vieira Jr. and S. P. Morato, "High-efficiency, argon-laser-pumped Nd:YLF laser system" *Applied Optics* **34** (21) 4295-4297 (1995).

[63] VLOC homepage, http://www.vloc.com/vlochome.htm.

[64] JENOPTIK Laserdiode GmbH homepage, http://www.jold.com/eng-sites/index.htm "Fiber-coupled passively cooled cw diode lasers" http://www.jold.com/eng-sites/products-ie.htm.

[65] M. W. Sasnett, "Propagation of multimode laser beams – the M^2 factor" *The Physics and Technology of Laser Resonators*, edited by D. R. Hall and P. E. Jackson, IOP Publishing, Bristol, New York, pp. 132–142 (1989).

[66] OZ Optics homepage, http://www.ozoptics.com "Non-contact style receptacle style laser to fiber couplers" http://www.ozoptics.com/dSheeets/noncontact_style.pdf

[67] H. W. Kogelnik, E. P. Ippen, A. Dienes, D. V. Shank *IEEE Journal of Quantum Electronics* **8** 373 (1972).

[68] Simulations with "Paraxia-Plus", Preview release 1.04.02 (2003) *SCIOP Enterprises and Stanford University*.

[69] C. Giulio *et al*, "High efficiency, 40 W cw Nd:YLF laser with large TEM_{00} mode" *Optics Communications*, **93** (1-2) 77-81 (1992).